WARWICK
THE UNIVERSITY OF WARWICK

A Thesis Submitted for the Degree of PhD at the University of Warwick

Permanent WRAP URL:
http://wrap.warwick.ac.uk/110794

Copyright and reuse:
This thesis is made available online and is protected by original copyright.
Please scroll down to view the document itself.
Please refer to the repository record for this item for information to help you to cite it.
Our policy information is available from the repository home page.

For more information, please contact the WRAP Team at: wrap@warwick.ac.uk

warwick.ac.uk/lib-publications

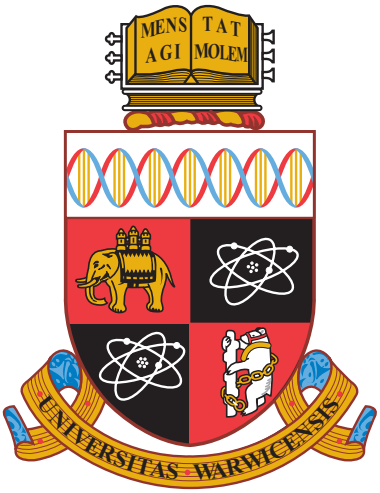

The Design and Analysis of Quartic Double Well Potential with Stochastic Resonance for Communication Systems

by

Nurhan Güneş

Thesis

Submitted to the University of Warwick

for the degree of

Doctor of Philosophy

School of Engineering

January 2018

THE UNIVERSITY OF WARWICK

Contents

List of Figures

Acknowledgments

It is a pleasure to thank those who made this thesis possible. First and foremost, sincere gratitude goes to my supervisors, Dr. Matthew D. Higgins and Dr. Mark S. Leeson, whose encouragement, guidance and support from the initial to the final level enabled me to develop an understanding of the subject whilst allowing me the room to work in my own way. I also wish to thank Dr. Alexander P. Nikitin for his comments and advices.

Secondly, I would like to thank the Ministry of National Education, the Republic of Turkey, for the scholarship helping me to focus on the study.

Thirdly, I also would like to express my deepest gratitude to my colleague Dr. Song Qui and his family for their warmth and kindness that conducts our close relation.

Last but not least, I am deeply grateful to my wife, Elif, and my son, Osman, and appreciative of all their love and understanding. I also express my thanks to our parents, Asiye & Şermi Güneş, Hatice & Sezai Alver, and Esen & Kadir Özkan. This thesis would not have been possible unless I was supported by all mentioned.

Declarations

I herewith declare that this thesis contains my own research performed under the supervision of Dr. Matthew D. Higgins and Dr. Mark S. Leeson, without assistance of third parties, unless stated otherwise. No part of this thesis was previously published or submitted for a degree at any other universities.

List of Publications

- N. Güneş, M. D. Higgins, and M. S. Leeson, "Stochastic resonator to detect bipolar binary pulse amplitude modulated signals; analysis, parameter-induced SR designs and sine-induced SR," *IET Signal Processing*, 10(9), 10171023. 2016.

- N. Güneş, M. S. Leeson, and M. D. Higgins, "The use of symmetric quartic potential well for noise filtering," *Fluct. Noise Lett.*, 1850019, 2018.

- N. Güneş, M. D. Higgins, and M. S. Leeson, "Deterministic and stochastic resonance in symmetric quartic potential well," *IEEE Signal Processing Letters*, To be submitted, 2018.

- N. Güneş, M. D. Higgins, and M. S. Leeson, "Modulation and Coding with symmetric quartic potential well," *Digital Signal Processing*, To be submitted, 2018.

Abbreviations

AWGN	Additive White Gaussian Noise
BER	Bit Error Rate
BPAM	Binary Pulse Amplitude Modulation
CDF	Cumulative Distribution
DC	Direct Current
DE	Differential Equation
DFT	Discrete Fourier Transform
DWP	Double Well Potential
FHN	FitzHugh-Nagumo neuron model
FPE	Fokker-Planck Equation
FSK	Frequency Shift Keying
LPF	Low Pass Filter
LRT	Likelihood Ratio Test
i.i.d.	independent and identically distributed
MMR	Output-Input Magnitude Ratio Response
NSR	Noise Induced Stochastic Resonance
ODE	Ordinary Differential Equation
PAM	Pulse Amplitude Modulation
PAM4	Four Level Pulse Amplitude Modulation
PDE	Partial Differential Equation

PDF	Probability Density Function
PSK	Phase Shift Keying
PSR	Parameter Induced Stochastic Resonance
PWPM	Pulse Width Position Modulation
SDE	Stochastic Differential Equation
SNR	Signal to Noise Ratio
SQPW	Symmetric Quartic Potential Well
SQUID	Superconducting Quantum Interference Device
SR	Stochastic Resonance
SSR	Supra-threshold Stochastic Resonance

Abstract

Non-linearity and noise are two phenomena that are expected to be essential to future advanced technologies. Although largely abstained, in general, from introduction into current communication systems, the counter-intuitive phenomenon called Stochastic Resonance (SR) can be introduced into communication systems in an innovative form. Therefore, in this thesis, the most prominent dynamical system in the SR field, the *double well potential*, namely the over-damped Duffing equation with symmetric bistable potential, has been studied in order to reveal its signal processing capabilities for communication systems.

Within this thesis, the double well potential was designed in order to detect a binary pulse amplitude modulated (BPAM) signal subject to a background noise. The bit-error-rate (BER) performance was enhanced by adding various resonant signals to the input. In addition, the eye patterns of system output indicated that, while decreasing BER, a resonant causes a strong fluctuation. It was eliminated by a use of two systems coupled in parallel, which provided further performance improvement. The results inferred that the double well potential performs filtering and modulation.

Following that, the double well potential was designed as a lowpass filter by determining the DC gain and cut-off frequency. Through simulations, as a filter, its noise suppression performance was shown to be better than that of various orders of Butterworth filters.

The analog and digital modulation capabilities of the double well potential have also been investigated. In order to clarify the relation between input signal and modulation parameters, the differential equation driving the output was solved, and thus the output was expressed as a function of modulation parameters. It was shown that the output is a multivariate analog modulated signal. In terms of digital modulation, the output of system processing a PAM signal has been interpreted by means of a Markov chain. The results indicated that this process consists of a convolutional coding and multidimensional modulation. In addition, the presence of noise induced coding was found. Finally, the system was designed to obtain a pulse width position modulated (PWPM) output. Throughout the project, detection, filtering, modulation and coding capabilities have been demonstrated, it has been concluded that the double well potential is an sophisticated signal processing tool.

Chapter 1

Introduction

1.1 Background and motivation

In any communication system, noise limits the sensitivity and accuracy, thereby the performance. Defining communications as a transmission of information from one location to another, it takes place in a medium called the *channel*. According to the *noisy channel coding theorem*, for reliable communications, the maximum amount of information that can be transmitted through a channel is determined by the *channel capacity*. As the channel is a physical medium, the power of the information signal is finite, and more importantly, a noise source is always present. In addition, this capacity is a function of the frequency band, called *bandwidth*, and power of information signal and noise. It can be improved by increasing bandwidth. However, the maximum capacity can reach to the upper bound defined by the *signal-to-noise ratio* (SNR). Therefore, the performance of a communication system is restricted by the noise [1].

The noise can be divided into four main categories; crosstalk, impulse noise, inter-modulation noise, and thermal noise. While the coupling between two or more signals and an instant release of charge carriers result in crosstalk and impulse noise, respectively, the inter-modulation noise is caused by the non-linear response

of device or medium. These are related to instrumental imperfections, atmospheric turbulence, harmonics from power line, broadcasting stations, etc. and can be reduced by shielding or instrumental improvements. The last one, thermal noise, results from random electron motion, and its power depends on the temperature and bandwidth. It is always present in any element of a communication system. These noise-induces can be reduced to arbitrary small values by means of significant achievements from various disciplines. However, in practice, they cannot be eliminated entirely [2, 3].

Moreover, noise reduction, on its own, can not help a system to reach the optimum performance led by the channel capacity. Although it can be accomplished by signal processing techniques and information encoding, this conventional approach to the noise treatment is possibly unrealistic when a system with micro and nano scale components are in the consideration. At such scale, in addition to the unaffordable complexity, these components may not be changed with an alternative, or should not be [4]. For instance, in nano-networks and molecular communication, biological cells, proteins, nucleic acids, etc. are considered as a system components that encode, decode, or carry the information [5,6]. In such systems, noise reduction can affect the functionality of these components, thereby causing the system failure. This has been already observed and demonstrated under the name of *Stochastic Resonance* (SR) [7].

SR is a counter-intuitive phenomenon showing that in a non-linear system, noise can be an indispensable ingredient. Although, it is already known that the non-linear systems in physics, engineering, biology, etc., exhibit deterministic resonance optimizing the system response, the stochastic resonance is a relatively new term probably due to the perception of noise. It is considered as an effect rather than a technique, and refers to an optimization of the system performance by means of noise. While this noise-induced phenomenon is observed in numerous systems regardless of the size or scale, they can be grouped into two categories; threshold

crossing and dynamical systems [8].

From the communication point of view, it has been proven that the threshold crossing systems with noise can perform fundamental signal processing tasks such as detection, quantization, and encoding [7]. While these are sufficient to call SR as a signal processing tool for communication systems, the same has not been inferred for SR in dynamical systems. Although their abilities such as signal amplification, noise coherent oscillation, are known, the dynamical systems with SR may not be endorsed for communication due to their strong non-linearity and inter-modulation property.

However, it is found that many devices working in resonant modes enhance the efficiency and performance. Dynamical systems are more capable when compared to threshold crossing ones in terms of signal processing. It is also anticipated that the properties of resonance play a significant role in future advanced technology [7, 8]. While the most prominent dynamical system in SR field is the *double well potential* (DWP), the potential well models are significant to researchers in explaining the reasoning behind probabilistic behaviours. For example, the motion of a particle in a DWP is used to model the dynamic behaviour of an superconducting quantum interference device (SQUID) [9], a finite square potential well is used to model the energy of the electron in a single quantum well [10], and a Morse potential well is used to model the vibrational structure of molecules [11]. Moreover, potential wells can exhibit the SR phenomenon, which occurs when a nuisance signal, such as noise, counter-intuitively, favours the system [12]. This combination of potentially beneficially behavioural phenomenon, coupled with the links to probabilistic concepts analogous in information theory, make DWP important for further consideration in the communications and signal processing fields. Therefore, the motivation of this Ph.D. research is to design and analyse the DWP, specifically for processing the fundamental communication signals.

1.2 Objectives

The objectives of this Ph.D. is to establish the DWP as a signal processing technique in communication, to enable its use in various cases where noise is either essential or dispensable signal, and to evaluate the performance enhancement. Therefore, this research has been separated into following specific tasks with corresponding objectives.

- Detection: The DWP needs to be designed to detect a weak information signal. The deterministic and stochastic resonances are supposed to be observed. The performance results should be inspected thoroughly in order to determine resonance conditions. The effect of coupling two double well in parallel is expected to be beneficial.
- Filtering: It is necessary to clarify the passband and stop-band of DWP and the effect on frequency components of the input signal and noise. Filtering capability also requires to be compared with a conventional filter.
- Modulation: The processes of functioning a modulation needs to be investigated and clarified by defining modulation parameters. It is expected to obtain an output equivalent to a conventionally modulated signal.
- Encoding: The decision process performed by DWP is also investigated. Then, the effect of noise on encoding process is expected to be illustrated.

1.3 Outline of the Thesis

The thesis is organised within 7 chapters. The first and last chapters are introduction and conclusion and the second chapter summarized the literature research. The remaining 4 chapters are going to describe each individual task. The highlights of these chapters are represented as follows:

- In Chapter 3, the DWP is designed to receive an information signal. The design is based on the output gain rather than the input signal. An information carrier, namely pulse amplitude modulated (PAM) signal, is applied to input, and the output is obtained from simulation. According to results, the design parameters are revised. From both design and simulation results, the conditions for SR occurrence are clarified. Then, the Gaussian noise and sine wave are introduced to observe stochastic and deterministic resonance effect on the bit error rate (BER) performance.

- In Chapter 4, the deterministic and stochastic signals alternative to Gaussian noise are added into the input and the extensive simulation is conducted in order to obtained the optimum performance for each resonant signal. The difference between performances are reported. Two DWPs connected in parallel are used to observe the possible noise cancellation. The outputs are examined in time domain by eye patterns. The relation between noise cancellation and performance improvement is reported.

- In Chapter 5, the DWP is designed as a baseband filter. The baseband gain and cut-off frequency are derived approximately, then adjusted according to the output's frequency spectrum. The effect of background noise on these properties are examined. BER performances from DWP filter and conventional filter are compared.

- In Chapter 6, the differential equation (DE) of the double well potential is approximately solved in order to obtain the output as a function of input. Input corresponding waveforms are defined.

- In Chapter 7, the modulation parameters are revealed and associated by analog and digital modulations. The decision process performed by DWP is presented by Markov chain. A PAM information signal is encoded. The state transition and trellis diagrams are also presented. The noise is used to trigger

encoding process off, and SR is observed. The DWP is designed to transform information signal into pulse position modulated signal.

Chapter 2

Systems with Stochastic Resonance

The first experimental observation of SR in a system with DWP was found in [13] which presented a significant SNR improvement for a bistable optical device: the bidirectional ring dye laser.

Misono et al. [14] demonstrated experimentally that a hybrid optical bistable system also experienced SR. In terms of optical signal processing, they preferred a hybrid system thanks to the capability of responding high speed signals. The system composed of an electro optic crystal with a $\lambda/4$ plate and a polariser, an avalanche photo diode (APD) converting the optical signal to electric signal and, finally, a comparator. The output of the APD was amplified and added to the bias of the crystal. This feedback made the system bistable. Then, SNR improvement peculiar to SR and the dependence of the noise correlation time on this improvement were observed in the case where the input was the output of the electro optic modulator driven by the sum of a sinusoidal signal and Gaussian coloured noise (This means that noise was added into the signal before it was transmitted). It was shown that the noise correlation time decreased output SNR. This system was served as a strong candidate SR device because of the advantages such as; low optical power

requirement and optical spectrum provided.

In [15], an experimental demonstration of an optical bistable system exhibiting SR was found. The sum of input signals, which are a binary pulse amplitude modulated (BPAM) signal and coloured noise, modulated the intensity of light, and it was received via a photo detector. Then, the results were examined in terms of Mutual information, and shown that SR depends on the noise cut-off frequency and bit rate.

SR phenomenon was also observed and demonstrated experimentally in; bistable SQUID loop [9, 16], Chua's circuit used for detection of a weak electromagnetic carrier signal [16], biological neural network, mammalian brain (suggested that a mechanism for amplification of weak electric field effect on the brain) [17], human visual perception [18], semiconductor laser with optical feedback [19], detection of pressure change on the sole of the human feet [20], microcavity polaritons under bistable conditions [21], the sensitivity of cantilever to a weak excitation, enabling transition between two states [22], detection of sub-threshold signals with carbon nano-tubes transistor [23].

These studies already exemplify the variety of noise, input signal, receiver and transmitter components. While this diversity expand the potential areas of applications, the remaining theoretical studies corresponding to SR phenomenon indicate that SR has numerous roles such as weak signal detection, synchronization and coherence, phase resetting etc. Although there is considerable variety on both field and studies, depending on the system models, SR can be classified in two categories; dynamical SR and threshold SR [7, 8, 24]. In this chapter, the fundamental systems studied in SR field have been introduced, and then the theoretical studies targeting SR phenomenon and corresponding systems specifically as a signal processing tool have been reviewed in order to evaluate their potential applications in communication systems.

2.1 Dynamical Systems

The term SR was first used by Benzi et al. in 1981 [25]. It was attempted to clarify the relationship between the quaternary climate records and external and internal mechanisms. The model of the earth climate was considered to be a DE with two stable steady state solutions. The external mechanism was the effect of the averaged solar radiation on the global earth temperature. In addition, the external mechanism had a periodic input due to changes in ellipticity of earths orbit. However it could not cause the dramatic changes in climate by itself. Therefore, the internal mechanism such as geodynamical events must have a role and its effect was considered a random variable. It was shown that this stochastic internal force could increase the effect of the small external force (which is likely to cause dramatic climate changes) and this was called stochastic resonance (SR) [25, 26].

The analytical theory of SR was first described in [27]. According to the theory, the SR occurred when the system was a dynamical system whose response $x(t)$ was derived by Langevin equation and its input was a weak periodic signal $(A\cos\omega t)$.

$$dx = [x(a - x^2) + A\cos\omega t]dt + \varepsilon dW \tag{2.1}$$

where W is for Wiener process representing the integral of Gaussian white noise process with intensity ε. In such system, the power spectrum of the output shows a peak at the frequency for a certain noise power.

In SR field, the dynamical systems are presented mainly under two models; Langevin equation and Duffing oscillator equation. While the original Langevin equation describes Brownian motion, which is the random movement of a particle in fluid due to collisions with the molecules of the fluid [28], the Duffing equation describes the hardening spring effect observed in several mechanical problems. However, Duffing equation can be treated as the equation of motion of a particle of unit mass in the quartic double potential well, and the harmonic oscillator model can be

used to introduce the Duffing equation as follows [8].

2.1.1 Damped Oscillator

The damped harmonic oscillator that exhibits SR can be modelled by Langevin equation. It is used to describe the motion of a particle whose mass is m with an applied friction γ.

$$m\frac{d^2x(t)}{dt^2} + \gamma\frac{dx(t)}{dt} = -\frac{d}{dx}U(x) + \sqrt{D}\xi(t) \tag{2.2}$$

where $\sqrt{D}\xi(t)$ is associated with a noise term $n(t)$, and considered as a stochastic process having a Gaussian probability distribution with correlation function and variance (intensity of stochastic force) D .

$$\langle n(t)\rangle = 0, \text{ and } \langle n(t)n(s)\rangle = D\delta(t-s) \tag{2.3}$$

where $\langle . \rangle$ denotes an average [7].

When the particle is heavily damped, the inertial term $m\frac{d^2x(t)}{dt^2}$ can be ignored. From this point, the equation is rewritten as the stochastic over-damped harmonic oscillator equation which helps us to understand the dynamics of the Duffing equation [7].

$$\frac{dx}{dt} = -\frac{d}{dx}U(x) + n(t) \tag{2.4}$$

2.1.2 Duffing Oscillator

The Duffing equation, modelling some oscillators, is a non-linear second order DE

$$\frac{d^2x(t)}{dt^2} + d\frac{dx(t)}{dt} + \omega_0^2 x + \beta x^3 = f\sin(\omega t) + n(t) \tag{2.5}$$

where the sinusoid is supposed to be amplified, $x(t)$ the system output, and $n(t)$ is given by Eq. (2.3) [8]. In [29] where it was over-damped, it was called the *standard*

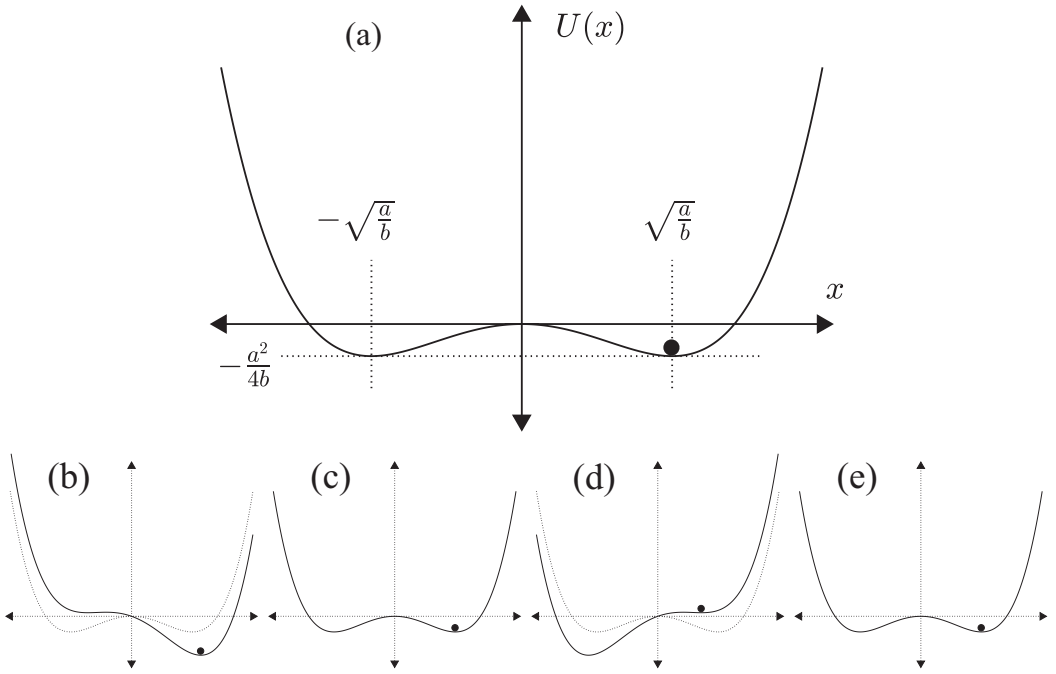

Figure 2.1: The representation of the two well potential or quartic potential (a) in Eq. (2.7) and the bending effect of the input signal disturbing the potential $U(x) + xA\sin(n\pi/2)$ where $a = 9$, $b = 1$, $A = 10$, $n = 1 - 4$ (b−e).

DWP system

$$\frac{dx(t)}{dt} = ax - bx^3 + A\sin(\omega t) + n(t) \tag{2.6}$$

where $a > 0, b > 0$.

2.1.3 Double Well Potential

In the case where $U(x)$ in Eq. (2.4) is a bistable potential given by Eq. (2.7), Eq. (2.6) is obtained. Therefore, the stochastic force denoted by $n(t)$ in Eq. (2.4) and $A\sin(\omega t) + n(t)$ in Eq. (2.6) can be considered as the system input.

$$U(x) = -\frac{a}{2}x^2 + \frac{b}{4}x^4 \tag{2.7}$$

When $a > 0$, $b > 0$, and $U(x)$ is plotted against x, the double well shape is obtained as in Fig. 2.1 and it becomes easy to comment on the system behaviour.

As can be seen in Fig. 2.1 (a), there are two minimums of the potential, $\pm\sqrt{a/b}$, and a barrier between them. In this case, the over-damped particle, staying in one of the minimums, can jump to the other minimum depending on the input signal and/or noise. If there is noise, not the signal, noise intensity play a role on the jumps. Therefore, increasing noise intensity makes the jumps occur more frequently. However, after a certain noise intensity, the frequency of the transitions does not increase at the same rate which occurs for smaller noise densities.

If there is signal, not the noise, the well potential is bended by the signal and the symmetry disappears as in Fig. 2.1 (b) and (d). Therefore, depending on the signal, one well becomes deeper than another. A transition or a jump can occur when the well, accommodating the particle, disappears; otherwise, the particle stays in the same well as in Fig. 2.1 (c) and (e). If there is signal with noise, the particle can exceed the barrier although the signal itself does not make the well disappear. This leads the output or the position of the particle to be likely to stay in the deeper well. This is where SR is observed; when the signal is weak, not to cause a transition, and the noise is present. In such conditions, at a certain noise intensity, output SNR has a peak as illustrated in Fig. 2.3 [7,30].

2.1.4 Other Potential Wells

There are also different bistable potentials in which the effect of SR has been observed; such as Hopfield neurons potential (x is the voltage of a cell membrane), SQUIDs loop potential (x is the magnetic field flux) [7,31], and a potential approximation for Schmitt trigger which is good example of a discrete two state system [30].

$$\begin{aligned} U(x) &= \alpha x^2 - \beta \ln(\cosh x), \\ &= \alpha x^2 - \beta \cos(2\pi x), \\ &= \beta\Big(\tfrac{1}{2}x^2 - \tfrac{1}{A\gamma}\ln(\cosh(A\gamma x))\Big) \end{aligned} \tag{2.8}$$

There are a considerable number of dynamical system model, and any other SR models from a monostable system to chaotic systems can be found in [32].

2.2 Threshold Crossing Systems

Threshold systems was considered as a basic model for the bistable dynamical systems and a simple threshold system was given by

$$y = \begin{cases} 0, & \text{for } x < \frac{1}{2}, \\ 1, & \text{for } x > \frac{1}{2}, \end{cases} \tag{2.9}$$

where y is the output, and x the input, the threshold 1/2 [33]. Such basic system exhibited noise induced threshold crossing effect. Although this initially considered as a type of dithering, but not SR, this consideration evolved with time such that dithering became a type of SR [34].

The threshold crossing effect is illustrated in Fig. 2.2. A sinusoidal signal as an input is applied to a threshold system. If the input amplitude is always smaller than the threshold, the system output does not change. When a noise is introduced to the input, the threshold can be crossed, which 1 occurs at the output for an instant. An increase in the noise variance leads the system to get more 1s for the input closer to the threshold, and less 0s for the input far away from the threshold. Therefore, there is an optimum noise variance ensuring the consistency of the sinusoidal period and the numbers of 1s and 0s. This consistency has been observed at the frequency magnitudes obtained by the discrete Fourier transform (DFT). The same process, with smaller steps of noise variance, providing the magnitudes at the sinusoid's frequency results in a typical curve of SR as in Fig. 2.3. In addition to the threshold non-linearity, the noise induced signal amplification in a static non-linear system was shown in [35].

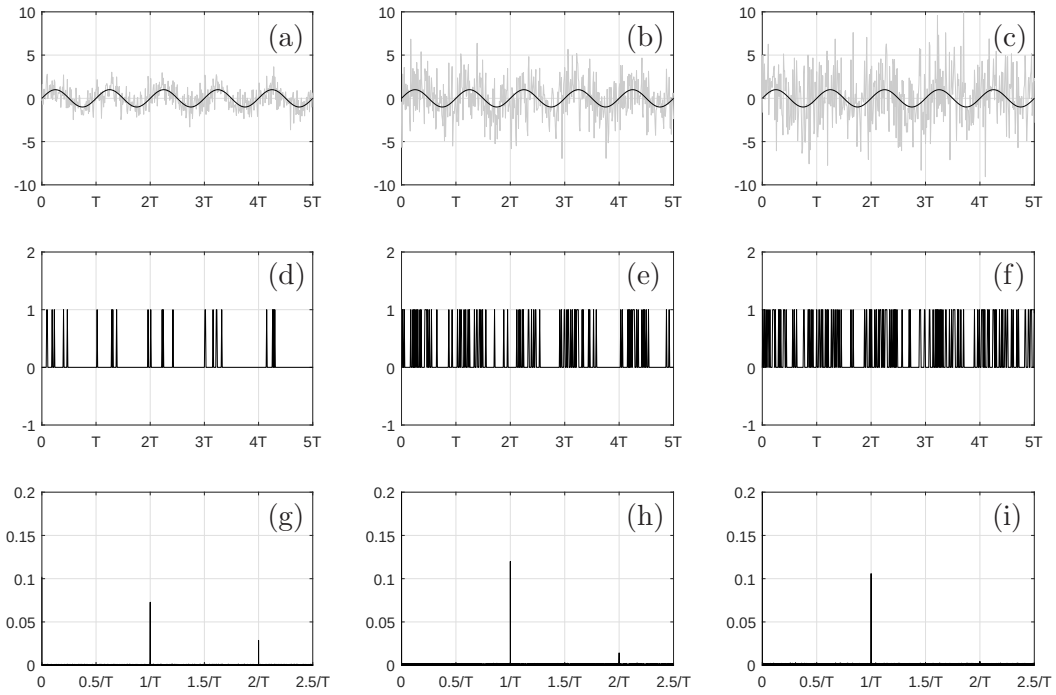

Figure 2.2: The illustration of the SR effect in a threshold device. The amplitude of input signal is 1 and threshold is 2. Figures on the first column are of input (black) with noise (gray) (a), output (d) and its frequency spectrum (g). The input is sampled at $t_s = T/100$ and the samples for noise follow $\mathcal{N}(\mu = 0, \sigma)$. For (a,b,c), σs are 1, 2, and 3 respectively.

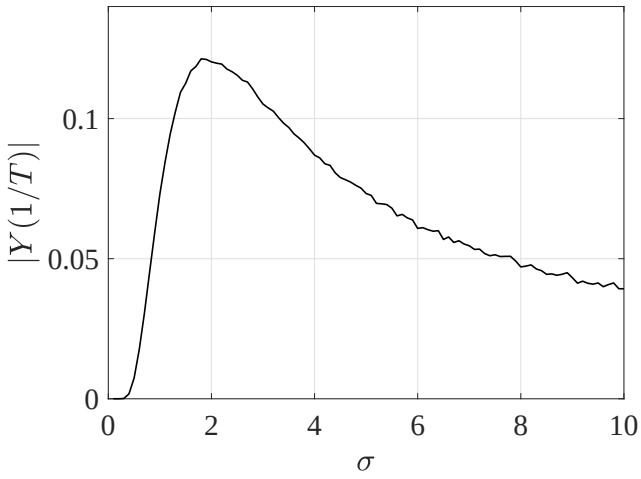

Figure 2.3: The magnitudes of $f = 1/T$ at the output, that provides the typical curve of SR

2.2.1 Array of Threshold Devices

In [36], a multi threshold system, similar to the analog-digital converter, was studied. A two-threshold system was defined by

$$y(t) = \begin{cases} -1, & \text{for} \quad x < -\frac{1}{2}, \\ 0, & \text{for} \quad -\frac{1}{2} < x < \frac{1}{2} \\ 1, & \text{for} \quad \frac{1}{2} < x \ , \end{cases} \tag{2.10}$$

where $x(t) = A\sin(\omega_0 t) + \xi(t)$. Where $A = 0.2$, the monitored SNR showed a curve like in Fig. 2.3 for a Gaussian noise. For a uniform noise, the peak SNR was higher than the other, and observed in a narrow noise power interval. Then the multi threshold system was examined in the similar way. The SNR tail corresponding to higher noise powers and peak SNRs were increased by the number of thresholds in coupling. It was concluded that the although SR like performance enhancement was observed, it was more adequate to associate this with dithering effect. However, it was shown that an array of threshold devices exhibited SR phenomenon and was able to recover the half of noiseless channel capacity, and furthermore, this was not limited by the signal being either deterministic or weak, thereby introducing the new term *supra-threshold SR* (SSR) [37–41].

2.2.2 Schmitt Trigger

The ideal Schmitt trigger circuit with the inputs; a sinusoid and noise, was also studied in SR field. Schmitt trigger was found to be applicable to examine the same SR phenomenon as in the case of the double well. In [30], a model of Schmitt trigger was given by

$$y = \text{sgn}(\gamma y - A\cos(\omega t) - n(t)) \tag{2.11}$$

where sgn is the sign function, γ the positive feedback constant, y the output. The theoretical derivation and simulation results indicated the presence of SR phe-

nomenon. Later, in [42], the Schmitt trigger was considered as a signal processing tool. As it simplifies the SR process by reducing the dynamics to just switching events, it was thought that the dependence of output SNR on input noise intensity would be easy to evaluate. Experimentally, SR was observed (also in [43]). However, the output SNR was always less than input SNR. It was indicated that SR process consisting of a single device is always lossy compared to standard spectral estimation techniques. In order to overcome this lack of SNR gain, an array of globally coupled devices was suggested. In addition to that, Schmitt trigger is limited to the switching events. However, with the focus of the system being dynamical (not the threshold one), a contribution in being able to provide the signal processing capability can have a significant impact on SR field.

2.3 Measure of SR

In [30], the essentials for SR were listed as a bistable system with a coherent signal and random noise and a output driven by internal dynamics of the system. The coherent frequency and intensity of the sinusoidal input were extended in [44, 45]. Gammaitoni et al. [26] gave the basic requirements of a SR effect. These were an energetic activation barrier (threshold), a weak coherent input (sub-threshold) and a source of noise. In contrast, Stocks [38] proved a new term supra-threshold SR which did not require the signal being sub-threshold. On the other hand, Mitaim and Kosko [32] stated that there was not any theorem answering which systems have a nonzero noise optimum although SR effect was observed in a large variety of systems from chemical and biological to electrical and magnetic systems.

Reasonably, the consequence of this variety led the performance measure of SR to be different from SNR to measures such as cross-correlation, mutual information [46], probability of residence time depending on the system and input signal. For example, when the signal is aperiodic or contains information, one may want

to know if the output corresponds with input signal or information in it. Then, cross-correlation or mutual information can be used instead of SNR [47]. Therefore, the essential measurements in the field of SR are presented below.

2.3.1 The First Assessment: Mean Exit Time

In [25], the output driven by Eq. (2.1) without a sinusoidal, jumps from one well to another after a random time τ. The mean exit (jump) time $E[\tau]$ is defined as the expected time duration the particle (output) stays in a well, or after how long the particle jumps.

$$E[\tau] \cong \frac{\pi}{a\sqrt{2}} \exp\Big(\frac{a^2}{2\varepsilon^2}\Big) \tag{2.12a}$$

$$Var(\tau) \cong \frac{\pi^2}{a^2} \exp\Big(\frac{a^2}{\varepsilon^2}\Big) \tag{2.12b}$$

When a weak sinusoid with A, small compare with $a^{3/2}$, is applied, the noise intensity ε can make the output $x(t)$ jumps following the weak sinusoid, and the output power spectrum shows a peak at the sinusoid's frequency, if ε is between the interval $\varepsilon_1 < \varepsilon < \varepsilon_2$.

$$\varepsilon_1 = a\left(\frac{1 - 4A/a^{3/2}}{2\ln(2\sqrt{2}a/\Omega)}\right)^{1/2} \tag{2.13a}$$

$$\varepsilon_2 = a\left(\frac{1 + 4A/a^{3/2}}{2\ln(2\sqrt{2}a/\Omega)}\right)^{1/2} \tag{2.13b}$$

2.3.2 Kramers Rate Theory

Kramers model for a chemical reaction defines the states of reactant and product as stable states of a particle in one dimensional asymmetric DWP. While the remaining degree of freedom for the reaction is considered as a fluctuating force $\xi(t)$, the particle

moves according to Newton's equation of motion in the form of a Langevin equation;

$$M\ddot{x} = -U'(x) - \gamma M\dot{x} + \xi(t) \tag{2.14}$$

where M is the mass, x reaction coordinates, $-M\gamma\dot{x}$ a linear damping force, and γ constant damping rate [48]. For moderate to strong friction, the escape rate from one well to another is given by

$$k_{A\to C} = \frac{\lambda_+}{\omega_b}\left(\frac{\omega_0}{2\pi}\exp(-\beta E_b)\right) \tag{2.15}$$

where E_b is the activation (barrier) energy $U(x_a) - U(x_b)$, x_a, x_b the stable states, $\omega_b^2 = -M^{-1}U''(x_b)$, a coefficient $\lambda_+ = -\gamma/2 + \sqrt{\omega_b^2 + \gamma^2/4}$. The inverse of this rate, $1/k_{A\to C}$, is given equal to average escape time τ_e. [48]. As found in [30], the system driven by Eq. (2.4) and Eq. (2.7), the mean first passage time (MFPT) was given by the Kramers time:

$$\tau = \frac{\sqrt{2}\pi}{a}\exp\left(2\frac{a^2/4b}{D}\right), \tag{2.16}$$

Similar to that, the first passage time density can be found in [49].

2.3.3 Signal to Noise Ratio

In [30], SR was defined as an increase in the output signal-to-noise-ratio (SNR) with increased input noise. Although the output signal was examined in the first study [25], the criteria of SR switched to SNR [16]. It was thought that using SNR as an indicator would be better due to the fact that the signal was periodic. This simplified the definition and made easy to evaluate this phenomenon.

Unfortunately, the evaluation of stochastic differential equations (SDEs) of these non-linear dynamical systems varies significantly depending on the nature behind them [50–52], and even for noiseless ones, deriving a solution requires mod-

ifications and approximations on the models [53, 54]. However, in the SR context, there is common treatment as follows.

Whether the signal is present or not, the Fokker-Planck equation (FPE) is generally used to evaluate Eq. (2.4). For example, in [55], the periodically forced FPE in a bistable potential was used to drive approximations for SR and SNR enhancement. That is

$$\frac{\partial P(x,t)}{\partial t} = -\frac{\partial}{\partial x}[C(x) + \epsilon h(x)\cos(\Omega t + \theta)]P(x,t) + D\left[\frac{\partial^2}{\partial x^2}\right]P(x,t) \tag{2.17}$$

where $C(x)$ is the drift term in the absence of forcing, D the diffusion coefficient, $\epsilon h(x)$ the forcing amplitude, respectively. In the same work, a systematic way to solve this equation was also presented. An evaluation of FPE's use was discussed in [29]. Then, the Kramers rate gives an approximate mean switching rate. However, this is a restricted solution and it is valid for the conditions where the system dynamics are one dimensional, stationary, and infinitely damped.

To make the solution more general in terms of various types of signal and noise, some approximations, such as adiabatic and reduced dynamics, must be made [31]. For example, applying these approximations, McNamara and Wiesenfeld [30] derived the output SNR denoted by R and the power spectrum of the output noise N (which is called Lorentzian shape) from Eq. (2.4) and Eq. (2.7);

$$R \approx \frac{\sqrt{2}aA^2c^2}{D^2}e^{-2U_0/D}, \tag{2.18}$$

$$N \sim \frac{2\alpha_0}{\alpha_0^2 + \Omega^2} \tag{2.19}$$

where $U_0 = a^2/4b$, $c = \sqrt{a/b}$, $\alpha_0 = \frac{\sqrt{2}a}{\pi}e^{-2U_0/D}$, and A is the sinusoidal signal amplitude. Furthermore, such expressions for asymmetric potential well were found in [56].

An alternative derivation was found in [57]. A theory of SR for weakly

damped Eq. (2.5) was presented where $d = 2$, $\omega_0^2 = -1$, $\beta = 1$, and $f = A$. Due to the weak signal approximation, the output was considered to have two part one was the response of a deterministic system to the input sinusoid and the other was the effect of noise on that deterministic system parameters. Then, the system output was written by $x(t) = s(t) + n(t)$ where $s(t) = \langle x(t) \rangle$ and n was the deviation from this mean. As a result, the non-linear system response was derived from the response of an effective linear deterministic system.

2.3.4 Mutual Information

In [46], an information theoretical aspect, the Mutual Information (MI) was suggested as a measure for SR phenomenon. The relation between an input (transmitted) signal and output (received) one was examined based on the transferred information. Defining a communication channel with the random input $x = \{-1, 1\}$ corrupted by a noise n, the output was given by a threshold function, $y = \theta(x + n)$, such that if $(x + n) > Q$ the threshold, then output is 1, otherwise $y = -1$. Where the probabilities P_y and $P_{\bar{y}} = 1 - P_y$ were for $y = 1$ and -1, respectively, the entropy of Y, $H(Y)$, conditional entropy of Y given X, and mutual information $I(X, Y)$ were given by

$$H(Y) = -P_y \log_2 P_y - P_{\bar{y}} \log_2 P_{\bar{y}} \tag{2.20}$$

$$\begin{aligned} H(Y|X) \quad &= P_x \Big(- P_{y|x} \log_2 P_{y|x} - P_{\bar{y}|x} \log_2 P_{\bar{y}|x} \Big) \\ &\quad + P_{\bar{x}} \Big(- P_{y|\bar{x}} \log_2 P_{y|\bar{x}} - P_{\bar{y}|\bar{x}} \log_2 P_{\bar{y}|\bar{x}} \Big) \end{aligned} \tag{2.21}$$

$$I(X, Y) = H(Y) - H(Y|X) \tag{2.22}$$

Then, the computed mutual informations for various thresholds and noise variances were illustrated. The SR-like effect was observed in any case except for the optimum thresholded one.

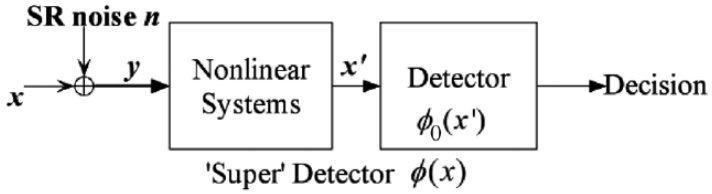

Figure 2.4: The generalized SR detection system [58].

2.4 Theoretical Studies

A mathematical theory which generalized the SR to the detection theory for fixed detectors was derived in [58]. It was stated that the performance improvement could be examined for any SR detectors in the literature by using this theory. Instead of SNR, the probabilities of detection and false alarm were considered to be the detection performance measure. They also gave an example illustrating the form of optimal noise pdf and the comparison between sign detectors performances where the input noises were Gaussian, uniform and optimal symmetric. Based on the theory, SR detection system was illustrated as in Fig. 2.4 in [58]. Additionally, the theory for variable detectors can be found in [59].

In [60], Eq. (2.6) was considered as a non-linear receiver by replacing the sine term with a BPAM signal. FPK equation was used to derive the probability density function (pdf) of the system output for BPAM levels, and the system parameters were normalized to provide more general solution. In addition to that, the time dependant variation of pdf was approximately expressed. Based on derived pdf and normalization, system parameters were adjusted for better performance, which was called the *parameter-induced SR* (PSR) method. The simulation results were presented to illustrate the performance enhancement. More importantly, it was stated that the non-linear receiver filtered the noise. For the same model, in [61], an adaptive parameter search method was applied to determine optimum b parameter resulting in better BER performance while the other variables were fixed.

Liu et al. [62] was also applied PSR method. As stated before, when the input noise intensity is over the optimum one, adding noise becomes useless. In the study, a BPAM input signal was first detected by proposed PSR which was based on the classical dynamical bistable system Eq. (2.6) in a form of

$$\frac{dy}{d\tau} = y - y^3 + \sqrt{\frac{b}{a^3}} A \sum_{i=1}^{+\infty} S_i G(\tau - iaT) + \sqrt{\frac{b}{a^3}} \sqrt{2D} n(\tau) \tag{2.23}$$

Then, the classical sign detector with LRT decoder provided the output signal. This time, PSR was based on tuning the parameters a and b related to the properties of signal and noise. The performance measure of the system was considered to be BER. The comparison between the performances with and without the PSR was indicated that the implementation of PSR based non-linear system enhanced the BER for the fixed optimum receiver. In addition to BPAM, in [63], another algorithm based on PSR was presented to detect binary phase shift keying (PSK) signals. However, PSR method presented in [60–63] are not applicable if the noise type, the resonant signal, changes.

2.5 Signal Processing Aspect

The earliest consideration of SR as a tool for signal processing was based on the amplification (gain) for detection. Although the use of only one system, called *resonator*, was not preferred due to the 2 dB loss at input-output SNR, an array configuration was suggested for achieving an SNR gain obtained with linear signal processing techniques [42]. Despite the SNR loss of a single resonator, SR is a bona fide resonance as it occurs any time when the stochastic switching rate matches the deterministic one [64]. Owing to this resonance property, and the observations and models from natural phenomena, SR was considered to be a common phenomenon, at first, in sensory biology [16, 65], then, in other fields.

Of particular interest to researchers, and a subject that has been studied

extensively in the literature, is that of DWP. As it has been shown that this system can exploit the background noise to improve the SNR [7,40,66,67], DWP is effectively implemented as signal processing block sets within the receiver architecture to take advantage of the its behaviours. Examples of implementation have been shown for binary PSK [63],FSK [68], minimum shift keying (MSK) [69], and BPAM [60–62, 70, 71]. Upon implementation, these block sets are more generically referred to as a *stochastic resonator*.

In terms of communication system but not in SR context, the use of non-linear dynamical systems was found under the name of chaos based communication and signal processing [72]. While chaos was defined noise like behaviour (deterministic noise), SR and noise induced performance improvement was only mentioned for the amplification property of Chua circuit and its potential SNR gain. Therefore, studies found in literature related to SR have been reviewed and classified as follows.

2.5.1 Amplification and Filtering

Non-linear and dynamical behaviours of SR systems can be used to amplify and filter communication signals.

In [73], the interaction between sinusoidal signal and noise in Eq. (2.6) was examined, and considered as stochastic filtration. Later, in [70], BPAM signal was applied to the same system instead of the sinusoidal, the comparison of error probability and filtering performance between the non-linear filter and matched filter was presented. Although the performance of non-linear one was not better than the other, it was found less sensitive to synchronization.

Referring to the energy transfer mechanism from high frequency area to low frequency area, a low pass filter configuration was demonstrated, and then, results were compared with a low pass Butterworth filter in [74]. Although the design and both filtering characteristics were not clear, a realization circuit for Eq. (2.6) was illustrated.

In [29], Eq. (2.6) was studied, and the relation between periodic input signal amplitude and frequency was presented. It was shown that the peak amplification factor was increased by the frequency. The maximum amplification was obtained where the frequency was smaller than $\exp(-\Delta U/D)$ (adiabatic limit) and the noise was absent. In addition, the maximum power amplification decreased by an increase in signal amplitude (strength). It was also mentioned that the system exhibited a power transfer amongst input sinusoidal, noise, and stochastic output. This energy transfer was considered in [75] not for amplification but for noise power extraction. A bistable oscillator, an inverted pendulum, was proposed to extract energy from ambient wide spectrum vibration, and Duffing oscillator was used to evaluate the design and results.

2.5.2 Detection

Threshold systems, although they are not dynamical but non-linear, can be examined in order to evaluate the detection capability of non-linear dynamical systems with SR as follows.

In [76], it was reported that the crossing detector (CD) was able to detect the input signal as low as 1/4 of the threshold. The SR effect was observed and the dependence of the signal frequency on the output SNR was identified. In addition, it was stated that faster comparator and longer output observation could lead to have better detection performance.

Comte and Morfu [77] proposed a receiver called stochastic resonator receiver. The digital input signal was considered to be in three case; not modulated, Amplitude Modulation (AM), and Frequency Shift Keying (FSK). The measure was the percentage of correctly interpreted bytes. It was experimentally shown that a sub-threshold digital signal could be retrieved by this receiver. They concluded that this was an alternative detection technique compared to the classical receiver based on amplification and filtering, especially for low power or long distance transmission.

Unfortunately, neither a theoretical explanation nor a comparison between classical receiver and proposed one was given.

In [78], the SR effect in linear sensors was studied. Although sensors are designed to have a linear input-output function, this linearity is always limited. When the input exceeds these limits, which is called saturation, the output experiences a strong distortion. According to the study, this distortion can be reduced by the help of SR effect. A parallel array of sensors was considered to be a SR structure. Sensors were modelled by soft and hard-limiting function. It was demonstrated that adding independent and identical distributed (i.i.d.) noises to every sensors improved the output SNR in both saturation cases; strong signal with and without Direct Current (DC) offset.

In terms of the effect of the multiplicative noise on SR, Guo and Tan [79] derived the mutual information of the Supra-threshold SR system. They also provided a comparison between the effects of multiplicative and additive noise intensities on the system performance. It was claimed that using additive noise intensity in order to tune SR was more effective rather than using multiplicative one. They also emphasized the importance of the proper threshold choice. In the study, where the multiplicative noise was injected into the system seems more realistic than in [80].

Zozor and Amblard [81] stated that when the performance of the detector was considered, SNR gain was more important than the maximum output SNR. The idea is that if the resonators SNR gain is lower than 1, the performance of a detector, which is placed after the resonator, cannot be improved. Thus, the aim is to make the gain greater than 1 at the optimum noise intensity which maximizes output SNR. From this point of view, it was demonstrated that the performance of some locally optimal detectors (LOD) using likelihood ratio test (LRT) can be improved by using SR unless the parameters of the detector are well-tuned.

2.5.3 Modulation and Synchronization

In [82], it was stated that chaotic systems could be used to design and generate signals for communication systems as resulting chaotic signals were broadband, difficult to predict, like noise. Additionally, it is also mentioned that some of these systems had self-synchronization property. Therefore, the Lorenz system was designed and used to create transmitted signal $u(t)$ and to recover the received signal u_r.

$$\begin{array}{lll} \text{Transmitter} & & \text{Receiver} \\ \dot{u} &= \sigma(v-u) & \dot{u}_r &= \sigma(v_r-u_r) \\ \dot{v} &= ru-v-20uw & \dot{v}_r &= ru-v_r-20uw_r \\ \dot{w} &= 5uv-bw & \dot{w}_r &= 5uv_r-bw_r \end{array} \tag{2.24}$$

These two systems were masking the information signal $m(t)$ and provide synchronization between transmitter and receiver by transmitting $s(t) = u(t) + m(t)$ and recovering $\hat{m}(t)$ from $s(t)$. Moreover the corresponding circuitry and test results were also provided in the same study.

The importance of synchronization in digital communications was pointed out in [83], and chaotic modulation and synchronization were suggested as alternative schemes for the poor propagation conditions. Then chaotic modulation schemes (chaos shift keying (CSK), differential CSK, chaotic on-off keying (COOK)) within different detection techniques were examined in the context of synchronization and noisy band limited channels [84].

An experimental demonstration based on the non-linear Fourier transform and non-linear frequency division multiplexing [85] was found in [86]. Although the non-linear processes were applied to the transmitted and received signals, SR was not mentioned.

2.5.4 Spectrum Sensing

In [87], a spectrum sensing method based on noise enhanced detection was proposed to improve detection performance of the receivers in cognitive radio networks. The energy detector (non-linear system) sensing was considered due to its low complexity, and, before the detector, a noise was added to the received signal. The probability of detection was derived based on binary hypothesis, and the improvement on the detection performance was presented.

2.5.5 Quantization: Encoding

In [88], it was stated that the dithered conventional quantizing system exhibited SR effect because of the statistical modification caused by dither. In [7, 89], the array of threshold devices was examined where the input was a supra-threshold random signal and each threshold experienced the same input but affected by independent noises. The presence of *bifurcation*, quantization, was shown. Its effect was modelled as a stochastic quantization and optimized by Fisher information.

This configuration was also associated with encoding as the threshold array maps each input value into a discrete output value. Considering that an output of a threshold device is a Bernoulli trial, then the array's sum can be defined as a random variable with Binomial distribution. This process, as well as the decoding of SSR output, was examined extensively in [7]. Furthermore, SSR encoding was studied also with a different threshold device(neuron) model, namely Integrate-and-Fire [90].

2.6 Performance Improvements of SR system

The systems with SR, regardless being dynamical or threshold, have various performance criteria. Depending on input signal, noise, purpose, available treatment etc. the performance improvement method and evaluation vary considerably. For instance, considering a sine wave is applied to the dynamical system to be amplified,

the gain and SNR can be chosen as criteria. In such case, mutual information is not required as a sinusoidal does not contain any information. However, if an information signal is introduced to the system, SNR can not be sufficient indicator. As the system is mixing the signal and noise, which causes intermodulation, the output is going to have information buried frequency components out of the band of interest. Therefore, previous studies targeting performance improvements of systems with SR has been reviewed and presented as follows.

In [91], SR was observed in a two dimensional potential with and without external signal, where the noise-induced frequency shift, coherent motion, and output SNR were examined. The results were obtained from the simulation of system's Langevin equations by Euler forward method.

The detection performance of Schmitt trigger model was improved by a threshold controlling scheme, proposed in [92]. Where the input was a weak sinusoidal and noise, the Schmitt trigger's upper and lower thresholds were modulated by another sinusoidal. It was stated that the same improvement was also applicable to a DWP system.

In [93], the FitzHugh-Nagumo (FHN) neuronal model, two dimensional limit-cycle oscillator, a simple representation for the firing dynamics of sensory neurons, was studied. It was shown that noise can benefit the non-linear system with weak aperiodic input signals as well as periodic ones. The term *aperiodic stochastic resonance* (ASR) was thereby introduced to the literature. In [94], a linearised FHN model was proposed, and owing to the linearisation, a transfer function was obtained by Laplace transform. The low-pass and high-pass filtering were associated with the membrane capacitance of the neuron model and recovery variable, respectively. The coloured noise was suggest instead of white noise in order to produce SR in real neural systems.

In [95], the over-damped DWP was considered, and the weak input signal was amplified by a high frequency sinusoidal instead of noise, which was called the

vibrational resonance VR. Although in that work, the relation amongst resonant amplitude, frequency, and signal parameters was obtained by calculation, the exact result can be found by assuming that the output of the double well is already a sinusoidal with an amplitude and the same frequency as the input. Then, the exact resonant signal is determined. In addition to the potential well, VR was found in an array of three level hard limiters [96].

Liu et al. [40] pointed out a different case where the input signal already had a destructive noise. This means that the system works optimally at the noise level, $D_m \neq 0$, however the input noise level is already higher than that, $D_j > D_m$. In such case, a noise injection increased overall noise level, thereby decreasing the performance. The suggestion was coupling N systems in parallel. It was shown that the more system was connected, the higher noise level was needed to obtain the optimum performance. This was already indicated by Stocks [38] in terms of mutual information.

Zhang and Xu [80] investigated the effects of system parameters, especially multiplicative noise intensity and the self-correlation times of multiplicative and additive noises. They stated that the multiplicative noise intensity did not have an effect on SR as significant as the additive one had. Then, they suggested that it was better to control SR by varying the multiplicative noise self-correlation time rather than the additive one. From the figures in [80], it can be found out that using multiplicative noise intensity may provide a maximum SNR slightly higher than using additive noise intensity. However, the multiplicative noise term was introduced to one of the system parameters, not to the input signal, which is contrary to what 'multiplicative noise' refers.

Shao and Chen [97] studied SR in time delayed bistable system, theoretically. The classical bistable system equation including a feedback was examined and the effective potential well function was derived. The feedback was the output signal

with a delay and strength;

$$\frac{d}{dt}x(t) = ax(t) - bx^3(t) + \epsilon x(t-\tau) + A\cos(\Omega t) + \sqrt{D}\xi(t). \tag{2.25}$$

The results indicate that the feedback intensity, ϵ, and time delay, τ, change the shape of bistable potential. While the feedback intensity is decreasing the maximum SNR, the effect of the time delay on the SNR depends on the feedback being negative or positive.

In [98], the chain of linearly coupled *stochastic resonator*s, typical over-damped oscillators, was used to improve output SNR. The performance enhancement of threshold-based neuron array for detection weak signals was demonstrated in [99]. The effects of white and colour noises were examined.

In [100], a piecewise non-linear potential derived by a sinusoid together with one additive and one multiplicative noise was studied. The approximate output SNR at the sinusoid frequency was derived, and it was shown that SNR curve, which is a function of the noise intensity, had a peak at non-zero noise. In addition to that, the effect of noise and signal properties on this peak was also presented. Similar to this study, the results for additive and multiplicative harmonic noise can be found in [101].

2.7 Conclusion

To sum up, for over three decades, the definition of SR has been extended. Today, SR is considered as noise induced performance improvement techniques. It can be observed and applied in many branches of science. For communication systems in terms of un-wanted signals, the initial aim is to suppress the noise, which is not always possible due to the non-linear and noisy nature of devices. Therefore, SR can be an alternative signal processing technique. It has been inferred that the DWP, given by Eq. (2.4) and Eq. (2.7), is the most prominent system in SR field.

Its signal processing applications were found mostly in amplification and detection, which is quite limited when compared with the threshold crossing systems. However, the DWP is supposed to be a more powerful tool owing to its non-linear internal dynamics. Therefore, DWP is examined as a signal processing technique throughout the following chapter.

Chapter 3

Resonance in Quartic Double Well Potential

3.1 Introduction

A Stochastic Resonator has been considered as an alternative signal processing tool because of its noise-induced performance enhancement ability. In this chapter, this resonator is used to detect bipolar BPAM signals. To clarify the relations amongst BPAM characteristics and the resonator parameters, steady states and transition time of the system are redefined. A precise and generalised resonator analysis is derived from these relations in order to identify the region in which the resonator benefits from noise. In addition to that, simple PSR designs are built based on this analysis in order to configure the resonator in the optimum region. Finally, Sine-induced SR based on using a periodic signal instead of noise is introduced to enhance the system performance and compared with noise-enhanced SR (NSR). It is shown that periodic SR provides a performance enhancement while it needs less power and does not require an adjustment relevant to the background noise. The results indicate that a resonator improves the receiver performance by eliminating noise if its parameters and BPAM characteristics are set accurately as given in PSR

designs, otherwise the resonator can benefit from either a noise as in NSR or a sine wave as proposed in this chapter. However, Sine-induced SR is superior to NSR in terms of output performance, power requirement and simplicity [102].

Existing methods at mitigating noise may be ineffective at low SNRs, whilst also being inapplicable at the nanoscale in terms of the signal processing and energy requirements [103]. SR, is an alternative signal detection technique [40,42], where, compared to removing noise, one uses noise to enhance the system performance. The SR term was first coined by Benzi *et al.* in 1981 [25,27] and since then, SR has been observed in numerous systems across many fields [24,26,47]. As more systems were seen to exhibit SR, several generalized theories on the subject have thus been presented [30, 58, 59], but essentially, SR means that the system performance is enhanced by the means of noise.

The performance of the systems exhibiting SR has a peak at a non-zero noise intensity. In the literature, there are two methods used to enhance the performance, namely, NSR, and PSR. In NSR, defining the type of resonant noise and its correlation time, the effectual intensity is determined [79, 80, 97]. If an adjustment is required, NSR needs the knowledge of the background noise, which can be obtained by adaptive search methods, and this makes the system more complex. Moreover, the power consumption of a noise source can be another problem. In PSR, the system parameters are determined for the optimum performance [62,63,81] and intrinsically differ from one type of input signals to another. Whilst there are many studies on weak periodic input signals, there is no basic and precise design methodology for a bipolar BPAM signal which is one of the fundamental communication signal. In addition to this, no research concerning the use of a deterministic (as supposed to noise) resonant signal could be found.

Therefore, in this chapter, the aim is to design a basic stochastic resonator for detecting BPAM signals and to subsequently increase the system performance by using a deterministic periodic resonant signal as supposed to noise. Since ex-

isting designs do not focus on the input signal, we define new parameters derived from the desired output and build a new stochastic resonator design based on the characteristic of the BPAM signal. The unique relation between the output and the system parameters is also clarified, and as a consequence, PSR methods are simplified. Then, a periodic signal is introduced as a resonant signal. It is found that the use of a periodic signal ensures a significant performance enhancement without tuning. To summarize, parameters defined to analyse the SR system with Langevin equation, a further performance enhancement in NSR by a sine wave, and simple designs for PSR are the key contributions of this chapter.

This chapter is organized as follows. In Sec. 3.2, the theory behind the stochastic resonator and its implementation is discussed and the method used to determine the design parameters explained and subsequently evaluated. The optimum configuration providing low BERs at low SNRs is also presented. Sec. 3.3 introduces the generalised analysis allowing the reader to identify any resonator configuration. Based on this analysis, simple PSR designs are also provided. In Sec. 3.4, the use of a resonator is taken further with the notion of using NSR and Sine-induced SR. Finally, the chapter is concluded in Sec. 3.5.

3.2 The Stochastic Resonator

The stochastic resonator, in this chapter, is a form of an over-damped Brownian motion in the symmetric quartic bistable potential [14, 31, 32, 66]. It is modelled as a feedback system in which the forward loop consists of an arbitrary amplifier with gain M followed by an integrator as shown in Fig. 3.1. The feedback loop consists of two amplifiers with gains a and b and two multipliers.

Defining the transmitted signal, $s(t)$, which is typically corrupted by an additive white Gaussian Noise (AWGN), $n(t)$, the input of the stochastic resonator,

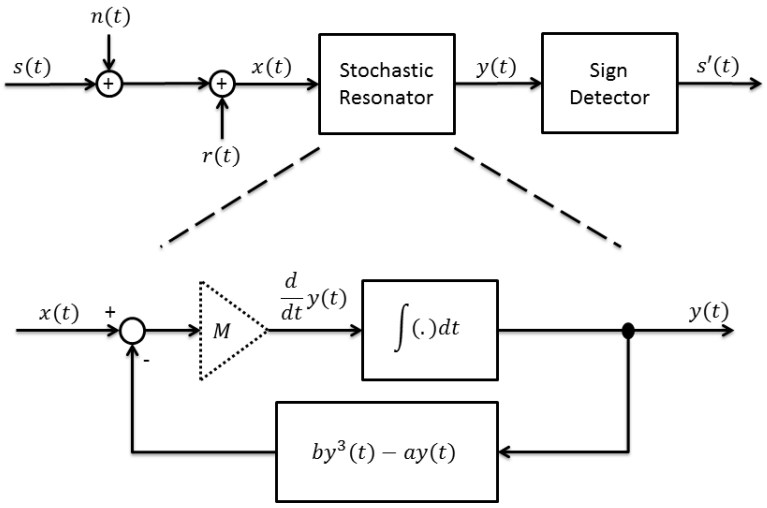

Figure 3.1: The BPAM receiver

$x(t)$, is given by

$$x(t) = s(t) + n(t) + r(t), \tag{3.1}$$

where $r(t)$ is an intentionally added resonant signal under the control of the system designer.

The integrator is based on the midpoint rule approximation which keeps the previous output, y_p, and the previous derivative, y'_p, in its memory. The output, $y(t)$ is thus

$$y(t) = y_p + \frac{y'_a + y'_p}{2} \times t_s, \tag{3.2}$$

where, to illustrate the system working as close to a continuous system as possible, $t_s = T_b/100$, and T_b is the bit interval of $s(t)$. Therefore, within this model there are three adjustable parameters, a, b and M, together with one controllable signal, $r(t)$, all of which will affect the output to the stochastic resonator, $y(t)$.

In order to achieve the aims of this work, the following process is required.

Firstly, in the absence of both $n(t)$ and $r(t)$, the steady state behaviour shall be analysed to determine the bounds of a and b. This is followed by incorporating knowledge of the systems transient behaviour such that a and b can be refined (if necessary) and M can be determined. The result of this section therefore is that, given some knowledge of $s(t)$, and still in the absence of $n(t)$ and $r(t)$, the system should operate without an error. It is then possible to begin the analysis into how $n(t)$ affects the performance and subsequently how $r(t)$ can be controlled to mitigate its effects.

3.2.1 Steady State Behaviours

Referring to Fig. 3.1, under the assumption that $M = 1$ for the duration of the steady state behaviour analysis, the resonator's output is derived from

$$\frac{dy}{dt} = ay - by^3 + x, \tag{3.3}$$

where $x(t)$ is only $s(t)$ and $s(t)$ follows a non-return-to-zero (NRZ) BPAM scheme, which can take only the values of either A or $-A$ during a bit interval T_b. In other words, it is assumed that the transmitter sends digital information by use of two rectangular pulses ($g_0(t) = -A, g_1(t) = A$). Each pulse is transmitted within the symbol interval of duration T_b ($0 < t \leq T_b$). Therefore, the transmitted signal is in the following form

$$s(t) = \sum_{i=1}^{+\infty} g_{B_i}(t - (i-1)T_b), \tag{3.4}$$

where B_i is a sequence of binary symbols. Each symbol is an identically distributed and independent random variable with $P(B_i = 1) = P(B_i = 0) = 0.5$.

The function of the detector is to decide which of two pulses was transmitted based on the sample taken at the end of each pulse. Therefore, the output bit

sequence can be given by

$$B_i^{out} = \begin{cases} 0 & , y(iT_b) < 0 \\ 1 & , y(iT_b) \geq 0 \end{cases} \tag{3.5}$$

For $s'(t) = sign(y(t))$ to have the same polarity as $s(t)$ does, a and b must be chosen carefully.

First of all, the resonator applies a barrier to the input. It can be calculated by determining the local maxima (or minima) of dy/dt where $x(t) = 0$, and be given by $h_b = \sqrt{4a^3/27b}$. $x(t)$ forces output to have the same signs when $A > h_b$. This is the first relationship between a, b and the magnitude of the input, A, for error free operation.

To explain this, consider Fig. 3.2. If $x(t) = A \geq h_b$, i.e a positive BPAM symbol greater than the barrier height, regardless of value of $y(t)$ at the same instant, $y(t)$ will settle to a positive value as required. If $x(t) = A < h_b$, i.e a positive BPAM symbol but with a magnitude lower than the barrier height, depending upon the value of $y(t)$ at the same instant, $y(t)$ may settle to the positive value, correctly, or the negative value incorrectly.

Secondly, it is needed to know exactly what $y(t)$ will be. Although making the barrier smaller than the input is enough for the polarity issue, later, it is going to be shown that the steady state matters when the bit interval is taken into account. By definition, the roots of Eq. (3.3) are the steady states, and there is only one real root if $A > h_b$. As is typical within any system that the output has a gain (or loss), k, the steady state can be given by kA where $x(t) = A$. If so, it must satisfy Eq. (3.3), which reduces to $0 = akA - bk^3A^3 + A$. Therefore, $A > h_b$ can be rearranged as $\sqrt{(ak+1)/(bk^3)} > \sqrt{(4a^3)/(27b)}$, which dictates that the parameter a times the gain k must be smaller than 3, $ak < 3$. And, the parameter b is determined by $(ak+1)/(A^2k^3)$.

As a result, the resonator parameters (a, b) are determined to make output

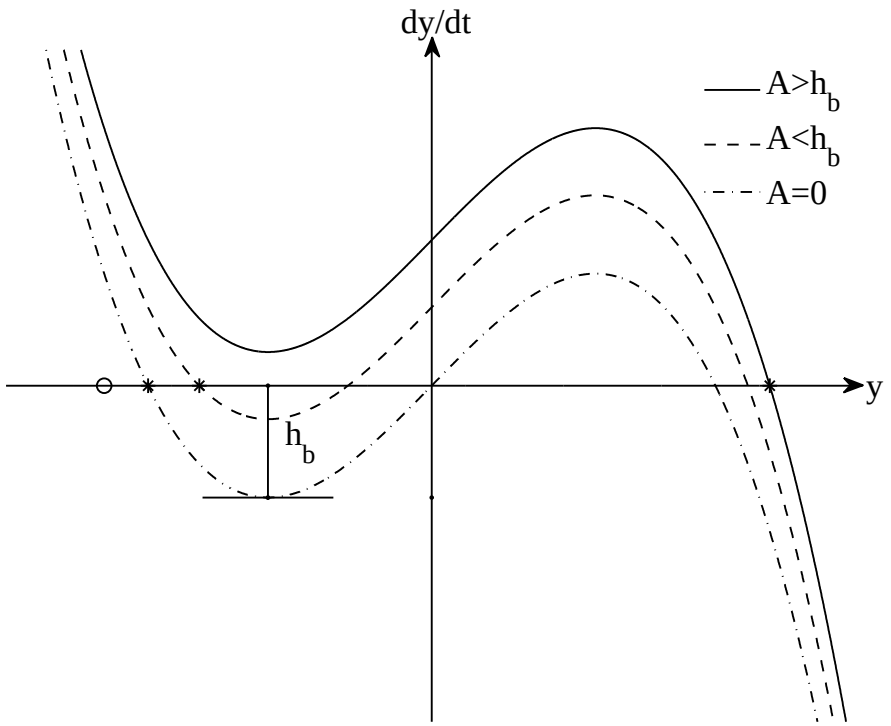

Figure 3.2: The derivatives of output where the output of the system is derived by the Langevin Equation, the noise is absent, and $x(t) = A$.

with a desired signs and gain, k. It is based on the steady states of Eq. (3.3) with the assumption of having a sufficient time for the output to become stable. However, the input is stable only for a period of time T_b, so the output may not reach the steady state within the same period.

3.2.2 Transient Behaviours

As has been discussed so far, upon an input change, the output $y(t)$ needs a finite time to transient from $-kA$ to kA when input $x(t) = A$. It is called the *transition time* t_r, and parameters (a, b) must be determined to satisfy $t_r < T_b$.

The transition time t_r can be derived from the integral of one over the derivative of output within the interval $[-kA, kA)$. Assuming that $y = -kA$ and $x(t) = -A$ at $t < 0$ and $x(t) = A$ for $t \geq 0$. In such case, $y(t)$ starts increasing

according to its derivative. Then, t_r is given by

$$t_r(y < kA) = \int_{-kA}^{y} \frac{dt}{dy} dy \tag{3.6}$$

It is preferred to use y as an upper boundary from which the transition shape can be obtained. In addition to that, the output never reaches kA theoretically. Due to the fact while y is getting closer to kA, dt/dy goes infinite. Therefore, the upper boundary should be smaller than kA so it is set to $y = 0.99 \times kA$ which means the system is working to a 1% steady state error.

To obtain the derivation of Eq. (3.6), the roots of Eq. (3.3) can be separated where $x = A$, and then, the right hand side can be rewritten as:

$$\frac{dy}{dt} = -b(y - kA)(y - r_1)(y - r_2), \tag{3.7}$$

where one root is kA and the $r_{1,2}$ is given by

$$r_{1,2} = kA\left(-\frac{1}{2} \pm i\sqrt{\frac{3}{4} - \frac{ak}{ak+1}} \right). \tag{3.8}$$

To be able to write down the expression for $t(y)$, p and q are introduced as

$$q = kA\sqrt{\frac{3}{4} - \frac{ak}{ak+1}}, \tag{3.9}$$

$$p = kA/2 \tag{3.10}$$

Such that, $r_{1,2} = -p \pm iq$. Thus, Eq. (3.6) becomes

$$t(y) = \frac{1}{-b} \int_{-kA}^{y} \left(\frac{D}{(y - kA)} + \frac{E}{(y - r_1)} + \frac{E}{(y - r_2)} \right) dy, \tag{3.11}$$

where,

$$D = \left((kA)^2\left(2 - \frac{ak}{ak+1}\right) + kA\right)^{-1}, \tag{3.12}$$

and

$$E, F = \frac{D}{2}\left(-1 \mp i\frac{1+p}{q}\right). \tag{3.13}$$

Finally, $t(y)$ is given by

$$\begin{aligned} t(y) = \frac{D}{-b}\Bigg\{ & \ln\left(\frac{y-2p}{-4p}\sqrt{\frac{p^2+q^2}{(y+p)^2+q^2}}\right) \\ & + \frac{2+p}{2q} \times \left(\arctan\left(\frac{q}{y+p}\right) + \arctan\left(\frac{q}{p}\right) + \pi u(y+p)\right)\Bigg\}, \end{aligned} \tag{3.14}$$

where $u(l) = 0$ while $l < 0$ otherwise 1 and where $-kA < y < kA$.

If variables D, p and q are represented by a function of ak and kA, and if b is written as $f_b(ak, Ak)/k$, then, Eq. (3.15) becomes $k \times f(ak, Ak)$. This can be simplified as $t_r = kt_n(ak, kA)$ where t_n is the normalized transition time, as a function of ak and kA. Fig. 3.3 illustrates the effects of kA and ak on t_n, and it is obvious that t_n goes to infinity while ak is getting closer to 3. Another point to note is that the effect of kA on the normalized transition length is not significant when compared to ak.

As the input signal has a bit interval, T_b, kt_n must be smaller than T_b in order the output to transient and settle down before the following bit comes, such that $kt_n < T_b$. Additionally, from Fig. 3.3, t_n is always greater than 2, which result in $2 < t_n < T_b/k$. However, the relation between k and the bit interval T_b causes an attenuation problem because k has been used for determining output steady state. For example, if the receiver is designed for BPAM signal with $T_b = 1$ ns, then k has to be smaller than 5×10^{-10}. Such attenuation is not practical.

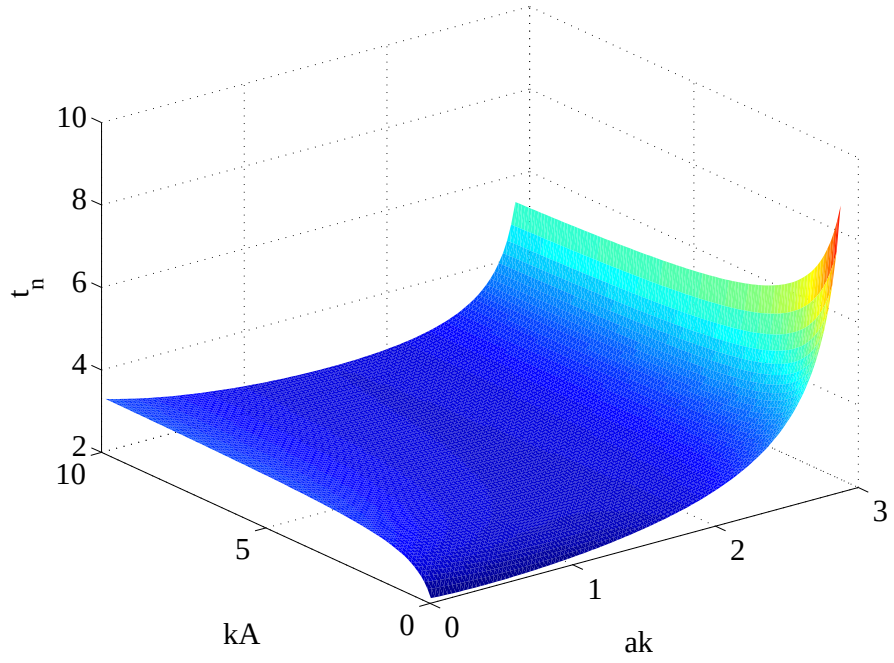

Figure 3.3: The effects of ak and kA on the normalize transition time, $t_n(y)$.

The attenuation problem can be solved by the parameter M in Fig. 3.1. Considering that t_r has k multiplier, the derivative of the output must have $1/k$ multiplier, and it does, which is obvious when Eq. (3.3) is re-written as

$$\frac{dy}{dt} = M\frac{1}{k}\left(aky - \frac{ak+1}{(kA)^2}y^3 + kA\right). \tag{3.15}$$

In Eq. (3.15), M is introduced to eliminate the effect of k on t_r and to have a control on the frequency response. It can be given by

$$M = m \times \frac{k}{T_b}, \tag{3.16}$$

where m is related to the normalized transition time t_n. That must be greater than t_n but does not have to equal to t_n so it is preferred to use different notations.

As a result, the new parameters used to define the resonator are kA for output steady state, ak for barrier height, and m for frequency response. A resonator can

be analysed and designed by only two of them as shown next.

3.2.3 Parameter Choices

The choice of parameters is critically important for the output performance of the resonator. First, an example with significant parameters is illustrated and then the optimum values based on the output performance is obtained.

The example is a resonator design with the parameters $ak = 1.5$ and $m = 3$. Given the input characteristics and desired output;

$$T_b = 10^{-9}\text{s},\ A = 1,\ y_{\text{desired}} = 1,$$

The design thus has the variables;

$$\begin{aligned} k &= y_{\text{desired}}/A = 1, \\ a &= ak/k = 1.5, \\ b &= (ak+1)/(A^2k^3) = 2.5, \\ M &= (mk)/(T_b) = 3 \times 10^9. \end{aligned}$$

The output of the stochastic resonator with these parameters can complete the transition in a bit interval time as illustrated in Fig. 3.4 (a) so that it can follow the input sign. When m is set to 1 which is smaller than the minimum normalized transition time $t_n(ak = 1.5, kA = 1) \simeq 2.46$, a bit interval is not long enough to complete the transition as illustrated in Fig. 3.4 (b). When $ak \geq 3$, $h_b \geq A$ so that the output sticks in either positive or negative side. Fig. 3.4 (c) illustrates the case where $ak = 3$. It is clear that, because of the barrier height h_b, the output does not change its sign while the input has both negative and positive values. As a result, in terms of design, there are two significant parameters with simple inequalities $0 \leq ak < 3$ and $m \geq t_n(ak, kA)$. However, these inequalities do not specify the optimum values of the parameters where the background noise is present.

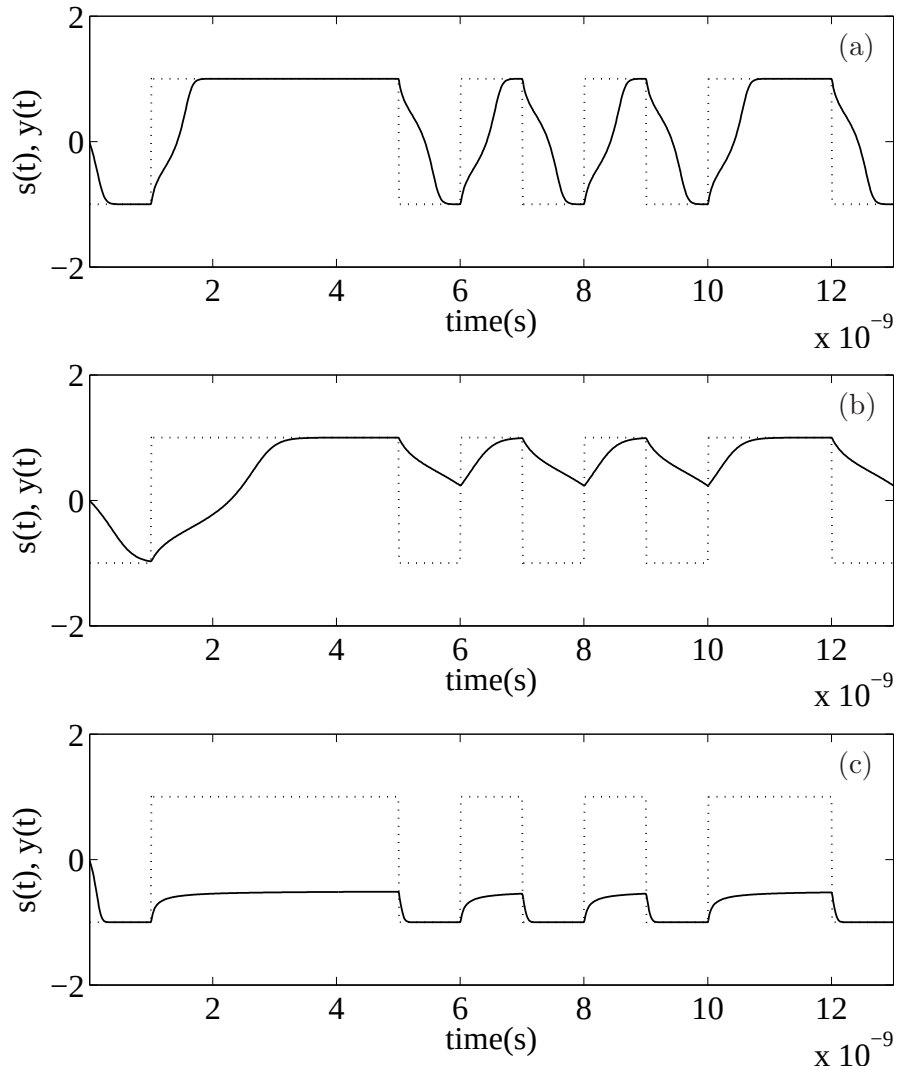

Figure 3.4: The output of stochastic resonators with (a) $ak = 1.5, m = 3$, (b) $ak = 1.5, m = 1$, and (c) $ak = 3, m = 3$ respectively. Note that $k = 1$, input is $s(t)$ with dash line, and output is $y(t)$ with solid line.

When the signal is weak, the presence of the background noise is supposed to increase the performance. This is valid for $ak \geq 3$. However, as Fig. 3.5, where SNR is $20\log_{10}(A/\sigma)$ and determined by $10\log_{10}(\sum(s[.]^2)/\sum(n[.]^2))$., indicates, if the signal is not weak ($ak < 3$), the background noise and the barrier h_b decrease the performance. Therefore, ak must be smaller than 1.

The other parameter m is directly related to the input signal frequency 1/Tb,

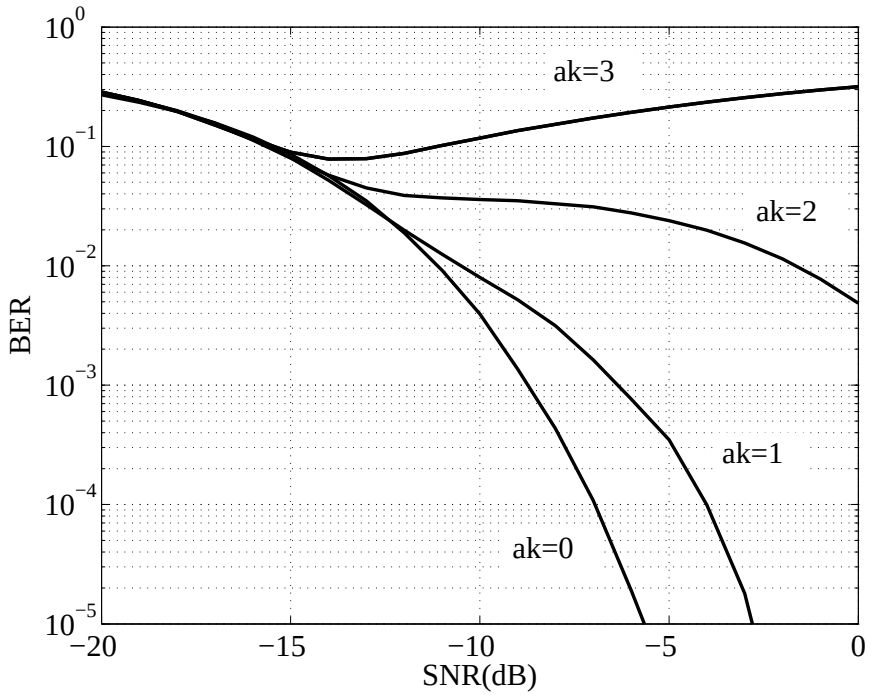

Figure 3.5: BERs where $m = 3$, $ak = \{0 : 3\}$, $x(t) = s(t) + n(t)$ and $n(t) \sim N(0, \sigma_n^2)$

and Fig. 3.6 indicates that $m = 3$ is almost optimum. When m is greater than that, the BER curve moves through the higher SNRs. When m is 2 and 1, the curve is shaped so that the BER slightly decreases at lower SNRs, but significantly increases at higher SNRs. Therefore, to have low BERs in general, m must be set to 3.

The stochastic resonator, whose output is given by Eq. (3.3), has been designed in a way different from those in the literature. It is based on the generalization of the parameters in terms of the signal characteristics. It provides a better understanding on the relations between the signal amplitude and the frequency response of the system. New parameters k, ak, kA, t_n, m and M are defined. It is emphasized that m and ak are the most significant parameters. They are used to determine the frequency response of the system and the barrier to the input signal amplitude. Finally, the optimum values of m and ak are specified by the means of the output performance. The application of this design on PSR method and further

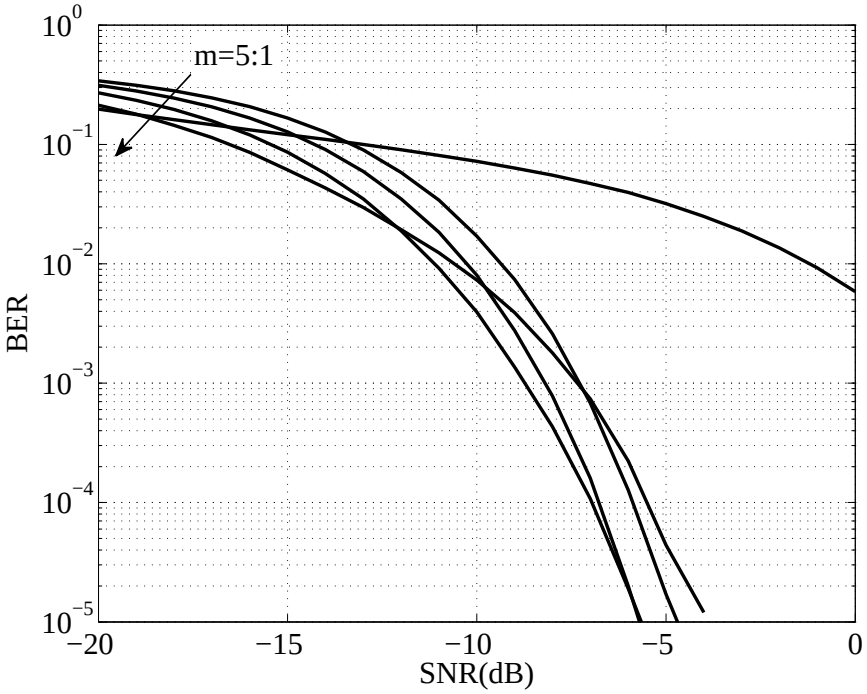

Figure 3.6: BERs where $ak = 0$, $m = 1:5$, $x(t) = s(t) + n(t)$ and $n(t) \sim N(0, \sigma_n^2)$

analysis are discussed in the next section.

3.3 Analysis and Design for PSR

The parameters defined in Sec 3.2 are used to analyse the stochastic resonator whose response depends on not only the bit interval but also the amplitude of the input signal. Although well-known transformations cannot be applied because of that, the new interchangeable parameters which represent those; a, b, M, A and T_b together help us to analyse and design the resonator.

Given a, b, M, A and T_b, parameters ak and m can be determined. First, to find out ak, the barrier obtained from Eq. (3.3) must be equal to the barrier derived by A and ak; $h_b = \sqrt{4a^3/27b} = \sqrt{4(ak)^3A^2/27(ak+1)}$. Then, ak and normalized

A can be given by

$$A = \sqrt{\frac{a^3(ak+1)}{b(ak)^3}} = \sqrt{\frac{a^3}{b}} A_n, \tag{3.17}$$

where

$$A_n = \sqrt{\frac{(ak+1)}{(ak)^3}}. \tag{3.18}$$

Secondly, to determine m and normalized T_b, ak in Eq. (3.18) and a are used in Eq. (3.16) as

$$m = MaT_b/ak = T_{bn}/ak, \tag{3.19}$$

where

$$T_{bn} = MaT_b. \tag{3.20}$$

These two normalizations have only one precise solution and bring out a fundamental analysis of a resonator. Fig. 3.7 is created by these normalizations. It can be used to determine m and ak parameters indicating the region in which resonator works. For example, if $A_n = 10$ and $T_{bn} = 100$, $ak \ll 1$ and $m \gg 3$. So the resonator works in the region where SR effect can not be observed ($ak \ll 1$), and BER is low at low SNRs ($m \gg 3$). Fig. 3.7 is more practical when compared to Eq. (3.18).

Similar to this analysis, PSR designs can also be simplified. Essentially, there are two possible tuning methods; the first one, PSR-1, is determining the optimum a, b, and M for a given A and T_b [60]. The second one, PSR-2, is determining the optimum input signal characteristics A and T_b where a, b, and M are given. The M parameter is set to 1 for the following designs to have more general expressions. As stated in Sec. 3.2.3, the variables for optimum BER performance must be chosen

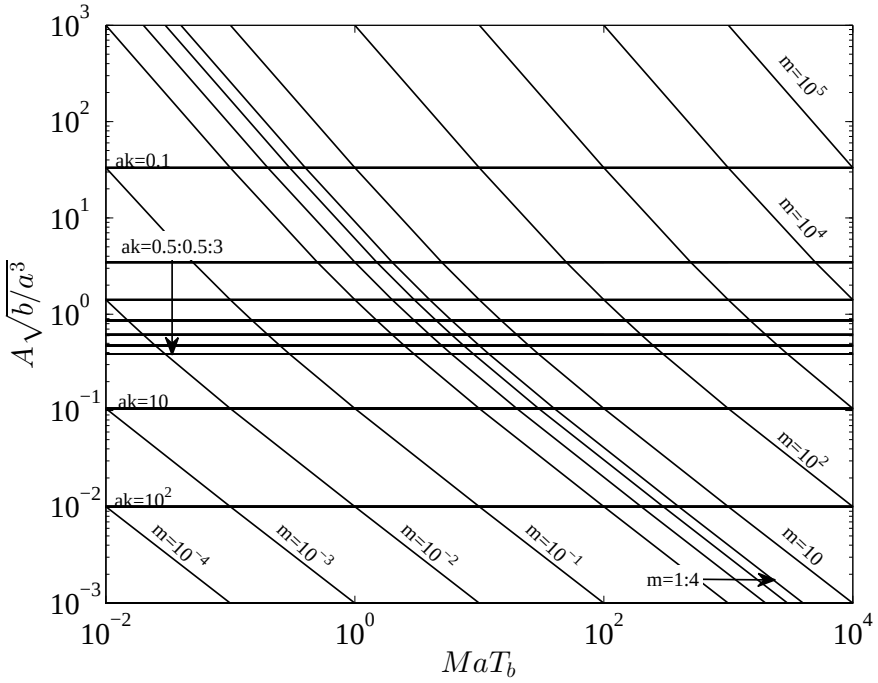

Figure 3.7: Normalized amplitude and bit interval with corresponding m and ak parameters

as $m = 3$ and $ak \ll 1$. For PSR-1, the resonator can be designed by

$$\begin{aligned} k &= T_b/m, \\ a &= ak/k, \\ b &= (ak+1)/(A^2k^3). \end{aligned} \tag{3.21}$$

For PSR-2, A and T_b are determined by Eq. (3.17) and Eq. (3.19) as

$$\begin{aligned} k &= ak/a, \\ T_b &= m \times k, \\ A &= \sqrt{\tfrac{a^3(ak+1)}{b(ak)^3}}. \end{aligned} \tag{3.22}$$

An analysis for a stochastic resonator and PSR designs have been given in this section. The analysis is based on determining m and ak by the normalized

amplitude and bit interval of the signal applied to the resonator. PSR methods are established in Eq. (3.21) and Eq. (3.22). Setting $m = 3$ and $ak \ll 1$ is sufficient to have an optimum BER performance for these designs. Although PSRs are simplified and provide significant performance improvement, they may not be applicable in some circumstances. When PSR is not available, another method, NSR, can be applied as discussed in Sec. 3.4.

3.4 NSR and Sine-induced SR

When the input signal, $s(t)$, is weak according to the system barriers, the output cannot transit. In this case, the resonant signal $r(t)$ can help the input to exceed the system barriers and improve the system performance. The resonant signal can be either a type of noise as in NSR method or a periodic wave as indicated in this section. These two resonant signals are going to be compared in terms of BER performances and power requirements.

NSR can be used when the parameters and the input characteristics are chosen to have a weak input signal. The PSR-1 design method of Sec. 3.3 is used to build the resonator to demonstrate an NSR application. Here, the input is a BPAM signal with $A = \sqrt{4/27}$ and $T_b = 9$. Critical parameters are set as $m = 3$ and $ak = 3$ to observe SR effect, and as a result, resonator parameters are $a = 1$ and $b = 1$. If there is only a BPAM signal at the input, the resonator output will show either positive or negative values depending on the first bit received as in Fig. 3.8 (a). When an AWGN resonant noise with an optimum power (BER is minimum at SNR, $20\log(A/\sigma) \cong -14$ dB in Fig. 3.5) is added to the input, the output starts to transient along with BPAM signal as shown in Fig. 3.8 (b).

However, with this method, NSR, suffers from some drawbacks. For instance, when background noise $n(t)$ is present, the resonant noise $r(t)$ has to be re-adjusted to have the optimum input SNR. Although it can be easily determined by $\sigma^2_{opt} =$

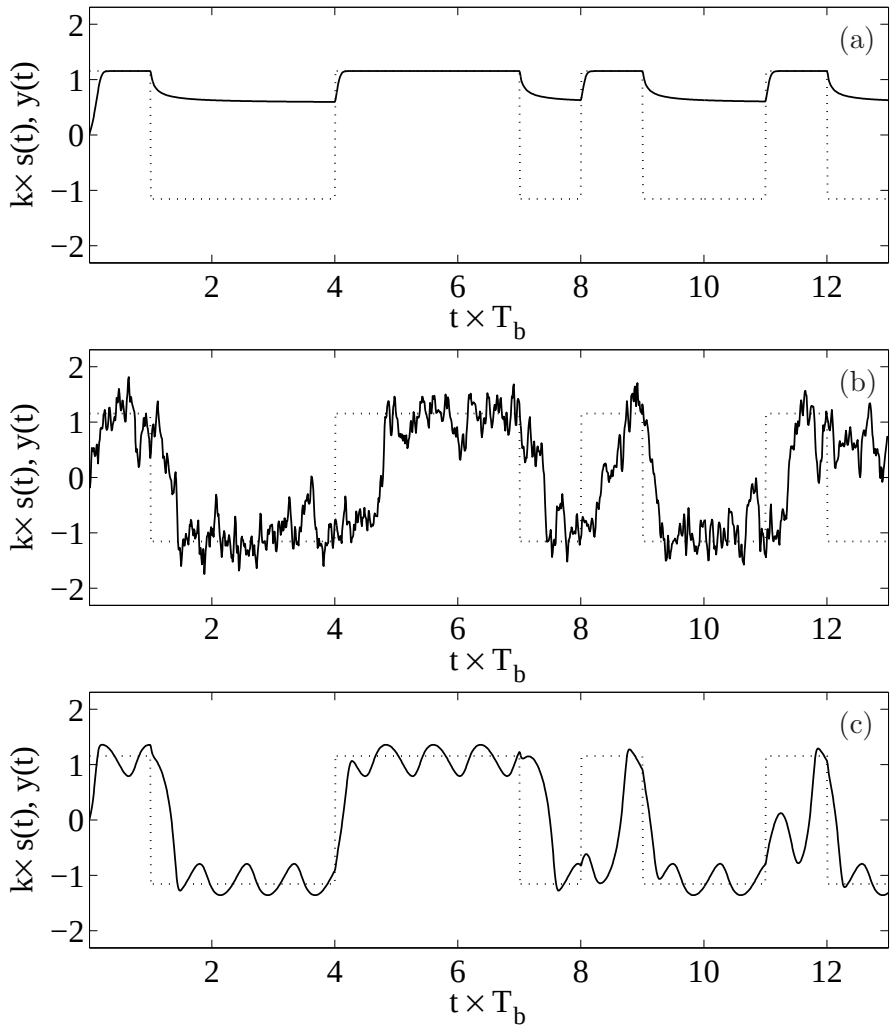

Figure 3.8: Outputs of the stochastic resonator with the parameters; $a = 1, b = 1$ and $s(t)$ is BPAM with $A = \sqrt{4/27}$ and $T_b = 9$. (a) $x(t) = s(t)$. (b) $x(t) = s(t)+r(t)$ where $r(t) \sim N(\mu = 0, \sigma_{opt} = 1.93)$. (c) $r(t) = 2A\sin(2\pi(1.3/T_b)t)$.

$\sigma^2_{n(t)}+\sigma^2_{r(t)}$, background noise power must be known. Even if $\sigma^2_{n(t)}$ can be measured, when $\sigma_{n(t)}$ is already higher than σ_{opt}, injecting any resonant noise $r(t)$ will cause a decrease in performance. Besides these drawbacks, as a source, resonant noise may demand high power, especially when background noise power is much less than the optimum one.

A periodic signal is suggested as an alternative to resonant noise. For the sake of simplicity, it is considered as a sine wave, $B\sin(2\pi ft)$, which can also help

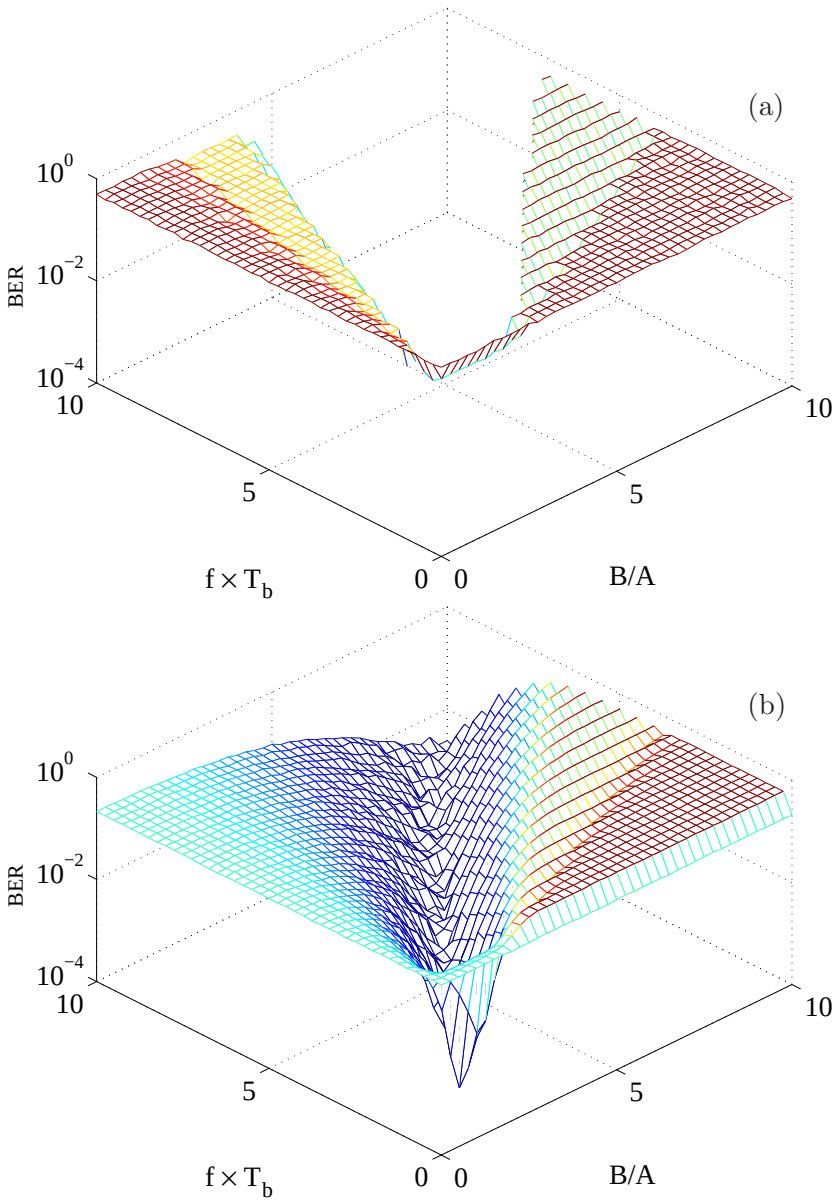

Figure 3.9: BERs where $r(t)$ is $B\sin(2\pi ft)$, and $\sigma_{n(t)} = 0$ and 0.68 respectively.

the input to exceed the system barrier as shown in Fig. 3.8 (c). It is aimed to detect effectual sine waves providing a significant performance improvement. BER performance results for various sine waves are illustrated in Fig. 3.9 where $\sigma_{n(t)} = 0$ and $\sigma_{n(t)} = 0.68$ respectively. When $\sigma_{n(t)} = 0$, there are many sine waves providing error free output signal of which performance cannot be plotted in log scale, and

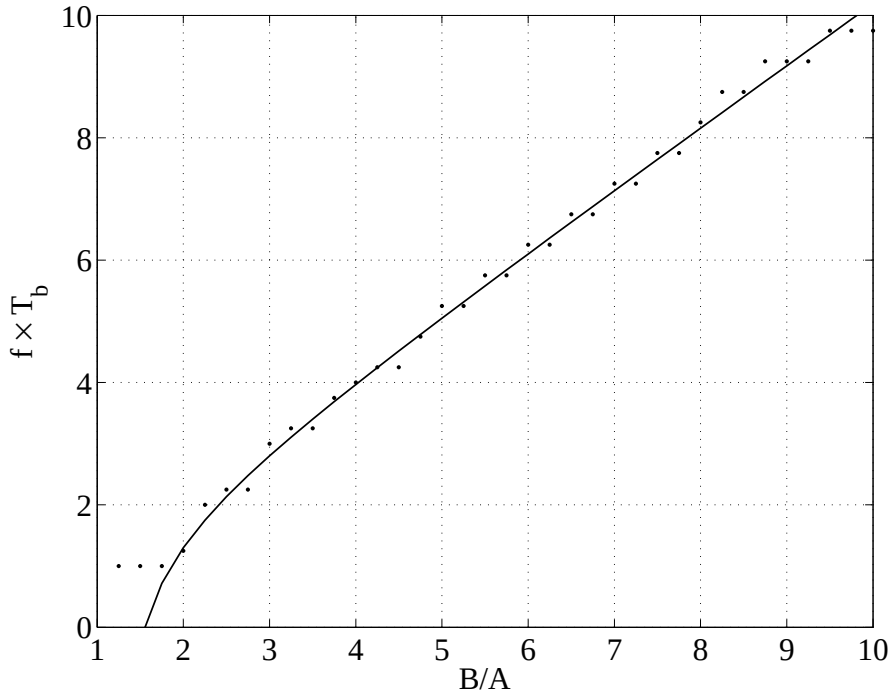

Figure 3.10: Frequency and Amplitude couples (dots) providing lowest BERs and fitted curve (solid) given in Eq. (3.23).

there is a pattern restricting the amplitudes, B, and the frequencies, f. Such as in Fig. 3.9 (b), this pattern is narrowed by the background noise ($\sigma_{n(t)} = 0.68$), thus, output is not error free any more. For this example where $m = 3$, $ak = 3$ and SNR $= -5$ dB, a basic curve fitting is applied to find out the best f and B couples as illustrated in Fig. 3.10. The fitted curve for resonant sine waves can be given by

$$f \times T_b = \frac{1}{1 - B/A} + B/A + 0.3. \tag{3.23}$$

Choosing $B \geq 2A$ and $f \geq 1/Tb$, the BER decreases significantly. On the other hand, the power of the sine wave is basically $B^2/2$. To consume less power, B must be $2A$ and f is thus $1.3/T_b$.

Both NSR and sine wave SR can be compared in terms of performance and power issues. It is clear from Fig. 3.11 that NSR cannot enhance the performance further than that obtained by the optimum background noise. However, sine wave

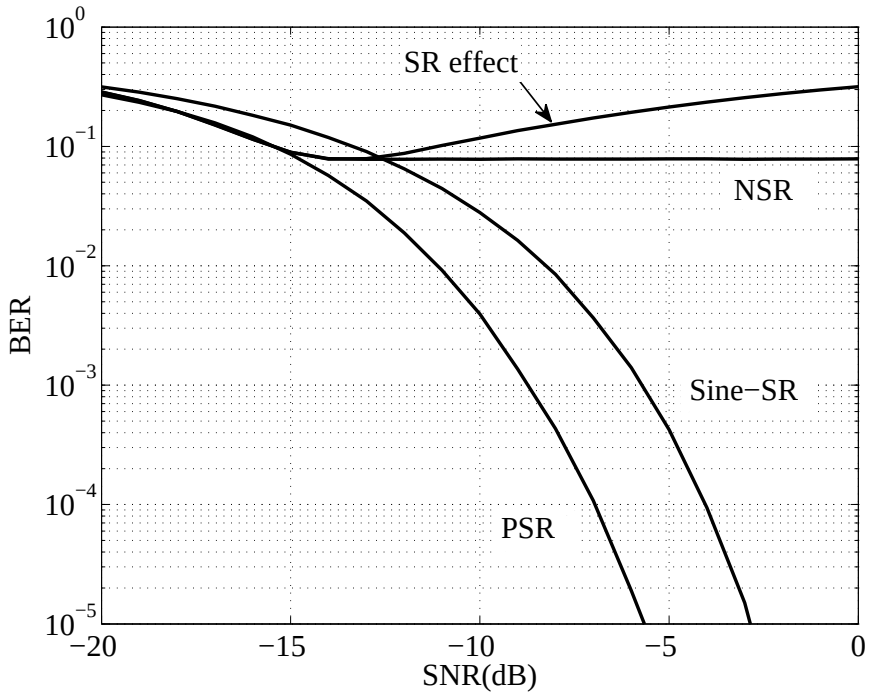

Figure 3.11: BERs where $x(t) = s(t) + n(t) + r(t)$ and $n(t) \sim N(0, \sigma_n^2)$. NSR performance with $r(t) \sim N(0, \sigma_r^2)$. Sine wave SR performance with $r(t) = 2A\ sin\ (2\pi(1.3/T_b)t)$.

SR decreases the BER as much as a PSR method does. When it comes to power requirement, it is seen that resonant noise power, $\sigma^2_{r(t)}$, is between 0 and σ^2_{opt}, while the power of sine wave is always $B^2/2$. The minimum power consumption in sine wave SR is only $10\log((B^2/2)/(A^2)) = 3$ dB so that $\sigma^2_{r(t)}$ is always greater than $B^2/2$ where SNR $>$ SNR$_{opt} + 3$ dB. It can be concluded that whilst sine wave SR needs less energy and does not requires an adjustment depending on background noise, it provides an increase in performance.

3.5 Conclusions

A stochastic resonator can be used as an alternative signal processing tool at low SNRs and potentially applications where size and energy considerations are paramount. Owing to the expressions given for steady states and transition time,

comprehension and application of this resonator becomes attainable. Furthermore, the analysis shown here simplifies the application of PSR methods. A resonator filters the background noise and thus, the system performance can be enhanced considerably by the means of only two parameters a and b. While digital filters are providing a similar performance with hundreds of coefficients, having only two coefficients may be the most significant advantages of the resonator. Finally, it was shown that a sine wave, proposed as a resonant signal instead of noise where PSR methods are not available, did not need a tuning process corresponding to the background noise. The evidence presented thus far supports the idea that a sine wave supplies a better performances enhancement while decreasing the complexity and power consumption.

Chapter 4

Deterministic and Stochastic Resonant Signals

In Chapter 3, a periodic signal, namely a sine wave, has been introduced to the input in addition to the noise. It has been shown that the sine wave can also resonate with the BPAM signal at certain amplitudes and frequencies, which is similar to the existence of a certain noise level in SR. However, they provide significantly different performance enhancements. For example, the sine wave can keep decreasing BER in response to the increase in SNR, while the noise only case is limited to the BER obtained at the optimum SNR. The presence of these two cases necessitates a study on the resonant signals, themselves.

In this chapter, the resonant signals are examined in four categories; deterministic signals, white noise with different distributions, colour noise, and band-limited noise. Signals defined in each category are applied to the resonator in Sec. 3.2, where the information signal and system design are given in Sec. 3.4.

4.1 Deterministic Resonant Signals

Deterministic signals, studied in here, are sine wave, square wave and triangle wave which are all periodic. The reason for calling them *deterministic* instead of periodic is that when they resonate with the BPAM, there is only one SNR for a given BER. It means that one can be determined from another. However, this is not possible for stochastic resonant signals as there are two SNR levels matching with one BER.

These deterministic signals can be defined by three parameters; amplitude, B, frequency, f, and phase, θ, where their expressions are given by

$$r(t) = \begin{cases} B\sin(2\pi ft+\theta) & \text{, sine wave} \\ B\ \text{sgn}(\sin(2\pi ft+\theta)) & \text{, square wave} \\ B\frac{2}{\pi}\arcsin(\sin(2\pi ft+\theta)) & \text{, triangle wave} \end{cases} \tag{4.1}$$

These parameters for resonant signals can be obtained by means of simulation which is similar to the parameter search performed in Sec. 3.4. As that search does not cover phase parameters, θ, the simulation can be extended by setting a random phase variable with uniform distribution for each SNR; $\theta \sim U(0, 2\pi)$. In addition to that, the system needs to be simulated also for SNRs lower than that of resonant background noise. Therefore, the search is carried out for lower SNRs (-14 dB and -17 dB) as well as for higher ones (0 dB and -10 dB).

The simulation set-up can be given as following. The system input, given in Eq. (3.1), consists of a BPAM signal, $s(t)$, with amplitude $A = \sqrt{4/27}$ and pulse (bit) duration $T_b = 9$ s, a background noise ,$n(t)$, and a resonant signal $r(t)$. The system parameters are $a = 1$ and $b = 1$. For the simulation, discrete forms $s[i] = s(it_s)$, $n[i]$ and $r[i]$ are defined where the sampling period is $t_s = T_b/100$ and i denotes ith sample. The resonant signals amplitude, B, and frequency, f, are normalized by corresponding parameters of $s(t)$.

The background noise samples are considered as Gaussian random variables

with zero mean and a variance, $n[.] \sim \mathcal{N}(\mu, \sigma^2)$. Then, SNR in dB is determined as in Sec. 3.2.3. Finally, the resonator output is obtained from Eq. (3.2).

The simulation is performed for each and every resonant signal with ($B/A \in \{0.5 : 0.5 : 10\}$, $fT_b \in \{0.5 : 0.5 : 10\}$). In order to obtain the BER, the signs of samples $y[iT_b/t_s]$ from a 1×10^3 bit long output are compared with those of $s[iT_b/t_s]$. The results are illustrated in Fig. 4.1, Fig. 4.2 and Fig. 4.3, for sine, square, and triangle waves respectively.

Results show that these deterministic signals can drastically improve the system performance. For some (B/A,fT_b) signal settings, no error is detected during the simulation at SNR = 0 dB. When the SNR is decreased to -10 dB, errors occur for any deterministic signal. However, BERs obtained from those (B/A,fT_b)s are still less than that of the noise, BER = $\log_{10}(0.08) = -1.1$ at SNR = -14 dB as given in Sec 3.4.

On the other hand, when SNR ≤ -14 dB, the deterministic resonant signals cannot provide a better BER performance than the noise. However, in that case, there is no need for a resonant signal as the background noise performs optimally. Therefore, it is necessary to specify (B/A,fT_b) parameters for SNR ≥ -14 dB.

In the figures (a) and (b) corresponding to SNR = 0 dB and SNR = -10 dB, it can be observed that the resonant signal parameter B/A is directly proportional to fT_b as the minimum BERs falling over the (B/A,fT_b) surface contours. Assuming that these lines overlap at the bottom of the BER surface, the coordinates (B/A,fT_b) of this bottom line give the resonant signals.

This contours can be obtained by means of a surface fitting. Due to the randomly chosen phase, BER varies from one (B/A,fT_b) to another. This causes a mismatching of minimum BERs. For example, it can be assumed that there is a function $f_{\text{minBER}}(B)$ which gives f resulting in minimum BER for a given B. Similarly, another function $B_{\text{minBER}}(f)$ can be considered.

When the minimum BERs are assigned as values of these functions, the

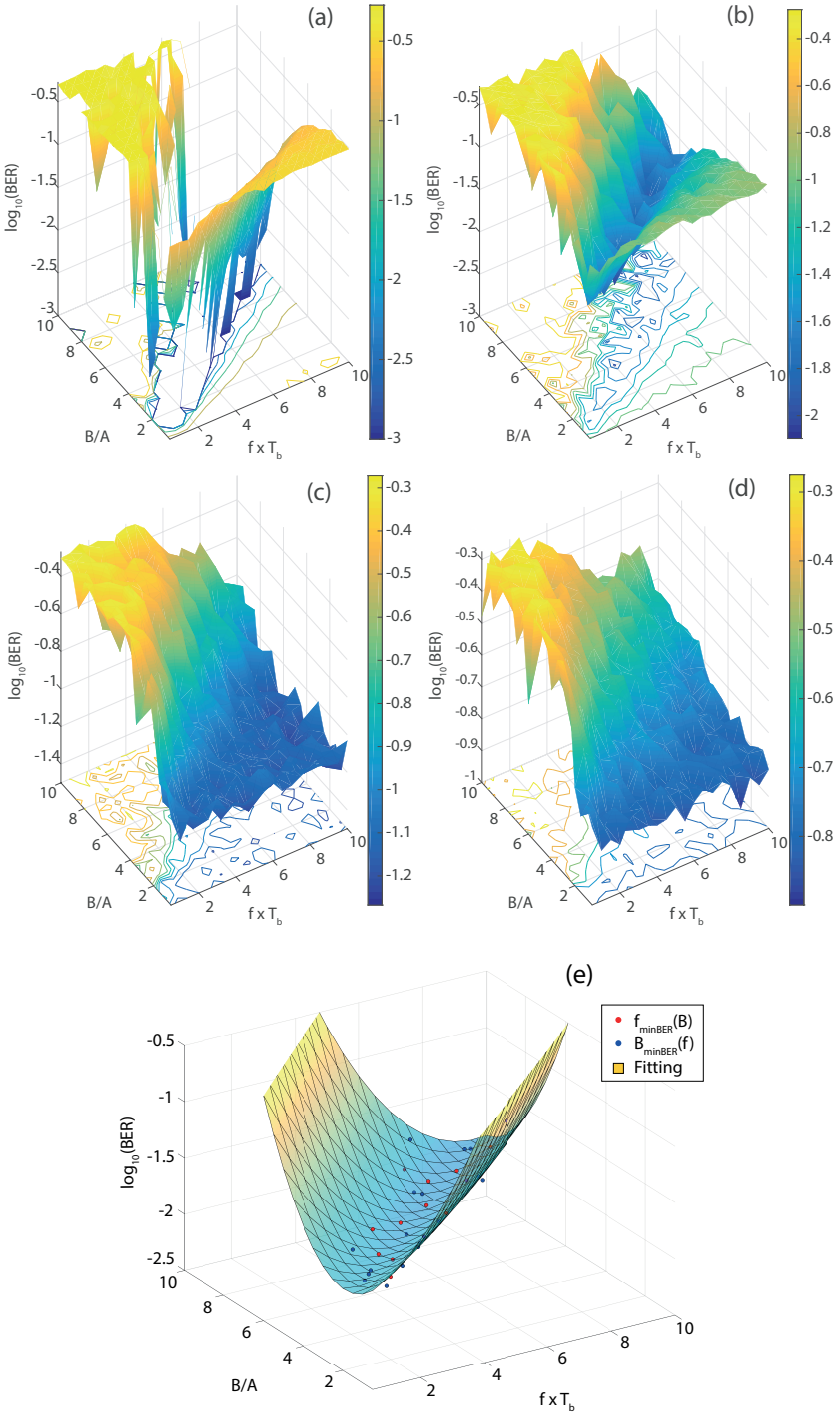

Figure 4.1: BER pattern search (a,b,c,d) for sine wave resonant signal where SNRs are set to $0, -10, -14, -17$ dB respectively. The phase parameter for each simulation is chosen randomly $\theta \sim U(0, 2\pi)$. The fitted surface (e) for minimum BERs at SNR$= -10$ dB.

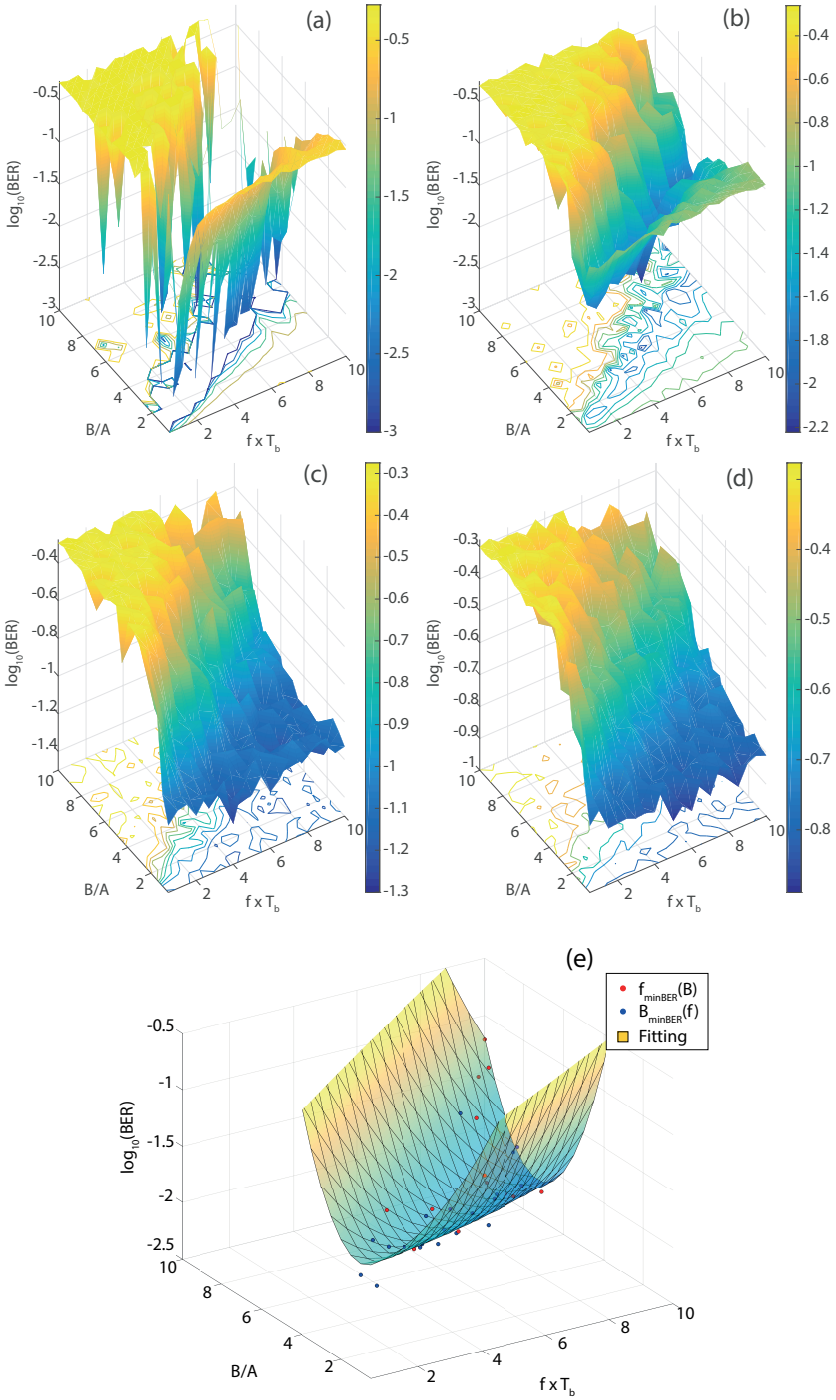

Figure 4.2: BER pattern search (a,b,c,d) for square wave resonant signal where SNRs are set to $0, -10, -14, -17$ dB respectively. The phase parameter for each simulation is chosen randomly $\theta \sim U(0, 2\pi)$. The fitted surface (e) for minimum BERs at SNR$= -10$ dB.

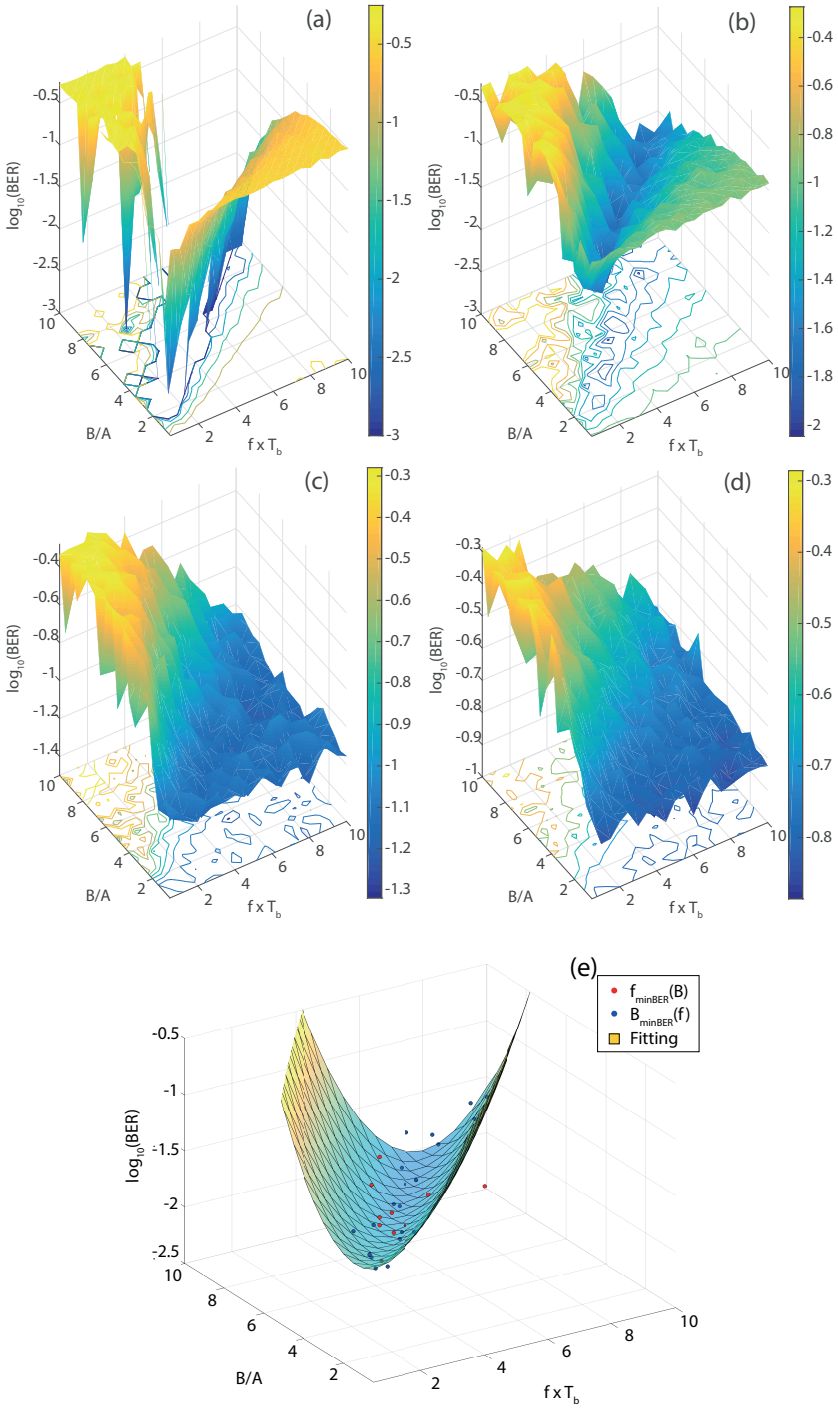

Figure 4.3: BER pattern search (a,b,c,d) for triangle wave resonant signal where SNRs are set to $0, -10, -14, -17$ dB respectively. The phase parameter for each simulation is chosen randomly $\theta \sim U(0, 2\pi)$. The fitted surface (e) for minimum BERs at SNR= -10 dB.

mismatching appears within a valley shaped surface. These BERs at SNR = −10 dB and fitted surfaces are illustrated in the 5th plots of the corresponding figures. For fitting, the function used is

$$\log_{10}(BER) = c_{0,0} + c_{1,0}\frac{B}{A} + c_{0,1}fT_b + c_{1,1}\frac{B}{A}fT_b + c_{2,0}\frac{B^2}{A^2} + c_{0,2}f^2T_b^2 \qquad (4.2)$$

When B/A is considered as a constant, the derivative of Eq. (4.2) in respect to fT_b provides the resonant fT_b as

$$\begin{aligned} 0 &= c_{0,1} + c_{1,1}\tfrac{B}{A} + 2c_{0,2}fT_b \\ fT_B &= -\tfrac{c_{0,1}+c_{1,1}B/A}{2c_{0,2}} \end{aligned} \qquad (4.3)$$

where the fitting results are $c_{0,1}$ = [0.1398, 0.0467, −0.0086], $c_{1,1}$ = [−0.1338, −0.1691, −0.1691], and $c_{0,2}$ = [0.0623, 0.0570, 0.1064] for [sine, square, triangle] waves, respectively.

The resonant signal parameters (B/A,fT_b) obtained from the surface fitting are illustrated in Fig. 4.4. In the first plot, it can be seen that the amplitudes are linearly proportional to the frequencies, and the triangle resonant signal needs amplitudes greater than square and sine waves at high frequencies.

Then the second plot, where the average power is defined by $1/N\sum_{i=0}^{N} r[i]^2$, shows that square and triangle resonant signals have almost the same average powers for a given frequency, and the sine wave always requires more power.

The third and fourth plots are for the BER comparison. It is shown that the higher the frequency the resonant signals have, the lower the BER can be achieved in exchange for a power requirement increase. In addition to that, the sine wave provides the lowest BERs at the lowest frequencies of $fT_b < 4$, while triangle and square waves need to be used at higher frequencies to obtain better BER performances.

Moreover, the resonant amplitudes are greater than the input A, and this causes the output to fluctuate, which makes the system phase sensitive. For exam-

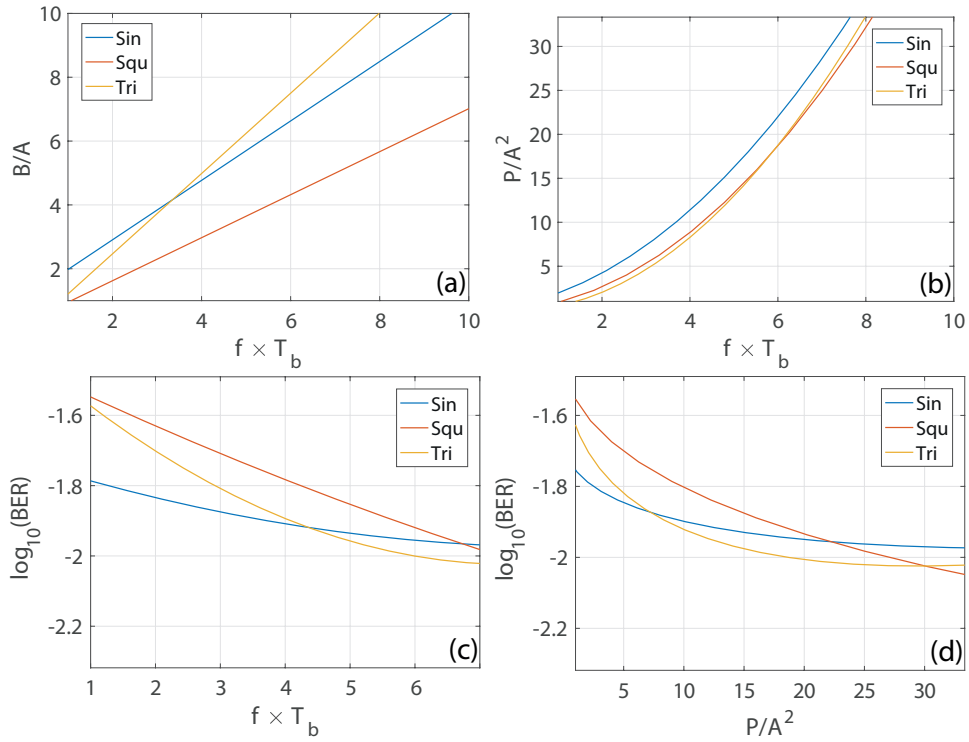

Figure 4.4: The resonant signal parameters obtained by surface fitting, with Normalized Powers P/A^2 and BERs.

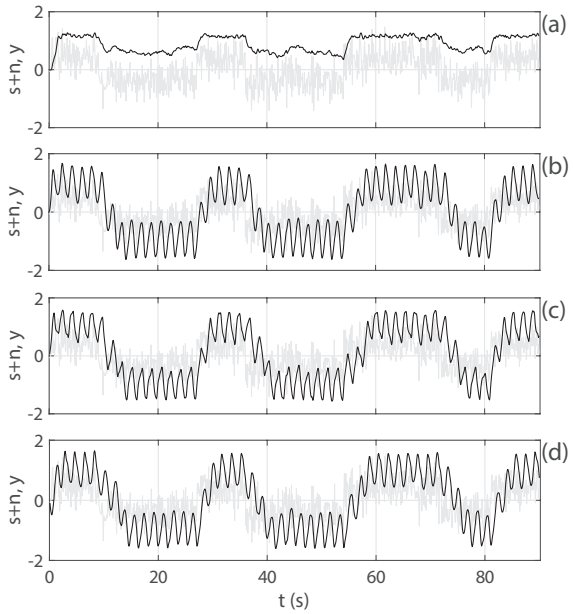

Figure 4.5: The outputs (black) of the resonator where there is no resonant signal, and where the resonant signals; sine, square, triangle at $fT_b = 5$ with $B/A = [5.7, 3.65, 6.24]$, are added to the input, $s + n$ (gray). SNR = 0 dB.

ple, if $fT_b = 5$, then Eq. (4.3) gives the resonant amplitudes $B/A = [5.7, 3.65, 6.24]$. While these signals are improving the system performance, they introduce a significant fluctuation to the output, which is illustrated in Fig. 4.5.

It can be seen that the resonant signals benefit the system in the same way as was shown in Chapter 3. They help the input to cross the barrier h_b and keep the output level until input changes. In addition to that, the fluctuations caused by the resonant signals have almost the same peak-to-peak values, although amplitudes at the input are considerably different.

Furthermore, it seems that the system itself has already suppressed the background noise. Considering the resonant free case, the output fluctuation is weak and it follows the input with a mean difference. As the decision threshold of the sign detector is not on that mean, it may lead to lower BERs if the threshold is determined accordingly. Similarly, a weak fluctuation is also present for outputs of the resonant signal. Together with the strong resonant effect, the weak random variation closes the gap for the threshold values. Therefore, the outputs with and without a resonant signal need to be analysed in terms of the decision threshold in order to clarify the benefit of the resonant signals. This can be analysed by the means of eye pattern.

4.1.1 Eye Pattern

The eye pattern reveals significant properties of the signals; such as the sensitivity to decision timing, optimum sampling time, peak distortion, etc. By definition, an eye pattern is obtained by plotting the delayed copies of the signal over and over. However, it may not be effective as the outputs being analysed here contains a high frequency component with noticeable magnitudes. As an alternative, considering the eye pattern as a screen with a number of pixels, if BER for every pixel is found and coloured accordingly, an eye pattern can be obtained.

With this method, eye patterns for the outputs are represented in Fig 4.6. The horizontal axis consists of a hundred samples. The vertical one is limited by the

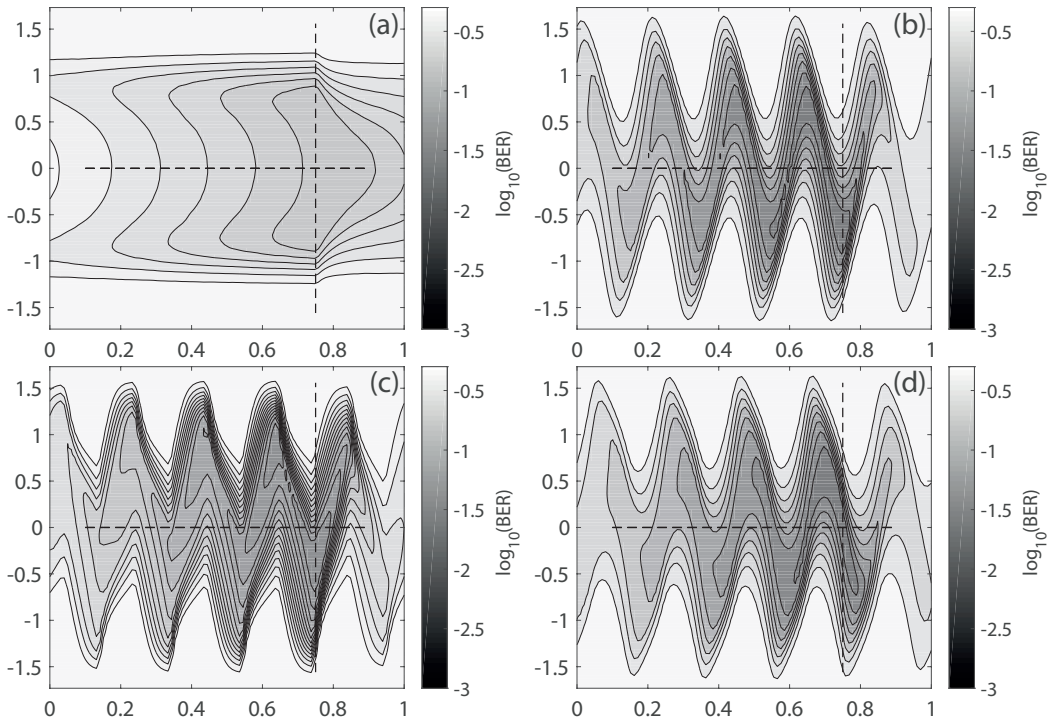

Figure 4.6: Eye patterns of outputs; without a resonant signal and with sine, square, triangle resonant signals, respectively where SNR $= -10$ dB

interval $(-1.5kA, 1.5kA)$ and divided by a hundred equally separated thresholds. For each threshold and sample, BER is calculated, and its value in log scale determines the colour. While 'black' denotes BER $= 10^{-3}$, 'white' is used for BER $= 0.5$. The corresponding colour bar is placed next to the pattern. The vertical dashed line indicates where the present bit ends and the next starts.

The first pattern in Fig 4.6 shows that the output without resonant signal does not benefit from a threshold value, but zero. As the BPAM signal does not cause a change in the output's sign, it follows the BPAM with a mean. This mean is present for both positive and negative outputs, and the noise causes output to switch from one mean to another randomly. However, as mentioned before, the noise is already suppressed by the resonator, so the random switching between these means occurs rarely and evenly at the given SNR. Therefore, setting a threshold according to one mean always fails when the output switch to another mean. The results are

$\log_{10}(\text{BER}) = -0.98$ and -0.93 at thresholds $\pm 0.71 = \pm 0.62\ kA$ and 0. As the difference between BERs is negligible, it can be said that the zero and optimum thresholds provide the same BER performance.

The other three eye patterns are for sine, square and triangle waves, respectively. It can be seen that these deterministic resonant signals decrease the BER significantly. However, the outputs become more sensitive to the decision time and threshold. As the lowest BER levels appear between two close periodic signals with high amplitudes, any independent change of the decision time and threshold can cause a drastic increase in BER.

For instance, when the resonant signal is absent, the minimum BER level is as wide as $0.23\ T_b = 23$ samples $\sim 1/4\ T_b$ at the zero threshold, and its height is about $1.8 = 1.56\ kA$ for decision sample at T_b. However, the minimum BER levels for sine and triangle waves are in a form of one period sinusoid, and the level for square wave is more like one period triangle. From the peaks of that one period forms, the maximum widths and heights for sine, square, triangle waves can be given by $[5, 6, 9]$ samples and $[0.4, 0.45, 0.49]\ kA$, respectively, while the corresponding BERs are $\log_{10}(\text{BER}) = [-1.95, -1.7, -1.95]$. Therefore, the deterministic resonant signals increase the BER performance in the exchange for shrinking the area of optimum decisions.

4.1.2 Resonators in Parallel

The optimum decision area can be widened by using two resonators connected in parallel. The shrinkage is mainly due to the fluctuation at the resonant frequency. Assuming that the phase does not vary from one pulse to another, the fluctuation can be considerably weaken by adding two outputs with resonant signals having π phase difference in between. This two-resonator configuration is illustrated in Fig. 4.7.

Similar to the simulation of a single resonator, the eye patterns are obtained

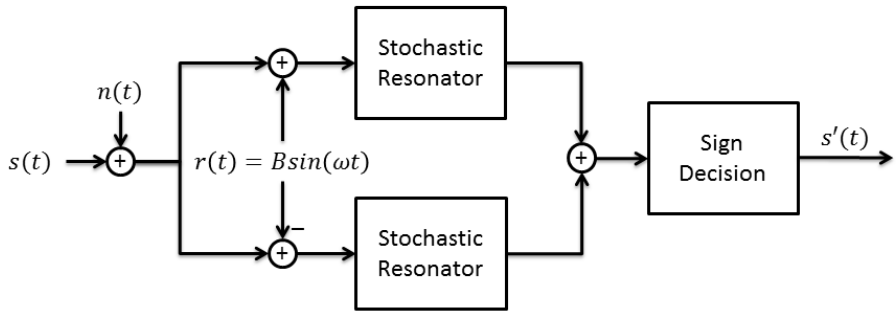

Figure 4.7: The two-resonator receiver dealing with the fluctuations caused by a sinusoidal resonant signal.

from 0.5 times the output sum, and presented in Fig. 4.8. The first eye pattern is for noise only inputs. As there is no resonant signal, two different noises with the same properties are applied. For the other three eye patterns, all inputs experience the same noise signal. The results for noise only, sine, square, and triangle waves can be summarized as following; the maximum widths are $[6, 16, 20, 13]$ samples, maximum heights are $[0.15, 0.33, 0.45, 0.33]$ kA, and $\log_{10}(\text{BER}) = [-1.36, -2.1, -2, -2.1]$, respectively.

The results show that BER performances are slightly increased by the use of two resonators in parallel, and more importantly the eye patterns are widened significantly. When the resonant is absent, the two resonators decrease BER from $10^{-0.98}$ to $10^{-1.36}$, and set the optimum threshold back to 0. When the resonant is introduced to the system, due to the π phase difference of resonant signals $(-\sin(\omega t) = \sin(\omega t + \pi))$, the fluctuation at the resonant frequency seems almost eliminated. The remaining fluctuation is about 5 times weaker at 2 times the resonant frequency. This results in 2 to 3 times wider eye patterns.

In terms of the pattern height, it is found that two resonator configuration causes the pattern to close by up to 33%. However, the optimum sampling area, $width \times height$, is increased, and its centre is also moved on to the zero threshold. Therefore, this coupling allow the output to be decoded in a feasible way. Further-

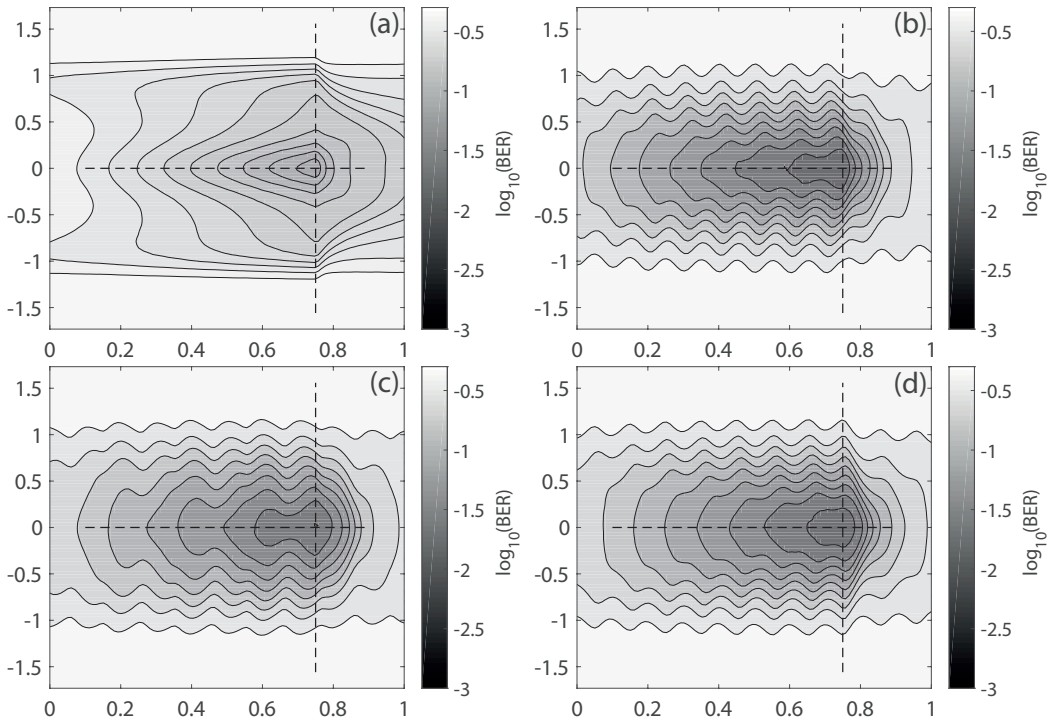

Figure 4.8: Eye patterns of outputs from two resonators; without a resonant signal and with sine, square, triangle resonant signals, respectively where SNR = −10 dB

more, better results can be obtained by using an array of resonators. In that case, the phases needs to be determined accordingly.

Finally, regardless of coupling, the deterministic resonant signals provide a BER performance improvement for SNRs higher than that of optimum noise as in Fig. 4.9. While the outputs are decoded by a single threshold, BER curve for the background noise is not monotonic and increases back to 0.5 at high SNRs. Another reason for that is the noise samples being Gaussian distributed. If there is a probability of receiving samples higher than the barrier h_b, then there is a probability of a change in mean which results in the decoding failure as in Fig. 3.4 and Fig. 3.8.

However, a periodic signal deliberately makes BPAM amplitudes greater than h_b within a period. In the resonance case, the amplitude and frequency of the periodic signal guarantee the resonator to switch and keep its output values according

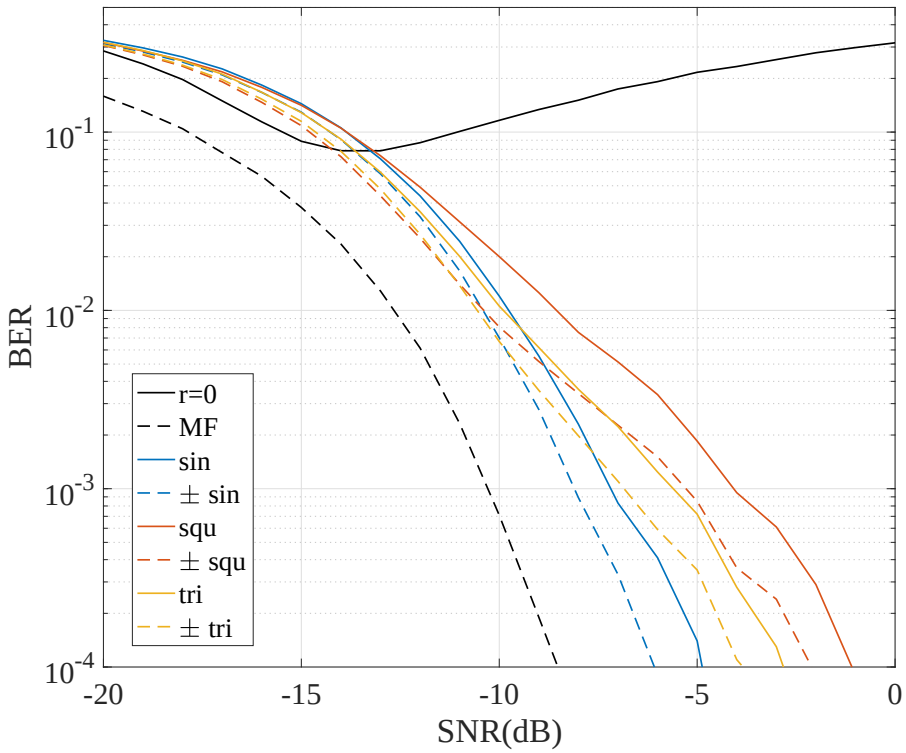

Figure 4.9: BER curves for resonant signals and for receiver configurations.

to BPAM input within the symbol interval. Therefore, any noise level distracts the system from synchronizing with the periodic resonant. As a result, the error rate monotonically increases in response to noise power increase.

4.2 White Stochastic Resonant Signal

A stochastic signal also resonates with the system and enhances the performance. In the previous section, the noise samples are i.i.d. random variables which are also the Gaussian white noise (flat power spectrum). It has been shown that the background noise leads the system to make less errors, and there is a minimum BER which the system can achieve at an optimum noise power. When the background noise power is less than that optimum power, the Gaussian white noise with adjunct power can be added deliberately in order to decrease the error probability. Therefore, the noise with sufficient power is called *stochastic resonant signal*. However, it is not limited by the type of distribution and the shape of the frequency spectrum.

The effect of probability distribution can be examined in terms of the average power of the resonant signal. While the probability of each value, that a random variable can take, is determined by its distribution, the average power, P_n, gives the expected square of that variable, $\lim_{K \longrightarrow \infty} \frac{1}{K} \sum_{k=1}^{K} r[i]^2$. Although the information of sign is removed, this expected power, together with the variable mean, defines an interval in which the signal spread out. In addition to that, if the resonant noise have a flat power spectrum, the mean requires to be zero. For these reasons, P_n is introduced to the resonant signal samples as below.

$$r[i] \quad = \begin{cases} \sqrt{3P_n}R & , R \sim \mathcal{U}(-1,1) \\ \sqrt{P_n}R & , R \sim \mathcal{N}(0,1) \\ \sqrt{P_n}R_1R_2 & , R_1 \sim \mathcal{N}(0,1), R_2 \sim \mathcal{N}(0,1) \end{cases} \tag{4.4}$$

In Eq. (4.4), the three different distributions; uniform, normal (Gaussian), and normal product are used to define the resonant signal where R is a random variable. The corresponding to cumulative distribution functions (CDFs) are illustrated in Fig. 4.10 to provide the comparison between resonant signals. For example, 60% of the resonants' samples are going to be between $[-1.1, 1.1]$, $[-0.8, 0.8]$ and

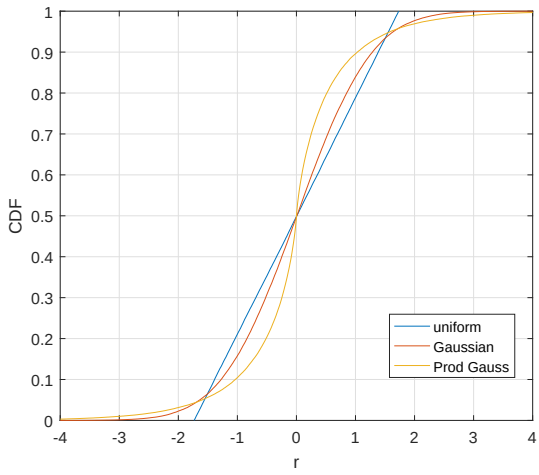

Figure 4.10: CDFs of the stochastic resonant signals with flat spectrum where $P_n = 1$.

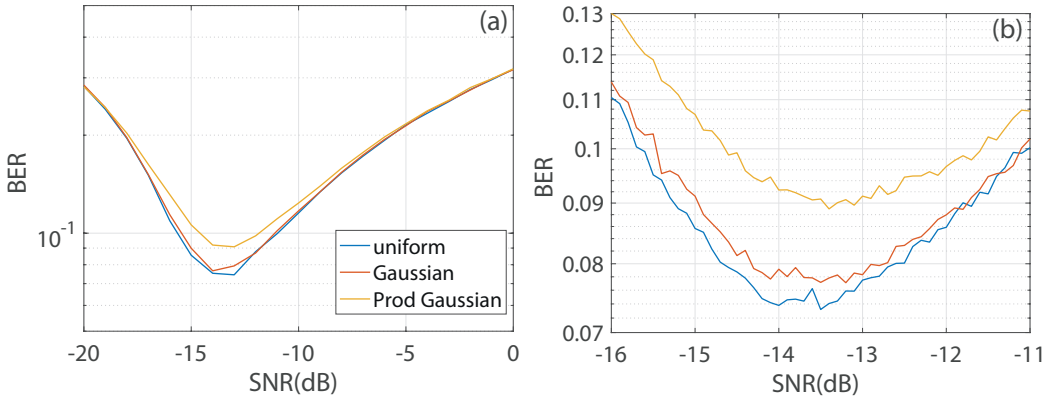

Figure 4.11: The BER performances of stochastic resonant signals with the flat spectrum and different CDFs. SNR increments; 1 dB (a) and 0.1 (b)

$[-0.5, 0.5]$, respectively. Similarly, the probabilities of a sample being greater than $\sqrt{P_n} = 1$ are 0.2, 0.15, and 0.1. Therefore, the resonant powers can be associated with the distribution differences.

In order to find out the power required for these stochastic signals to resonate with the system, BER performances are obtained from the simulation of 10^5 bits long input where the background noise is absent. The results in Fig. 4.11 (a) and (b) show that the resonant powers are 13 dB -14 dB and the corresponding BERs $\approx 0.07-0.09$. Due to the simulation of a certain number of bits, these BER curves fluctuate within

the 95% confidence interval $\pm\sqrt{10^5(0.9)(1-0.9)}\ 2/10^5 = \pm 1.8\times10^{-3}$. Therefore, it can be inferred that, a flat spectrum stochastic signal whose samples are uniformly distributed provides a better BER performance than those with normal and product distributed samples.

More importantly, regardless of the distribution type, a stochastic signal interacts with the background noise. While a deterministic resonant works with the system and BPAM, the background noise is regarded as a destructive signal. However, when the resonant is stochastic, the background noise becomes a part of the resonance process. According to the central limit theorem, this involvement results in a stochastic signal to be a normal distribution with the sum of operands' power. Therefore, the stochastic resonant signals also need to be analysed together with the background noise.

In Fig. 4.12, the simulation results for this analysis are presented. In the first column (a,d,g), it can be seen that noise-resonant interaction is mainly based on their powers. For example, where both distributions are normal, the result's distribution is also normal. Therefore, BER levels in Fig. 4.12 (d) appears as a quarter circle whose centre is at zero SNRs. Moreover, these levels are symmetric with respect to xy axis, which is expected for the sum of two normal random variable.

In addition to that BER performance depends on the shares of noise and resonant in the power required for resonance. Considering Fig. 4.12 (a,d,g), (a) and (g) are not symmetric. While $\log_{10}(\text{BER}) = -1.1$ level of (a) is slightly wider at the noise SNR = 0 dB, a different level appears for the same noise power in (g). This is because these resonant signals and noise have different distributions, and the result distribution, thereby BER curve, is shaped based on their powers.

The two resonators coupled in parallel are also simulated to examine the random fluctuations of output. The results are presented in Fig. 4.12 (b,e,h) and (c,f,i). It is inferred that the phase information of the stochastic signal can be conveyed to the output. In (b,e,h), the resonant signals differ only in phase, and

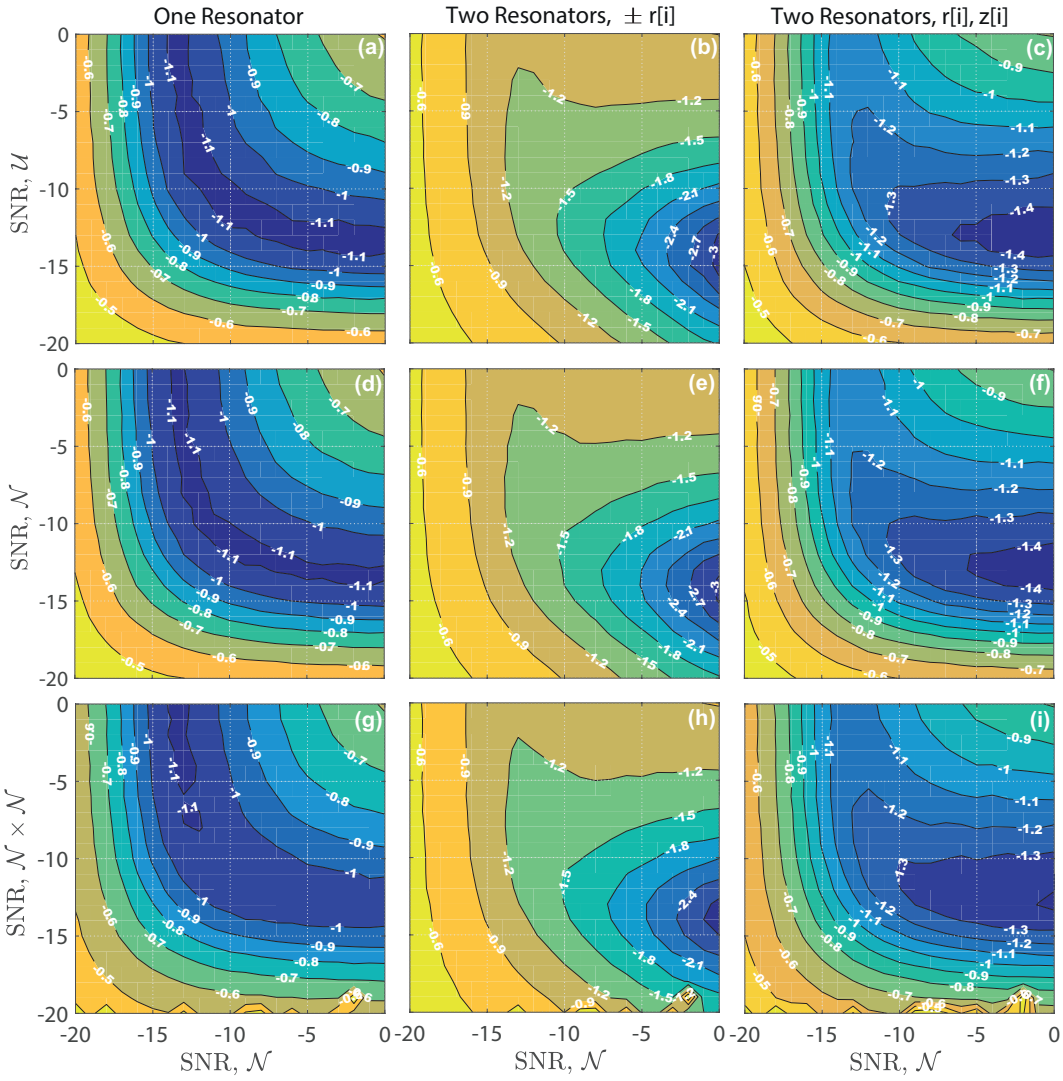

Figure 4.12: BER performances of the stochastic signals where the background noise is present. The rows are for different distributions, and the columns are for system configurations. $\pm r[i]$ means each resonator experiences the same absolute value, while $r[i], z[i]$ indicates that there are two i.i.d. signals. SNRs are in dB. While SNRs for horizontal axes (background noise) are obtained from BPAM power over noise power, those for vertical axes are from BPAM power over corresponding resonant's power. BER levels are given by $\log_{10}(\text{BER})$.

they are uncorrelated in (c,f,i), whilst the BPAM inputs are always the same for both resonators. The results indicate that there is a significant noise cancellation based on wide spectrum phase matching. While different resonant signals (c,f,i) can provide about 0.3 BER decrease, those with π phase difference (b,e,h) lead BER to decrease drastically from $\log_{10}(\text{BER}) = -1.1$ to -3.

In summary, the white stochastic signals resonate with the given system. Its performance depends on the power and distribution of these signals. If two stochastic signals are added, the performance is founded on the total power and the distribution whose power dominates the sum. In addition, when the system is in resonance, its output provides the optimum information about the phase of stochastic signal as well as that of BPAM. This makes the noise cancellation applicable.

4.3 Colour and Band-limited Noise

In the Section 4.2, the white stochastic signal, which has a flat frequency spectrum, has been studied. While *white* refers to the flat spectrum, other colours are used to mention different type of spectrum. Their difference is based on the relation between frequencies and their powers. For example, the *brown* noise describes the power spectrum of noise whose density is proportional to one over the square of frequency, $1/f^2$. Similarly, the *violet* noise refers to the derivative of white noise whose power density is proportional to f^2. In addition to that, the spectrum of a deterministic resonant signal has either one frequency component or one with its harmonics, and the powers are proportional to f^2. While there is a similarity between f^2 noise and resonant power, spectrum of resonants are different. Therefore, in this section, a pre-processed stochastic signal is applied to the system in order to examine the effect of colour and bandwidth.

In order to obtain stochastic signals differ in colour and bandwidth, Gaussian white background noise can be processed in the frequency domain. When its DFT

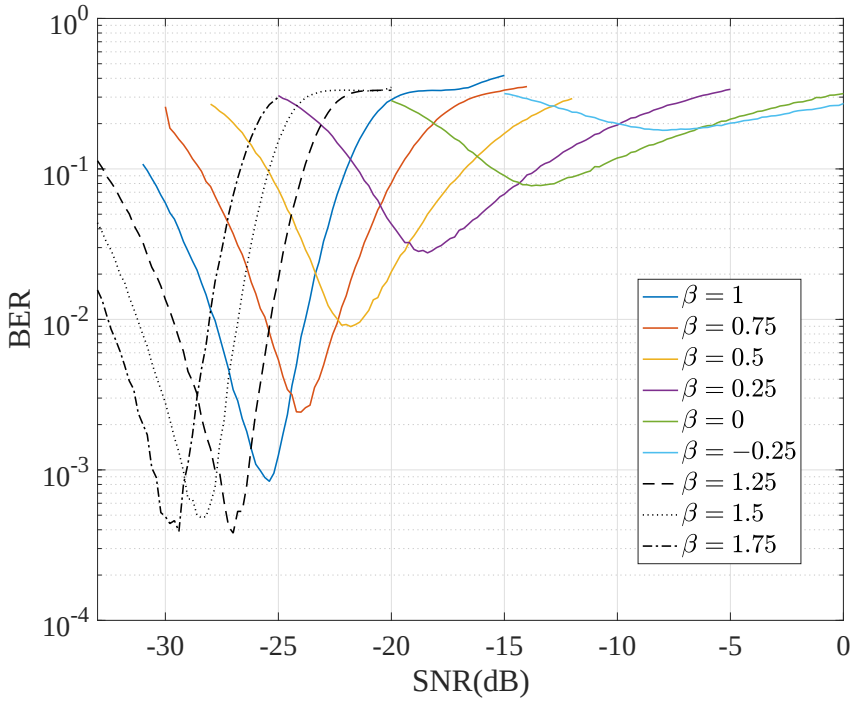

Figure 4.13: BER curves obtained from the simulation with color noises where there is no other resonant and background noise.

is calculated, the magnitude spectrum can be modified by a function to satisfy the required frequency-power relation. For different colors, this function is considered as f^{β}, and for bandwidths, a rectangular function is used. After the spectrums are formed, the inverse DFT provides the real valued signals. Then, they are solely introduced to the system in order to observe the resonance.

When system with the inputs; colour noise and BPAM, is simulated, it is found that colour noise formed by $\beta > 0$ is more effective in terms of BER performance. The simulation results are presented in Fig. 4.13 where SNR is the ratio of average powers in dB. As f^{β} is introduced in magnitude spectrum, here, $\beta = 1$ refers the violet noise. It can be seen that the optimum BERs are decreasing by the increase in β. That is because the difference between noise power in and out the BPAM's base-band depends on *beta*. The greater β is, the more noise power moves out of the base-band.

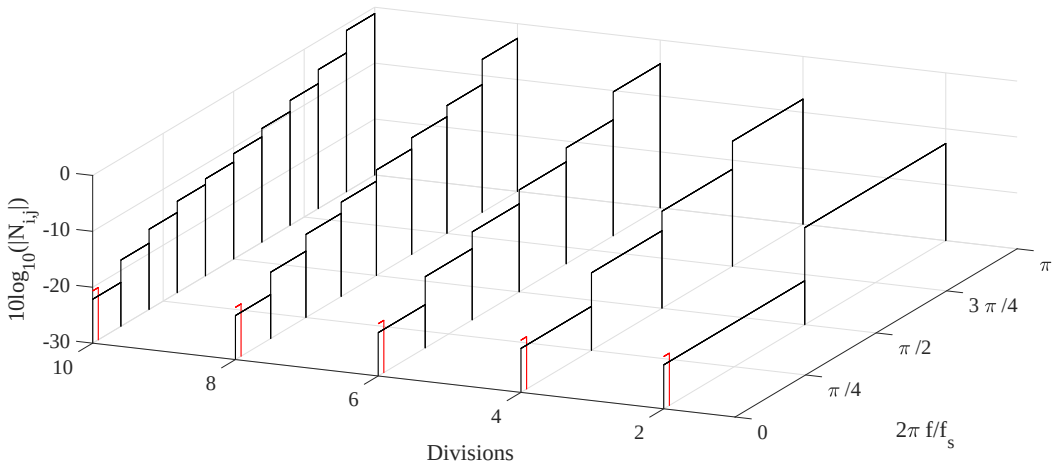

Figure 4.14: Magnitude spectrums of band-limited noises where the resonance is observed for each one.

This infers that BER can decrease more if the noise is removed from the band of interest. Therefore, its frequency spectrum is limited by rectangular functions shown in Fig. 4.14. The magnitude of each one represents the noise power which provides optimum BER. The results are given in Fig. 4.15. As the first ones in each division introduce noise power to the band of interest, their BERs are close to that of $\beta = 0$. Although, the others do not have any component in that band, they cannot provide BERs smaller than that of $\beta = 0.75$.

These two types of noise lead a greater decrease in BER compare to the white noise, while their power requirements differ significantly. In order to achieve BER less than the one of optimum white noise, the $\beta > 0$ colour noise needs to be applied with a power higher than the one required for the white noise's best performance. However, the band-limited noise can provide such BER at lower power cost, if the noise band is set out of the band of interest. Moreover, with five times less power requirement, the base band-limited noise can perform as same as the white noise.

In conclusion, the decrease in BER is limited due to the presence of a stochastic signal, regardless of its properties. For colour noise, it has been observed that optimum BER for $\beta > 1.25$ did not decrease further. For band-limited noise, the optimum BER was rather limited as it was shown that the performance is propor-

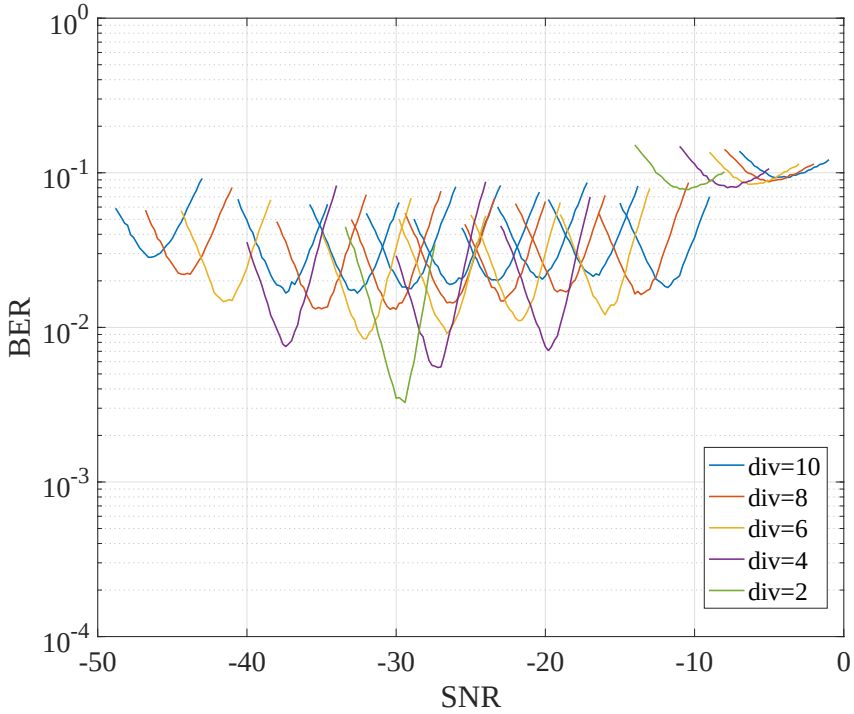

Figure 4.15: BERs of the band-limited noises where 'div' indicates the bandwidth, and the results for each segment from 0 to π are placed from left to right.

tional to the bandwidth. Nevertheless, they are alternative resonant signals as they enable the trade-off amongst bandwidth, error rate, and power requirement.

4.4 Conclusion

In this chapter, deterministic and stochastic signals are examined in terms of their potential use for the resonance. It has been shown that deterministic ones, namely periodic signals, whose frequencies are proportional to amplitudes, can resonate with the system and BPAM signal. As their effects are systematic, the background noise loses its resonant property and becomes the only source of BER increase. On the other hand, such a relation between frequency and amplitude causes strong fluctuations especially in the first harmonic that makes the system phase sensitive. The eye pattern analysis refers that the phase does not vary by the symbol interval. Therefore, the first harmonic is eliminated by using two resonators in parallel.

The stochastic signals are studied in three categories; distributions of white noise, noise colour, and band-limited noise. As the background noise is considered white Gaussian distributed, the use of another white resonant signal either with the same distribution or with a different one did not make a important change in the performance and power requirement. Then, the coupled resonators are used. The results indicates that if the background noise is lower than the optimum one, the performance can be improved significantly by introducing the same resonant to the both system with π phase difference, which is similar to the noise cancellation in theory.

The colour and band-limited noises are obtained by modifying the spectrum of white Gaussian noise. The modification is performed by f^{β} and rectangular functions. These noises are considered as alternatives to the white noise and they provide a trade-off amongst power, bandwidth and performance.

More importantly, it can be inferred that the results demonstrate signs of signal processing applications such as filtering and modulation. Especially where the resonance occurs, BER performance and difference between input and output signals indicates that the system suppresses high frequency components; thereby making the base-band ones more noticeable at the output. In terms of modulation, when the deterministic resonants and band-limited noise have no overlap with the band of interest, the output presents harmonics of deterministic ones and base-band noise components. Therefore, this system needs to be examined in term of filtering and modulation capabilities.

Chapter 5

The Use of Symmetric QPW for Noise Filtering

In this chapter, a symmetric quartic potential well (SQPW) is considered for use as a low-pass filter in BPAM receivers. By using the BPAM input to force a change in the shape of the well, the output can be considered as the position of a particle in the well. The potential well has been designed to pass the BPAM signal and suppress the background noise. Within the chapter, DC gain and cut-off frequency are defined where the potential well is subject to a noise free single pulse. The effects of the background noise are also discussed. These initial results are applicable to other pulse modulation methods. Moreover, it is revealed that the cut-off frequency plays a significant role on the BPAM detector. Finally, a new result for the probability of error is introduced which clearly shows that the potential well filters out the background noise as much as a low-pass Butterworth filter does.

5.1 Introduction

The potential well considered here, namely SQPW, which is not necessarily double well, also has a filter like response which thus results in an SNR gain. The frequency

response has a pattern similar to a Low Pass Filter (LPF) [30, 34, 73], and in some cases, linear response functions can therefore be derived [66,94]. What can be noted is that of all the papers given so far, none of them list their main focus as designing this SQPW as a filter, focusing instead their efforts upon the SNR gain itself. Thus, whilst they do provide analysis along the lines of SNR, BER, Mutual Information etc., the fundamental filtering characteristics; like DC gain and cut-off frequency, are not presented as a focused contribution.

Therefore, this chapter aims to make a significant contribution to the field by designing the SQPW as an LPF within a BPAM receiver. Through a process of designing the SQPW to pass a BPAM signal and attenuate the background noise, an analytical definition for the DC gain and cut-off is shown. This result, novel in itself, is then validated through simulation of the SQPW and an output-input magnitude ratio response (MRR). Further to this, the effect of the background noise on the MRR is then investigated. Finally, the primary result of the chapter, that of two equations that define both the probability of error and cut-off frequency for the SQPW, are shown. These two final closed form equations are new to the literature.

5.2 Receiver Model

The aim is to design a receiver that consists of a SQPW and a detector defined in Sec. 3.2, and shown in Fig. 3.1.

5.2.1 SQPW

In this chapter, SQPW's input is considered in the form of Eq. (3.1) where the received BPAM signal, $s(t)$, is defined by Eq. (3.4), and where the channel is assumed to corrupt the signal by the addition of white Gaussian noise, $n(t)$, with autocorrelation function $\langle n(t)n(t+\tau)\rangle = N_0/2\ \delta(\tau)$. The SQPW's output, $y(t)$, evolves according to Eq. (3.3), then it is sampled by the detector based on Eq.

(3.5).

5.2.2 Filter Design

It is known that at high frequencies the output power of the SQPW falls off [30, 66]. Considering that the input noise has a flat spectrum, this fall-off results in an attenuation. Therefore, $|Y(f)|/|S(f) + N(f)|$ needs to show this attenuation, which can be defined as an output-input magnitude ratio response (MRR) function $|H(f)|$. Although this notation is used for linear systems, it is found convenient whilst seeking a filter like response.

Assuming that a pulse is applied to the input, and the SQPW is designed to provide a pulse like shape corresponding to the input, then it can be said that the SQPW allows that pulse to occur in its output [102]. As the pulse signal is baseband, this SQPW passes the low (baseband) frequencies. Therefore, the MRR $|H(f)|$ needs to show the same relation.

In terms of DC response of the SQPW, as defined in Sec. 3.2.1 where the output is $y = k \times A$, the DC gain of LPF can be considered as

$$|H(0)| = k. \tag{5.1}$$

The frequency response is a more complex problem, and is related to the timing. Although the SQPW's response in time domain is carefully examined in Sec. 3.2.2, the understanding of frequency response can be simplified by an example as follows. Considering the SQPW's output, $y(t)$, reaches ckA at $t = T$ where $0 < c \leq 1$, the integral of Eq. (3.3) from $t = 0$ to T can be given by

$$ckA - (-kA) = \int_0^T (ay - by^3)dt + \int_0^T Adt, \tag{5.2}$$

where T is the specific time. In order to simplify Eq. (5.2), the output is assumed anti-symmetric, which makes the integral of y^3 zero. Thus, it can be written that

$1 < T/k \leq 2$ which shows that $T = 2k$ is the critical time for the output to be stable at the end of each pulse. Therefore, the SQPW passes the transmitted signal if $T_b \geq 2k$, which means that the cut-off frequency of the system is

$$f_c \leq 1/(2k). \tag{5.3}$$

5.3 Simulation Method and MRR

The design above can be verified by a simulation. This requires a specific treatment, known as SDEs, and needs to be considered in discrete time.

5.3.1 Heun Scheme

The output of the chosen SQPW evolves according to Eq. (3.3) which is a one dimensional SDE and can be solved by SDE integration schemes.

Firstly, it has to be written in the generic form that is given by $x = f(x) + g(x)\xi(t)$, where x represents y, $f(x) = ay - by^3 + s(t)$, $g(x) = \sqrt{N_0/2}$, and $\xi(t) \sim N(0, 1)$. Considering the discretization, the formal integration with the step size h is given by

$$x(h) - x(0) = \int_0^h (f(x) + g(x)\xi(t))dt. \tag{5.4}$$

Secondly, a method to solve this integral has to be chosen. In [51], SDE integration schemes; Euler Scheme, Exact Propagator, Heun Scheme and Full Algorithm are provided with their accuracies. Among those methods, the Heun scheme is considered since it promises a better accuracy and needs less computational effort. It is applied in two steps as,

$$x_1 = x(0) + \sqrt{\frac{N_0}{2}}Z(h) + hf(x(0)) \tag{5.5}$$

$$x(h) = x(0) + \sqrt{\frac{N_0}{2}}Z(h) + \frac{h}{2}(f(x_1) + f(x(0))) \tag{5.6}$$

where $Z(h)$ is a Gaussian random variable with zero mean and a variance which is equal to the step size h [51].

5.3.2 MRR without Noise

To verify the design, a pulse without the noise term is applied to make the output change from $-kA$ to kA, then the frequency response is obtained from $|H(f)| = |Y(f)|/|S(f)|$ by calculating the DFTs of both input and output.

As it is desired for the pulse to occur at the output, hereafter the potential barrier is eliminated by $a = 0$ and consequently there is no more restriction upon A. The fact is that increasing $|A|$ leads a to lose its effect on the output, and the minimum width of the well, that dominates the maximum output values, depends on b. Additionally, k is set to T_b/m where $m > 2$. Then, the simulation is carried out for different m parameters, which shows how the frequency response evolves.

The results are illustrated in Fig. 5.1. Defining $|H(f_c)|/k = 1/\sqrt{2}$ where f_c is the cut-off frequency, it is found that m shifts $|H(f)|/k$ and consequently the cut-off frequency is well-fitted by the expression

$$f_c \approx \frac{0.2047m}{T_b} \approx \frac{1}{5k}. \tag{5.7}$$

Here, Eq. (5.7) verifies via simulation that Eq. (5.3) is correct. Defining the bandwidth from DC to the first null in the frequency spectrum, $m = T_b/k \geq 5$ keeps the signal bandwidth in the pass-band.

By simulation, the design has been verified. It is found that the DC gain is $|H(0)| = k$ as determined previously where $T_b > 2k$. As can be seen, this is equal to Eq. (5.1), thus verifying its correctness. Moreover, decreasing k shifts the $|H(f)|$ curve towards higher frequencies.

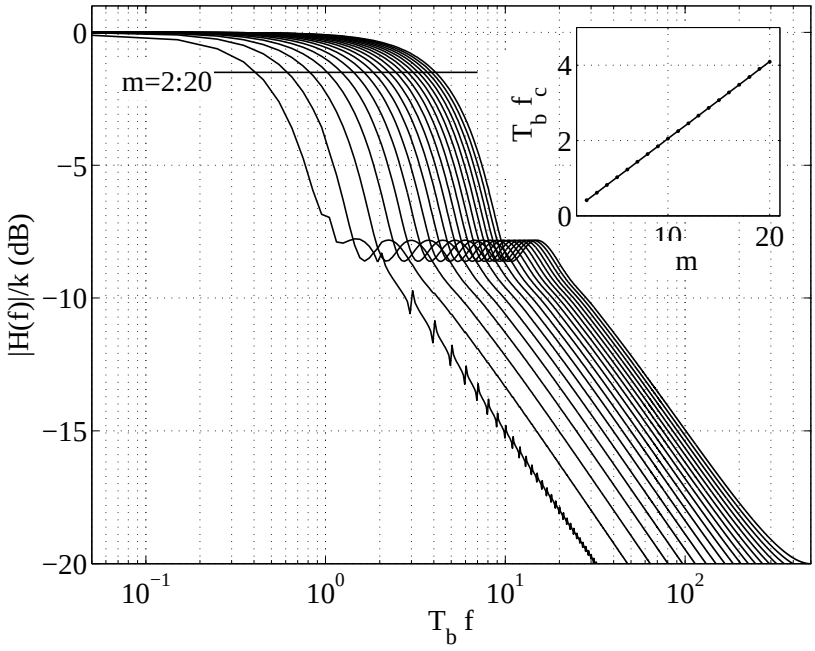

Figure 5.1: Normalised frequency response $|H(f)|/k$ where $a = 0$, $b = 1/(k^3A^2)$, $k = T_b/m$, $m = 2 : 20$ (from left to right). The input is $A = 1$, $T_b = 1$, and $t_s = T_b/10^3$. The insert gives the normalised cut-off frequencies of each curve.

5.3.3 MRR with Noise

The MRR is dependent on not only the transmitted signal but also the noise term. Although the noise term was not taken into account previously, those features of the MRR must be considered as references. When the noise term is considered, accordingly, the MRR changes.

To define the input noise power, the SNR per bit is used as the noise has an infinite number of frequency components. It is denoted by γ_b and given by $\mathcal{E}_b/N_0$ where $\mathcal{E}_b$ is the pulse energy and equals to A^2T_b for BPAM signal [1].

Then, in order to observe the effect of noise, the SQPW is simulated. The results are illustrated in Fig. 5.2. It shows that the slope in the attenuation band stays almost the same and the noise can decrease DC gain considerably.

The noise plays a significant role on f_c. Although the slope does not change,

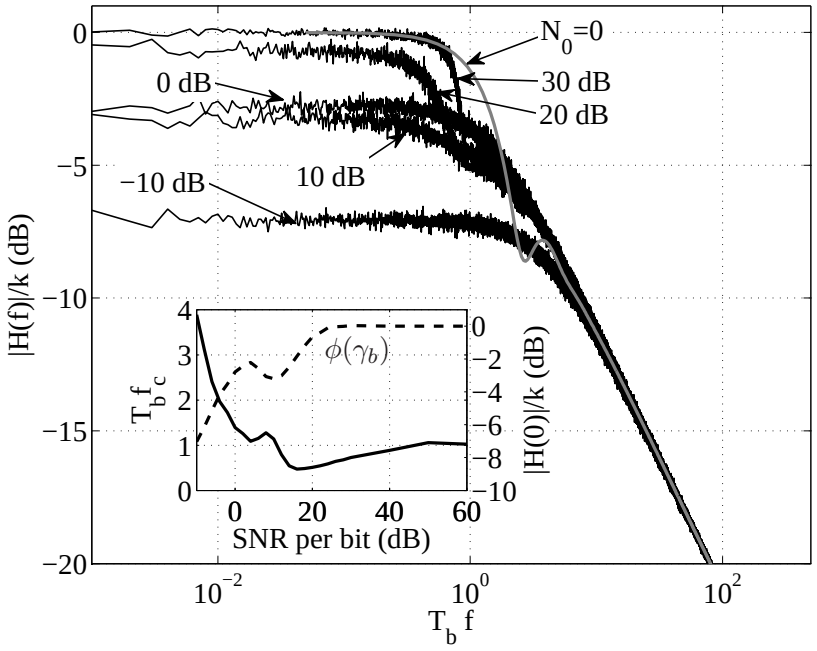

Figure 5.2: Normalised frequency response $|H(f)|/k$ where $a = 0$, $b = 1/(k^3A^2)$, $k = T_b/m$, $m = 5$, $A = 1$, $T_b = 1$, $\gamma_b = -10 : 10 : 30$ dB, and $t_s = T_b/10^3$. The insert illustrates the normalised cut-off frequencies (solid) and DC gain (dashed).

DC gain varies depending on γ_b. By definition, f_c is determined from $|H(f_c)| = |H(0)|/\sqrt{2}$. Thus, the cut-off frequency can be derived from

$$\frac{10\log(\phi(\gamma_b)) - 10\log(|H(0)|/k)}{\log(T_b f_c^N) - \log(T_b f_c^0)} \approx -10\frac{\text{dB}}{\text{decade}} \tag{5.8}$$

where $\phi(\gamma_b)$ is a function of γ_b, f_c^N and f_c^0 are the cut-off frequencies with and without noise respectively. Therefore, f_c can be written in a general form as

$$f_c = \frac{1}{ck\phi(\gamma_b)}, \tag{5.9}$$

where c is a coefficient. Assuming that $\phi(\gamma_b)$ is always positive and it tends towards 0 while decreasing γ_b, the noise increases f_c.

In concluding this key result, it implies that at high SNRs, the noise slightly

decreases f_c, whilst, at low SNRs, it decreases the DC gain and increases the cut-off frequency.

5.4 BER Performance of Receiver

5.4.1 The Effect of Cut-off Frequency

Besides the MRR, the error performance is also needed to validate the filtering capability of the SQPW. If the noise is filtered out, the output SNR must be greater than that of the input. As the output SNR is generally used to obtain the probability of error, the BER of SQPW can provide the SNR at the output. In order to reveal the BER performance of the receiver, it is simulated under various γ_b.

Assuming that transmitted signal power stays in $1/T_b$ bandwidth, for ideal case, the output SNR would be $\gamma_b T_b$ and increasing cut-off frequency only makes more of the noise component pass. If so, for the receiver, the output SNR can be given by $\mathrm{SNR_o} = \gamma_b / f_c$ where $f_c > 1/T_b$.

To verify this relation between $\mathrm{SNR_o}$ and f_c, the BER performance of the receiver is obtained by means of simulation. For each γ_b, simulations continue until the 100^{th} error occurs. The results are illustrated in Fig. 5.3 where the BER curves from left to right belong to the SQPW with increasing m parameter. The BER curves follow the same trend, shifted in m. This change in BER, corresponding to f_c given by Eq. (5.9), becomes more noticeable when the curve fitting is applied. It is found that the error probability P_e (also BER) curves are well-fitted by

$$P_e = \frac{1}{2}\exp\left(-\frac{\gamma_b}{(c_1 m + c_2)} - \frac{1}{c_3}\right), \tag{5.10}$$

where $c_1 = 0.2911$, $c_2 = 0.0424$, and $c_3 = 16.2$ with an RMSE = 0.06861 for the inside of the exponential. Fitted curves are also illustrated in Fig. 5.3. Considering

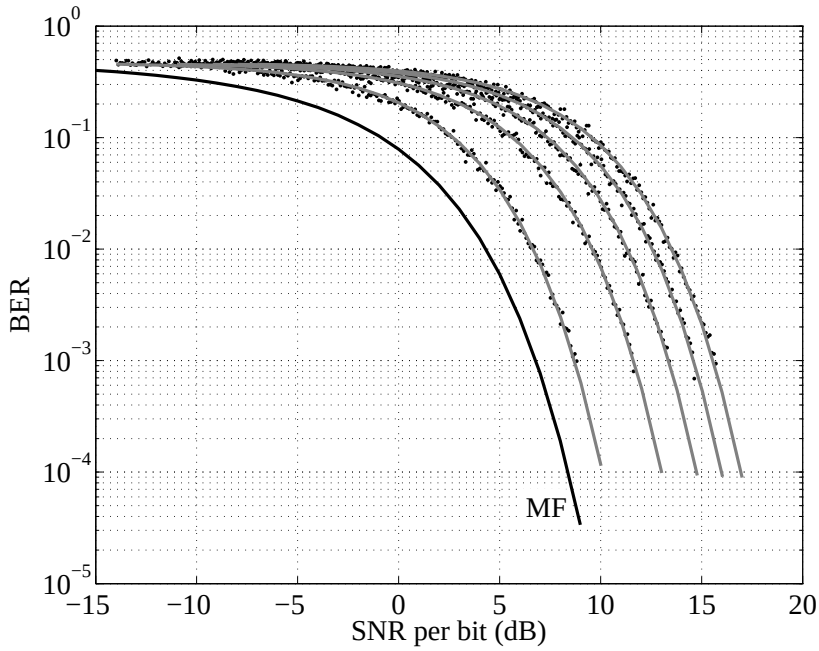

Figure 5.3: BER performance of the receiver where $a = 0$, $b = 1/(k^3A^2)$, $k = T_b/m$, $m = 4 : 4 : 20$ (from left to right), $A = 1$, $T_b = 1$, and $t_s = T_b/10^3$. The black curve with 'MF' mark illustrates BER performance of the receiver with the matched filter instead of the SQPW.

that $m > 2$ and $\gamma_b \gg c_1 m/c_3$, Eq. (5.10) can be rewritten as

$$P_e = \frac{1}{2}\exp\left(-\frac{\gamma_b}{c_f T_b f_c}\right), \tag{5.11}$$

where c_f, the filter coefficient, is about $0.2911/0.2047 = 1.422$. Note that, in general, the BER is a function of the output SNR in the form of mean over deviation. Therefore, $\gamma_b/(c_f T_b f_c)$ is directly related to the output SNR of the SQPW, which proves that the input signal frequency components below f_c passes. In addition to that, BER expression Eq. (5.11) is a supplement to the BER equation of PSR based receiver given in [62]. While the latter one is for the case where input is weak compared to the barrier potential $A \ll h_b$, the former one, Eq. (5.11), is for $A \gg h_b$.

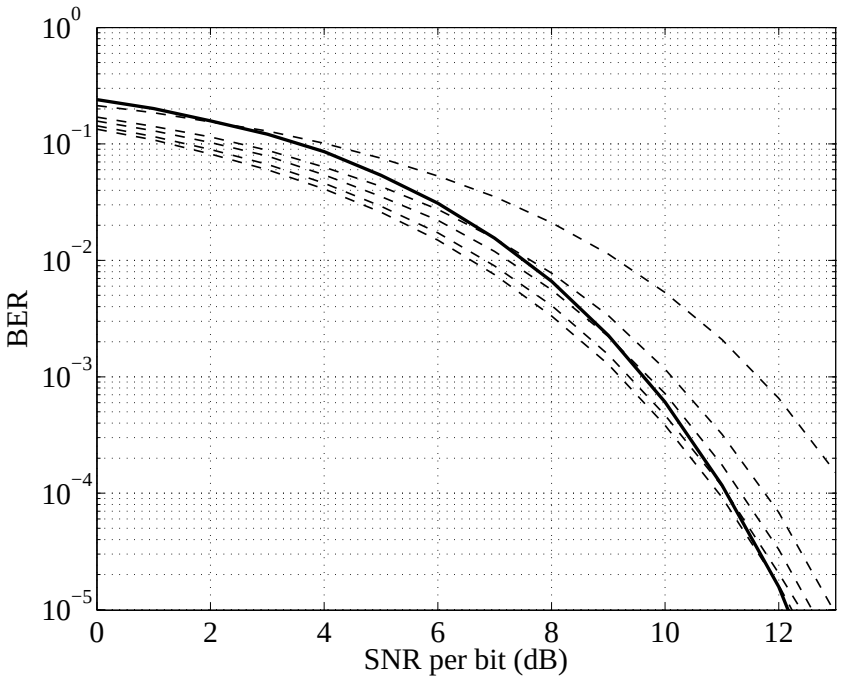

Figure 5.4: BER performances of the receiver accommodating either a SQPW (solid) or a Butterworth filter(dashed). The SQPW is with $a = 0$, $b = 1/(k^3A^2)$, $k = T_b/m$, $m = 5$, $A = 1$, $T_b = 1$, and low-pass Butterworth filters are with cut-off frequency $1/T_b$, and the orders $1 : 5$ (from right to left). The time step is $t_s = T_b/10^2$.

5.4.2 BER Comparison with Butterworth LPF

It has been shown that the output SNR is inversely proportional to the cut-off frequency. Now, it is desired to compare the SQPW with a conventional filter.

Considering Fig. 5.1 and Fig. 5.2, $(|H(f)|/k)^2$ has no ripples in the pass band, and in the stop band there is a -20 dB/decade slope like a 1^{st} order Butterworth filter. However, the SQPW's stop band consists of two slopes; the first slope starts from the -3 dB point, applies to a short frequency range, varies with SNR, and it is steeper than the seconds slope that is fixed at -20 dB/decade. This is an advantage of the SQPW at higher SNRs compared to the Butterworth filter having a cut-off frequency at -3 dB regardless of the filter order. On the other hand, the SNR dependency of its cut-off frequency becomes destructive at lower SNRs.

The effect of this SNR dependency can be observed from the BER perfor-

mance of the receiver accommodating a SQPW and a low-pass Butterworth filter separately. The results are illustrated in Fig. 5.4 and verify that, at SNRs lower than 2 dB, since a 1^{st} order Butterworth has a fixed cut-off frequency, less error occurs in the output, whilst the SQPW provides an error performance as good as a 5^{th} order Butterworth at SNRs higher than 12 dB.

5.5 Conclusions

In this chapter, a SQPW was designed as a low pass filter for use in BPAM receivers. The DC gain and cut-off frequency were defined and verified by the SDE simulation where the potential barrier was not present and where the SQPW was subject to only one pulse. Then, the effect of noise was examined and discussed. Following that, an expression for the error performance of BPAM receiver with a SQPW was obtained and compared with one having the Butterworth filter instead, which also validates the filtering capability of the SQPW.

As the SQPW is a non-linear system, these filter characteristics vary with input signals. In addition to that, the SR phenomenon was not observed, consequently the SQPW performance lags behind the matched filter because of having no potential barrier. However, such a SQPW becomes imperative if traditional ones can not be realised, even though its non-linearity and performance are not favourable when compared to the traditional signal processing methods.

As a result, the DC gain and cut-off frequency presented in this work provides a firm base for the studies on SQPW with pulse modulation methods. The use of SQPW as a filter is revealed for the cases where the input dominates the potential barrier, so that the design provides an over-all noise suppression.

The possible further directions can be; investigating the effect of barrier on the MRR and connecting that effect with SR phenomenon, comparing the performances of different pulse modulation methods, and seeking an alternative decision

making strategy.

Chapter 6

Derivation of Waveforms

6.1 Introduction

Throughout the previous chapters, it has been shown that a certain fluctuation on the input signal which is either deterministic or stochastic, helps in extracting more information from the output. The aim was to increase the input by adding a fluctuation in order to overcome the limits; the system barrier and long transition period. However, these limits can be considered as design parameters for the modulation and coding processes owing to the fact that the system equation has a cubic term which indicates the self modulation.

The modulation is performed by the means of system roots. As mentioned before, DWP has three roots; one is always real and others are either real or complex roots depending on the input strength. As a result of this, a set of root dependent waveforms occurs. The output is composed of corresponding waveforms defined by the input from this set.

When there are three real roots, the output settles down at one of two possible levels based on previous output level. Having that information, it means the output has at least one bit redundancy. Therefore, the coding property can be seen as a recursive convolutional encoding.

In this chapter, in order to evaluate the output of DWP, the expressions of roots dependent waveforms are going to be presented under adequate approximations by attempting to solve system's DE. In other words, the waveforms composing DWP's output are expressed by functions of the input signal, time, and initial condition.

6.2 Homogeneous ODE

The expression given for DWP is a stochastic non-linear partial differential equation (PDE). A system driven by DWP has a response that varies from one input signal to another. It also depends on the past values and those in turn determines the asymptotes restricting the output's value. Here, the evaluation will begin by starting with simplifying the equation, and then finding approximate expression for the waveforms. These expressions are going to provide a novel solution and to help to perceive the potential of modulation capability.

The response of DWP evolves depending on initial conditions, input signal and the time. A function of only these ingredients for the system response can be written by the means of the roots; such that, a simple arrangement provides a promising first order non-linear ordinary differential equation (ODE).

The homogeneous form of DWP's DE is obtained by setting the input $x = 0$. Although it has a trivial solution, the analysis of that solution is not the same due to the fact that its Fourier transform ends up with hyper-geometric functions. However, for evaluating the modulation capability, it provides the waveforms assigned to the input zero, and they are different in phases and frequencies.

$$\frac{dy}{dt} = ay - by^3 + x \tag{6.1}$$

Firstly, the DE given above needs to be solved in order to determine the waveforms.

The solution for $x = 0$ can be obtained by separation of variables;

$$\begin{aligned}
\tfrac{dy}{dt} &= ay - by^3 \\
&= by(\sqrt{a/b} - y)(\sqrt{a/b} + y) \\
&= \tfrac{b}{\frac{b/a}{y} + \frac{-b/2a}{y-\sqrt{a/b}} + \frac{-b/2a}{y+\sqrt{a/b}}} \\
&= \tfrac{2a}{\frac{d}{dy}\ln\left|\frac{y^2}{y^2-\frac{a}{b}}\right|} \\
\tfrac{dy}{dt}\tfrac{d}{dy}\ln\left|\tfrac{y^2}{y^2-\frac{a}{b}}\right| &= 2a \\
\tfrac{d}{dt}F &= 2a \text{ where } F = \ln\left|\tfrac{y^2}{y^2-a/b}\right|,
\end{aligned} \tag{6.2}$$

then,

$$\begin{aligned}
\textstyle\int \frac{d}{dt}F\ dt &= \textstyle\int 2a\ dt \\
F(t) - F(t=0) &= 2at - 0 \\
F(t) &= F_0 + 2at \\
\tfrac{y^2}{y^2-a/b} &= \mathrm{sgn}(y_0^2 - a/b)e^{F_0+2at} \\
y^2 &= \tfrac{a/b}{1-\mathrm{sgn}(y_0^2-a/b)e^{-F_0-2at}}.
\end{aligned} \tag{6.3}$$

As a result, the expression for y can be written as below and it gives real values when $t \geq 0$.

$$y(t) = \mathrm{sgn}(y_0)\Big(\frac{a/b}{1 - \mathrm{sgn}(y_0^2 - a/b)e^{-F_0-2at}}\Big)^{1/2} \tag{6.4}$$

The same solution can be derived by reducing the DE to a linear one. As this DE is also a Bernoulli Differential Equation, manipulating the derivative by substitution $y = e^w/\sqrt{u}$ should give Eq. (6.1);

$$\begin{aligned}
ay - by^3 &= \tfrac{dy}{dt} \\
&= w'\tfrac{e^w}{\sqrt{u}} - \tfrac{u'}{2}\tfrac{e^w}{(\sqrt{u})^3} \\
&= w'y - \tfrac{u'}{2}e^{-2w}y^3
\end{aligned} \tag{6.5}$$

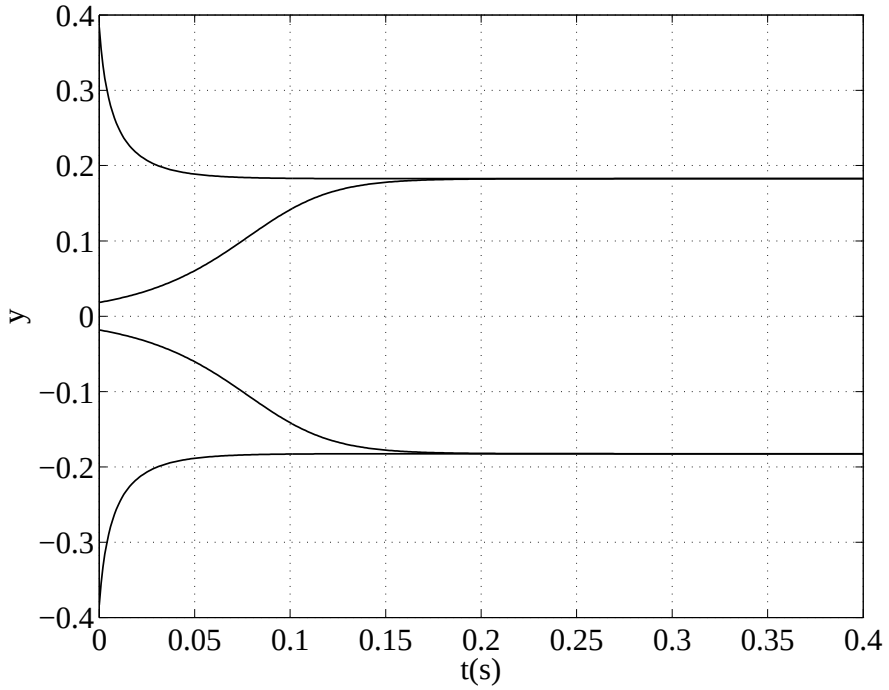

Figure 6.1: The output curves obtained from Eq. (6.4), where $m = 5$, $ak = 5$, $A = 1$, $T_b = 1s$. The initials are $y_0 = \pm 2.1\sqrt{a/b}, \pm 0.1\sqrt{a/b}$

then, the result is a system of DEs;

$$\begin{aligned} \frac{dw}{dt} &= a \\ \frac{du}{dt} &= 2be^{2w} \end{aligned} \tag{6.6}$$

which can be easily solved and provides the solution when w and u are placed back into the dummy function.

$$y = \frac{e^{at+c_1}}{\sqrt{\frac{b}{a}e^{2(at+c_1)}+c_2}} \tag{6.7}$$

Obviously, Eq. (6.7) is equivalent to Eq. (6.4), and the constants c_1 and c_2 can be determined. These equations are also the waveforms as they are assigned to one single input $x = 0$, which makes this process more accurately called modulation.

For the case where input $x = 0$, the waveforms in time domain are illustrated in Fig. 6.1. It shows two stable states, and how the output approaches them. When y_0 is greater than the stable state in magnitude, it needs less time to settle and the

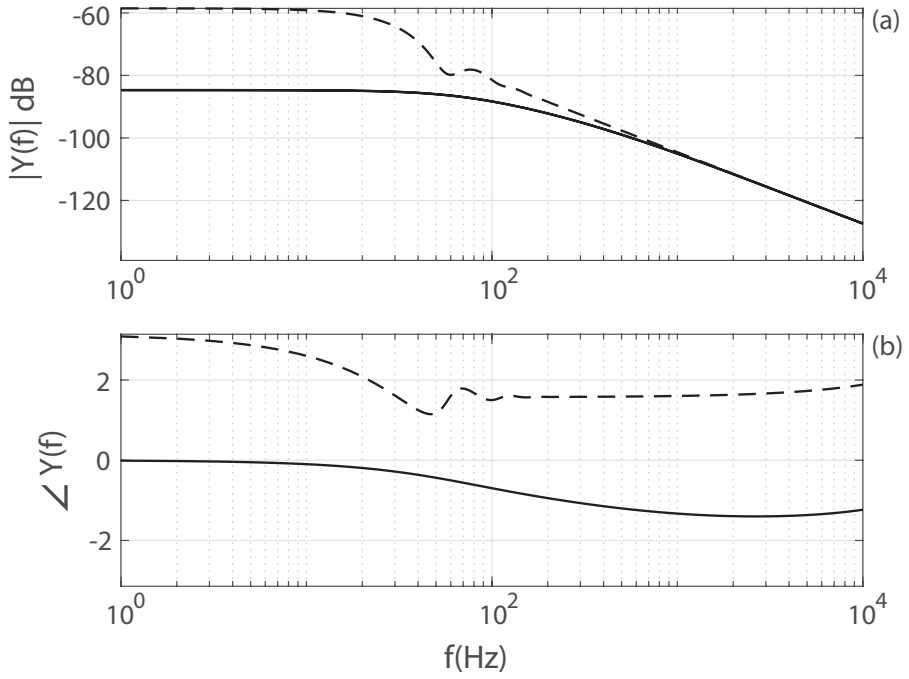

Figure 6.2: The phase and frequency spectrum of waveforms obtained from Eq. (6.4), where $m = 5$, $ak = 5$, $A = 1$, $T_b = 1s$. The initials are $y_0 = 1.99\sqrt{a/b}$ (solid), $0.01\sqrt{a/b}$ (dashed).

derivative is monotonic, otherwise, settling takes more time and the derivative is not monotonic.

The phase and frequency spectrum of these waveforms are also illustrated in Fig. 6.2. In order to make an adequate comparison, the initial outputs are set to the same distance from the stable state, namely; $\pm 0.99\sqrt{a/b}$, and then, the waveform, which settles in a short period, is modified to make both have the same start and end values in time. Finally, DFTs are calculated.

Fig. 6.2 shows that there is almost a 30 dB difference in magnitude at low frequency range, while the high frequency components are almost the same. On the other hand the difference between their -3 dB points is about 70 Hz. This is due to the transition periods and shapes. For example, in Fig. 6.1, these periods are 0.05 and 0.15 s, so it is expected for the first one to have three times more bandwidth. In addition to that, the shapes are approximately like a spike and a ramp, therefore,

spike one's energy in respect of the steady state is less than the ramp one as seen in the frequency spectrum.

As a result, even if the input is zero, there are 4 alternative waveforms that output can have. These are different in phase, frequency, and energy. The choice is based on the initial condition, which means that this is a modulation scheme with memory. Certainly, one single input is not the case for communication, so following this, the inhomogeneous DE needs to be solved.

6.3 Inhomogeneous ODE

Considering that x is not zero but a constant, the r.h.s of Eq. (6.1) still has three roots. However, depending on the value of x, there is at least one real root, and the other two may have imaginary parts. This happens when the constant is greater than the barrier, $|x| > h_b$. Nevertheless, the output still evolves in one particular direction and that can be obtained by applying the same methods.

6.3.1 Separation of Roots

But, first, the roots needs to be known. The r.h.s of Eq. (6.1) is a so-called *depressed cubic*, $y^3 + py + q = 0$, and with the help of *Cardano's formula*; the roots can be given by

$$\begin{aligned} r_l = \quad & \left(\tfrac{-1+\sqrt{-3}}{2}\right)^l \sqrt[3]{-\tfrac{q}{2} + \sqrt{\tfrac{q^2}{4} + \tfrac{p^3}{27}}} \\ & + \left(\tfrac{-1+\sqrt{-3}}{2}\right)^{2l} \sqrt[3]{-\tfrac{q}{2} - \sqrt{\tfrac{q^2}{4} + \tfrac{p^3}{27}}}, \end{aligned} \tag{6.8}$$

where $l = 0, 1, 2$, and an alternative representation can be

$$\begin{aligned} r_1 &= u_+ + u_- & & & u_+ &= \tfrac{1}{\sqrt[3]{2b}} \sqrt[3]{x + \sqrt{x^2 - h_b^2}} \\ r_2 &= zu_+ + \overline{z}u_- & \text{where} & & u_- &= \tfrac{1}{\sqrt[3]{2b}} \sqrt[3]{x - \sqrt{x^2 - h_b^2}} \\ r_3 &= \overline{z}u_+ + zu_- & & & z &= \tfrac{-1+\sqrt{-3}}{2} \end{aligned} \tag{6.9}$$

Additionally, note that there are some algebraic relations between roots as follows;

$$r_2 + r_3 = -r_1 \tag{6.10a}$$

$$r_1^2 = u_+^2 + u_-^2 + 2\frac{a}{3b} \tag{6.10b}$$

$$r_2 r_3 = u_+^2 + u_-^2 - \frac{a}{3b} = r_1^2 - \frac{a}{b} \tag{6.10c}$$

$$u_+ u_- = \frac{a}{3b} \tag{6.10d}$$

These roots appear in Eq.(6.1) as below;

$$\begin{aligned} \tfrac{dy}{dt} &= -b(y - r_1)(y - r_2)(y - r_3) \\ &= -b(y - r_1)(y^2 + r_1 y + r_1^2 - \tfrac{a}{b}) \\ &= -b(y - r_1)(y - r_1 z_-)(y - r1 z_+) \\ &= \left(\tfrac{A}{y - r_1} + \tfrac{B}{y - r_1 z_-} + \tfrac{C}{y - r_1 z_+}\right)^{-1} \end{aligned} \tag{6.11}$$

where,

$$r_1 z_\pm = -\frac{r_1}{2} \pm \sqrt{\frac{a}{b} - \frac{3}{4} r_1^2} = -\frac{r_1}{2} \pm w \tag{6.12a}$$

$$w = \sqrt{a/b - 3r_1^2/4} \tag{6.12b}$$

$$A, B, C = (a - 3b r_{1,2,3}^2)^{-1} \tag{6.12c}$$

$$B, C = A\Big(-\frac{1}{2} + \frac{3r_1}{4w}\Big), A\Big(-\frac{1}{2} - \frac{3r_1}{4w}\Big) \tag{6.12d}$$

and, r_1 is set to be the always real root. To satisfy $|r_1| > |r_{2,3}|$,

$$r_1 = \frac{\mathrm{sgn}(x)}{\sqrt[3]{2b}} \left[\sqrt[3]{|x| + \sqrt{x^2 - h_b^2}} + \sqrt[3]{|x| - \sqrt{x^2 - h_b^2}} \right] + \delta(x)\sqrt{\tfrac{a}{b}} \tag{6.13}$$

As the roots are defined into a standard form, and their relations are given,

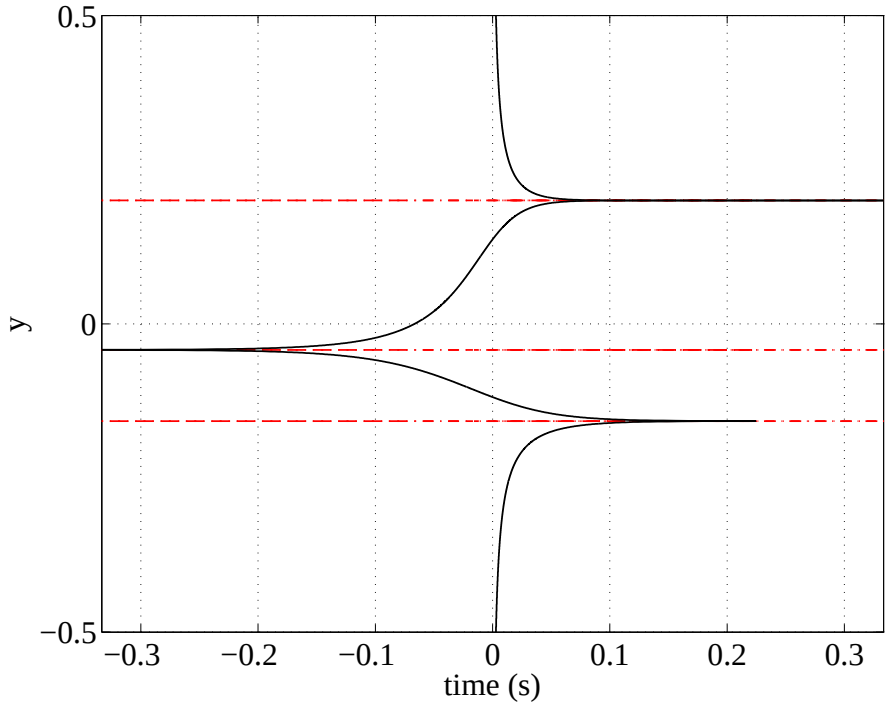

Figure 6.3: The function of time $t(y)$ given by Eq. (6.14), where $m = 5$, $ak = 5$, $A = 1$, $T_b = 1s$, $y = 2.5[-r_1, r_1]$.

a time function $t(y)$ can be derived from Eq. (6.11);

$$\begin{aligned} \frac{dt}{dy} &= A\frac{d}{dy}\ln|y-r_1| + B\frac{d}{dy}\ln|y-r_2| + C\frac{d}{dy}\ln|y-r_3| \\ t &= (-B-C)\ln|y-r_1| + B\ln|y-r_2| + C\ln|y-r_3| \\ &= A\Big(-\tfrac{1}{2}+\tfrac{3r_1}{4w}\Big)\ln|\tfrac{y+r_1/2+w}{y-r_1}| + A\Big(-\tfrac{1}{2}-\tfrac{3r_1}{4w}\Big)\ln|\tfrac{y+r_1/2-w}{y-r_1}| \end{aligned} \tag{6.14}$$

For the case where all roots are real, Eq. (6.14) is illustrated in Fig. 6.3. It can be seen that there are three horizontal asymptotes which correspond to the roots of the system, and the time t increases while y moves towards to the stable roots.

6.3.2 Transformation

However, in order to define the waveforms associated with the constant input, x in Eq.(6.1), the output y needs to be given as a function of time $y(t)$. To do so, Eq.

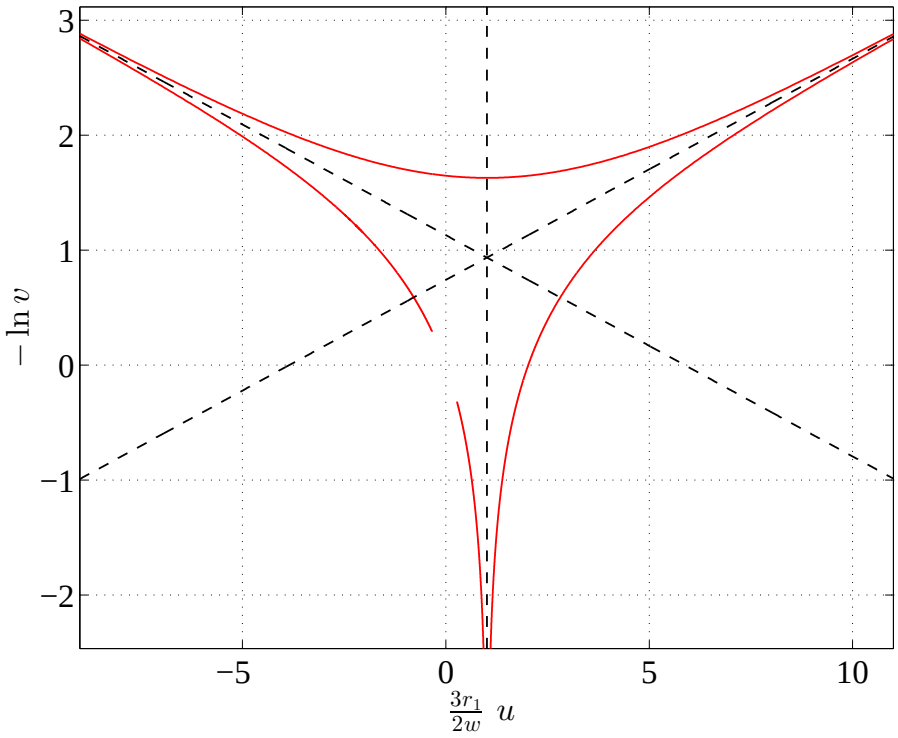

Figure 6.4: The relation between two functions given by Eq. (6.16), where $m = 5$, $ak = 5$, $A = 1$, $T_b = 1s$, $y = 5[-r_1, r_1]$.

(6.14) can be transformed by the expression

$$\begin{aligned} |\tfrac{y+r_1/2}{y-r_1} + \tfrac{w}{y-r_1}| &= ve^{u} \\ |\tfrac{y+r_1/2}{y-r_1} - \tfrac{w}{y-r_1}| &= ve^{-u} \end{aligned} \tag{6.15}$$

where

$$\begin{aligned} v &= \left|\left(\tfrac{y+r_1/2}{y-r_1}\right)^2 - \left(\tfrac{w}{y-r_1}\right)^2\right|^{1/2} \\ u &= \tfrac{1}{2}\ln\left|\tfrac{y+r_1/2+w}{y+r_1/2-w}\right| \end{aligned} \tag{6.16}$$

then Eq. (6.14) becomes

$$\begin{aligned} t/A &= \ln\left[(ve^{u})^{-\frac{1}{2}+\frac{3r_1}{4w}}(ve^{-u})^{-\frac{1}{2}-\frac{3r_1}{4w}}\right] \\ &= -\ln v + \tfrac{3r_1}{2w}u. \end{aligned} \tag{6.17}$$

As a result, the time, t, becomes simply a sum of two functions of y, namely;

$\ln v$ and u. These have a non-linear relation, and one can be expressed by a function of another. This is illustrated in Fig. 6.4 which shows the asymptotes of these relations. As y has three real roots, there are three asymptotes. The vertical one belongs to the biggest root r_1 which is always real. The one on the left comes from the second biggest root, and the third is from the root close to the zero.

In order to make the r.h.s. of Eq. (6.17) have a single variable either u or $-\ln v$, the asymptotes can be used to transform one into another, and those can be derived from

$$\begin{aligned} -\ln v &= -\tfrac{1}{2}\ln\left|\tfrac{y+r_1/2+w}{y-r_1}\right| - \tfrac{1}{2}\ln\left|\tfrac{y+r_1/2-w}{y-r_1}\right| \\ u &= \tfrac{1}{2}\ln\left|\tfrac{y+r_1/2+w}{y-r_1}\right| - \tfrac{1}{2}\ln\left|\tfrac{y+r_1/2-w}{y-r_1}\right| \end{aligned} \tag{6.18}$$

The vertical asymtote, VA, where $y = r_1$, is

$$\begin{aligned} -\ln v &\longrightarrow -\infty \\ c_1 &= \tfrac{1}{2}\ln\left|\tfrac{y+r_1/2+w}{y+r_1/2-w}\right|_{y=r_1} \\ VA : u &= c_1, \end{aligned} \tag{6.19}$$

and, the oblique asymptotes OAs can be given as below. The OA on the r.h.s of Fig. 6.4 is for $y = -r_1/2 + w$, as;

$$\begin{aligned} -\ln v \longrightarrow \infty &\ , \ u \longrightarrow \infty \\ c_2 &= \ln\left|\tfrac{y+r_1/2+w}{y-r_1}\right|_{y=-r_1/2+w} \\ OA : -\ln v &= u - c_2. \end{aligned} \tag{6.20}$$

The OA on the l.h.s of Fig. 6.4 is for $y = -r_1/2 - w$;

$$\begin{aligned} -\ln v \longrightarrow \infty &\ , \ u \longrightarrow -\infty \\ c_3 &= \ln\left|\tfrac{y+r_1/2-w}{y-r_1}\right|_{y=-r_1/2-w} \\ OA : -\ln v &= -u - c_3. \end{aligned} \tag{6.21}$$

These three asymptotes intersect each other at the same point;

$$(u, -\ln v) \quad = (c_1, c_1 - c_2). \tag{6.22}$$

These asymptotes also belong to two logarithmic functions, namely; ln(cosh(.)) and ln(sinh(.)), which can be derived from Eq. (6.15) as well, and can be given by

$$-\ln v = \begin{cases} \ln\left(\cosh(u - c_1)\right) - c_s, & r_3 > y > r_2 \\ \ln|\sinh(u - c_1)| - c_s, & \text{elsewhere} \end{cases} \tag{6.23}$$

where $c_s = \ln|\sinh(0 - c_1)|$ and $r_1 > 0 > r_3 > r_2$. Before attempting to place these expressions into Eq. (6.17) in order to derive $y(t)$, the second case, where only one of the roots is real, needs to be given. To do so, the same steps are followed and similar results are obtained;

$$-\ln v = \ln|\sin(u^* - c_1^*)| - c_s^* \tag{6.24}$$

where $u^* = \arctan(-iw/(y + r_1/2))$, $c_1^* = u^*(y = r_1)$, and $c_s^* = \ln|\sin(c_1^*)|$, and finally, Eq. (6.17) needs to be modified as

$$t/A = -\ln v + \frac{3r_1}{-2iw}(u^* + c_\pi), \text{where} \;\; c_\pi = \begin{cases} \pi, & u^* < 0 \\ 0, & u^* \geq 0 \end{cases} \tag{6.25}$$

Up to this point, the time function $t(y)$ is derived from the inhomogeneous ODE, Eq. (6.14), then transformed into Eq. (6.17) by applying Eq. (6.16). Following that, the relation between variables used for transformation is clarified by Eq. (6.23) and Eq. (6.24). As a result, t can be expressed by a function of one variable, u. However, its inverse, $u(t)$, is unknown, so the asymptotes given above are going to used for inversion by introducing relevant hyperbolas.

6.3.3 Inverse Function

The first case is when $-\ln v = \ln(\cosh(u - c_1)) - c_s$. Defining $Y = -\ln v - (c_1 - c_2)$ and $X = u - c_1$ moves the asymptotes' centre to the origin. Then, the curve is assumed to be a hyperbola given by

$$\begin{aligned} Y^2 - X^2 &= d^2 \\ Y &= \sqrt{X^2 + d^2} \end{aligned} \tag{6.26}$$

where $d^2 = (-cs - (c1 - c2))^2$, if so, the inverse of Eq. (6.17) can be derived as;

$$\begin{aligned} \tfrac{t}{A} &= \sqrt{(u - c_1)^2 + d^2} + (c_1 - c_2) + \tfrac{3r_1}{2w}u \\ 0 &= k_1 u^2 + k_2 u + k_3, \text{where} \begin{cases} k_1 &= (1 - \frac{9r_1^2}{4w^2}) \\ k_2 &= \frac{3r_1}{w}(\frac{t}{A} - (c_1 - c_2)) - 2c_1 \\ k_3 &= c_1^2 + d^2 - (\frac{t}{A} - (c_1 - c_2))^2 \end{cases} \\ u_+ &= \tfrac{1}{2k_1}\Big(- k_2 + \sqrt{k_2^2 - 4k_1k_3}\Big) \end{aligned} \tag{6.27}$$

which provides one of the waveforms as below;

$$\begin{aligned} \tfrac{1}{2}\ln\Big(\tfrac{y - r_2}{r_3 - y}\Big) &= \tfrac{1}{2k_1}\Big(- k_2 + \sqrt{k_2^2 - 4k_1k_3}\Big), \text{where} |r_1| > |r_2| > |r_3| \\ y_{23}(t) &= r_3 + \frac{r_2 - r_3}{1 + \exp\Big(-\frac{k_2}{k_1} + \frac{1}{k_1}\sqrt{k_2^2 - 4k_1k_3}\Big)} \end{aligned} \tag{6.28}$$

The second case is $-\ln v = \ln|\sinh(u - c_1)| - c_s$. This time, one asymptote is Y axis, so the previous hyperbola is replaced with;

$$\begin{aligned} Y &= X - \tfrac{d_2}{X} \\ X &= \tfrac{1}{2}(Y + \sqrt{Y^2 + 4d_2}) \end{aligned} \tag{6.29}$$

where $d_2 = (2c_1 - c_2)c_1$ and $u > c_1$. Then, the inverse can be obtained from Eq.

(6.17);

$$\begin{aligned}
\tfrac{t}{A} &= Y + (c_1 - c_2) + \tfrac{3r_1}{2w}\tfrac{1}{2}(Y + \sqrt{Y^2 + 4d_2} + c_1) \\
0 &= k_1 Y^2 + k_2 Y + k_3, \text{where} \begin{cases} k_1 &= (1 + \tfrac{3r_1}{2w}) \\ k_2 &= -(k_1 + 1)(\tfrac{t}{A} - (c_1 - c_2) - \tfrac{3r_1}{2w} c_1) \\ k_3 &= (\tfrac{t}{A} - (c_1 - c_2) - \tfrac{3r_1}{2w} c_1)^2 - \tfrac{9r_1^2}{4w^2} d_2 \end{cases} \\
Y_- &= \tfrac{1}{2k_1}\left(- k_2 - \sqrt{k_2^2 - 4k_1 k_3} \right) \\
&= -\ln v - (c1 - c2)
\end{aligned} \tag{6.30}$$

which provides another waveform as below;

$$\begin{aligned}
-\ln v &= \tfrac{1}{2k_1}\left(- k_2 - \sqrt{k_2^2 - 4k_1 k_3} \right) + (c1 - c2) \\
\tfrac{(y + r_1/2)^2 - w^2}{(y - r_1)^2} &= e^\theta, \text{where } \theta = \tfrac{1}{k_1}\Big(k_2 + \sqrt{k_2^2 - 4k_1 k_3} \Big) - 2(c1 - c2) \\
y_{13}(t) &= \tfrac{1}{2(1 - e^\theta)}\Big(- r_1(1 + 2e^\theta) + \sqrt{r_1^2(1 + 2e^\theta)^2 - 4(1 - e^\theta)(r_1^2(1 - e^\theta) - a/b)} \Big)
\end{aligned} \tag{6.31}$$

In the same way,

$$\begin{aligned}
\tfrac{t}{A} &= Y + (c_1 - c_2) + \tfrac{3r_1}{2w}(-\tfrac{1}{2}Y - \tfrac{1}{2}\sqrt{Y^2 + 4d_2} + c_1) \\
0 &= k_1 Y^2 + k_2 Y + k_3, \text{where} \begin{cases} k_1 &= (1 - \tfrac{3r_1}{2w}) \\ k_2 &= -(k_1 + 1)(\tfrac{t}{A} - (c_1 - c_2) - \tfrac{3r_1}{2w} c_1) \\ k_3 &= (\tfrac{t}{A} - (c_1 - c_2) - \tfrac{3r_1}{2w} c_1)^2 - \tfrac{9r_1^2}{4w^2} d_2 \end{cases} \\
Y_\pm &= \tfrac{1}{2k_1}\left(- k_2 \pm \sqrt{k_2^2 - 4k_1 k_3} \right), \\
\theta_\pm &= -2Y_\pm - 2(c_1 - c_2) \\
y_*(t) &= \tfrac{-1}{2(1 - e^\theta)}\Big(r_1(1 + 2e^\theta) + \sqrt{r_1^2(1 + 2e^\theta)^2 - 4(1 - e^\theta)(r_1^2(1 - e^\theta) - a/b)} \Big)
\end{aligned} \tag{6.32}$$

where $*$ stands for the outer root choice. For r_1 or 1, the θ_+ is put into the r.h.s., and, for r_2, θ_- is used.

The hyperbolas given by Eq. (6.26) and Eq. (6.29) are shown in Fig. 6.5.

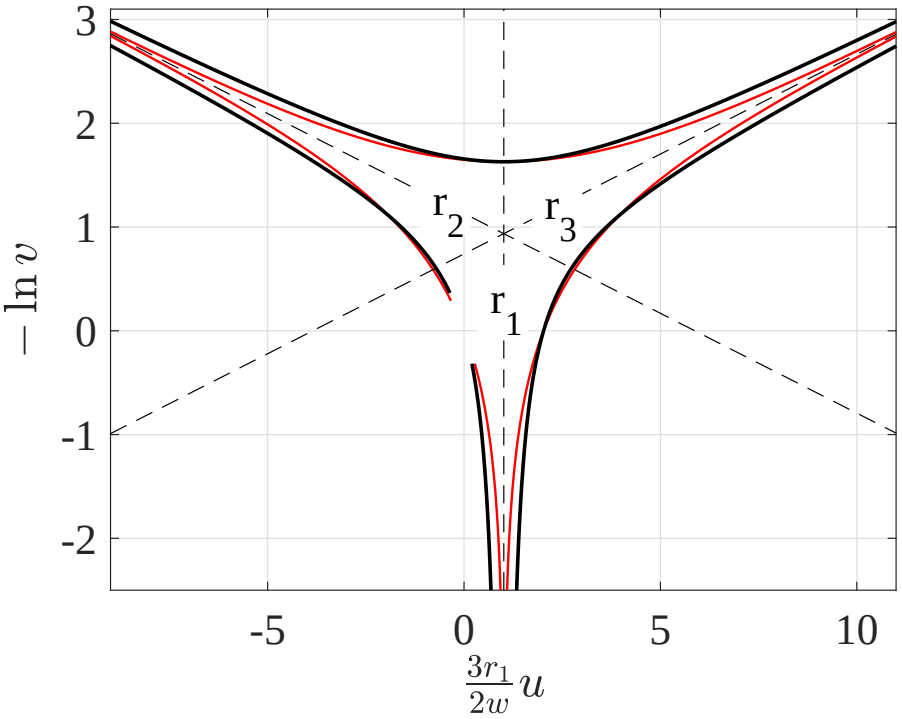

Figure 6.5: The hyperbolas(black) modelling the curves of $(-\ln v, u)$ (red), where $m = 5$, $ak = 5$, $A = 1$, $T_b = 1s$, $y = 5[-r_1, r_1]$.

It can be seen that the exact curves of $(-\ln v, u)$ and the hyperbolas have similar patterns approaching corresponding asymptotes. They intersect each other at the points set by d and d_2. Increasing the number of such point can make the hyperbolas closer to the exact curves. However, this also ends up with three or higher degree polynomials of $-\ln v$ and u.

A higher degree polynomial may not be necessary at this point because the output functions, $y_*(t)$s, give almost the exact (y, t) curves as in Fig. 6.6. In addition, for the higher ak, the outputs, $y_*(t)$s, are so close to those obtained from $t(y)$ that the dummy function method, used in Subsection 6.2, may provide more details on $y(t)$.

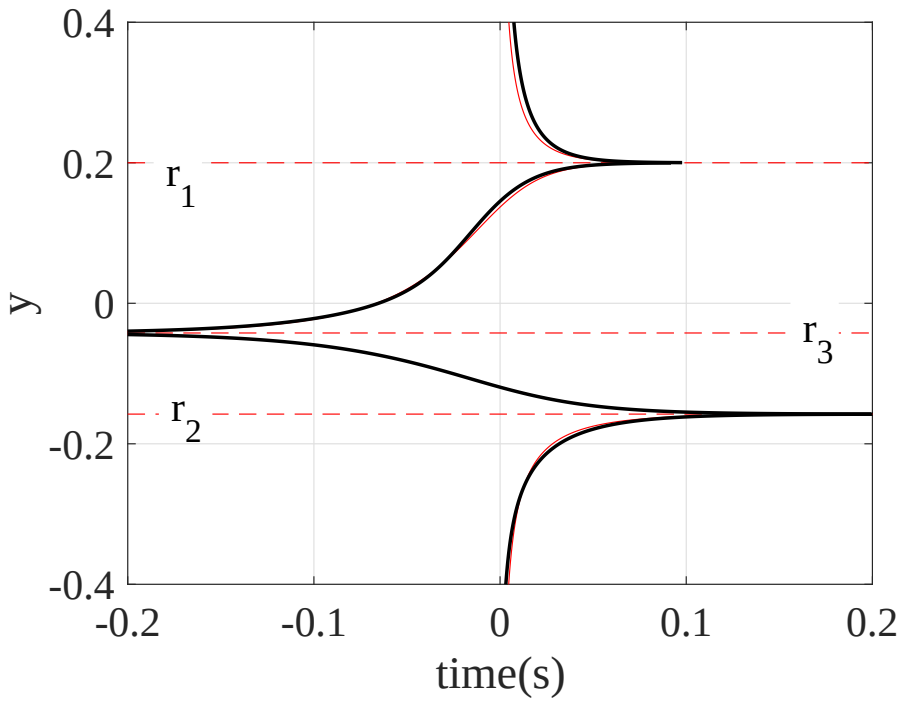

Figure 6.6: The output $y(t)$(black) compare to $t(y)$(red), where $m = 5$, $ak = 5$, $A = 1$, $T_b = 1s$, $y = 5[-r_1, r_1]$.

6.3.4 Dummy Function

The dummy function method is a powerful tool. The homogeneous ODE is solved by both root separation and dummy function methods. For an inhomogeneous ODE, although the former method has allowed us to derive an approximate $y(t)$, it fails when roots cannot be defined. Compared to that, the dummy function is capable of solving the Bernoulli ODEs without any linearisation as shown for a homogeneous case, the derivation of Eq. (6.7). However, the dummy function method needs the ODE in a homogeneous form, therefore the constant, x, is replaced by one of the root form; $x = -ar_1 + br_1^3$, and the output variable is changed with $y = g + r_1$ to

find a homogeneous form.

$$\begin{aligned}
\tfrac{dy}{dt} &= ay - by^3 + x \\
\tfrac{d(g+r_1)}{dt} &= a(g+r_1) - b(g+r_1)^3 - ar_1 + br_1^3 \\
\tfrac{d(g+r_1)}{dt} &= ag + ar_1 - b(g^3 + r_1^3 + 3r_1^2 g + 3r_1 g^2) - ar_1 + br_1^3 \\
\tfrac{dg}{dt} &= (a - b3r_1^2)g - b3r_1 g^2 - bg^3
\end{aligned} \tag{6.33}$$

If it is assumed that g is a product of single variable functions whose derivatives are a product of derivative of the corresponding variable and power of those functions, a system with simpler ODEs can be built. For example, considering a variable, $w(t)$, is a function of t, and a exponential function of which, $z(w) = e^w$, then, the derivative of z with respect to t gives

$$z = e^{w(t)},\ z' = w'z. \tag{6.34}$$

For other powers,

$$\begin{aligned}
z = \tfrac{1}{w} &\ ,\ z' = -w'z^2 \\
z = \tfrac{1}{\sqrt{w}} &\ ,\ z' = -\tfrac{w'}{2}z^3 \\
z = \tfrac{1}{\sqrt[3]{w}} &\ ,\ z' = -\tfrac{w'}{3}z^4 \\
z = w^k &\ ,\ z' = w'kz^{\frac{k-1}{k}}, k \neq 1
\end{aligned} \tag{6.35}$$

There are 2 and 3 powers of g in Eq. (6.33). So, the dummy function needs to have three variables; w, v, u, in the power related forms; e^w, $1/v$, $1/\sqrt{u}$. Then, assuming that g is equal to the dummy function that is the product of those variable functions;

$$g = e^w\ \frac{1}{v}\ \frac{1}{\sqrt{u}}, \tag{6.36}$$

and its derivative;

$$\frac{dg}{dt} = w'\frac{e^w}{v\sqrt{u}} - \frac{v'}{v^2}\frac{e^w}{\sqrt{u}} - \frac{v'}{2(\sqrt{u})^3}\frac{e^w}{v}. \tag{6.37}$$

It is also assumed that the derivative of dummy function with respect to t

is also equal to the derivative of g. But, first, it needs to be written in the same polynomial form. To do that, the variables which are with their own derivatives can be replaced by corresponding g representations obtained from Eq. (6.36) without moving the derivatives, which results in

$$\frac{dg}{dt} = w'g - v'\frac{\sqrt{u}}{e^w}g^2 - \frac{u'}{2}\frac{v^2}{e^{2w}}g^3. \tag{6.38}$$

In the case of these coefficients being equal to those of Eq. (6.33), three DEs can be obtained;

$$\begin{aligned} w' &= (a - b3r_1^2), \\ v' &= 3br_1\tfrac{e^w}{\sqrt{u}}, \\ u' &= 2b\tfrac{e^{2w}}{v^2}. \end{aligned} \tag{6.39}$$

It can be seen that w does not vary with v or u, but t. So, if v and u can be expressed as a function of w, then the dummy function will be the solution to the inhomogeneous first order non-linear ODE.

The transitive relation between v and u can be resolved by dividing one by another and making the derivatives include their own variables. Such that;

$$\frac{u'}{v'} = \frac{2be^{2w}\sqrt{u}}{3br_1v^2e^w} \longrightarrow \frac{u'}{2\sqrt{u}}\frac{v^2}{v'} = \frac{e^w}{3r_1} \longrightarrow \frac{(\sqrt{u})'}{(-\frac{1}{v})'} = \frac{e^w}{3r_1} \tag{6.40}$$

Now, it can be assumed that the numerator and denominator have a similar structure like,

$$(-\frac{1}{v})' = k\theta'e^\theta \quad \text{and} \quad (\sqrt{u})' = \frac{k\theta'}{3r_1}e^{\theta+w} \tag{6.41}$$

where k is a constant, θ is a function of t, and θ' is its derivative with respect to t.

$$v = -(ke^\theta + c_v)^{-1} \tag{6.42}$$

If this v is placed into Eq. (6.39), a base expression can be obtained as;

$$\begin{aligned} v' &= \frac{k\theta' e^{\theta}}{(ke^{\theta}+c_v)^2} = 3br_1 \frac{e^w}{\sqrt{u}} \\ \sqrt{u} &= 3br_1 e^w \frac{(ke^{\theta}+c_v)^2}{k\theta' e^{\theta}} \\ g &= -\frac{1}{3br_1} \frac{\theta'}{1+\frac{c_v}{k}e^{-\theta}} \end{aligned} \tag{6.43}$$

which is the derivative of $\ln(e^{\theta} + c_v/k)$. It shows that Eq. (6.28), Eq. (6.31), and Eq. (6.32) are in accurate forms. The exponentials found in their denominator, namely θs, can be used for further derivations through an exact solution, or one may solve the system of DE given by Eq. (6.39). However, the inverse functions are well defined, which is sufficient to use them in order to represent waveforms created by the DWP in response to its input.

6.4 Conclusion

In this chapter, the output of DWP has been derived for both homogeneous case (no input) and inhomogeneous case (step function input), and, as a result, the inverse functions, namely waveforms, have been obtained. All these waveforms fit into the model given by Eq. (6.43) which may provide an exact solution for DWP.

In addition, as the waveforms have been expressed by functions of variables; input, time and initial output only, the DWP's response to the input can be associated with conventional modulation methods. However, the modulation property needs to be study along with the waveform allocation conditions, hence it has been shown that the occurrence of waveforms depend on both the input and initial output. This allocation process can be associated with conventional coding methods.

Chapter 7

QDWP as Modulator and Encoder

The modulation is the process of changing the information signal from one form into another. For analog modulation, parameters of a carrier waveform, mostly sinusoidal, are varied by the information signal. For digital modulation, a set of pre-defined waveforms are assigned to the information bit sequences. By this definition, a system driven by Eq. (6.1) performs both forms of modulation at the same time. Therefore, in this chapter, one of the waveforms composing DWP's output is examined in order to evaluate analog modulation capability. Then, in terms of digital modulation, the waveform allocation is represented by Markov chain, which highlights the coding capability of DWP. Finally, both the effect of noise on coding process, and the use of DWP as a modulator are clarified by simulations of case studies.

7.1 Analog Modulation

In analog modulations, a waveform called the carrier changes continuously in response to the information signal. In the case of carrier being a sinusoid, the modu-

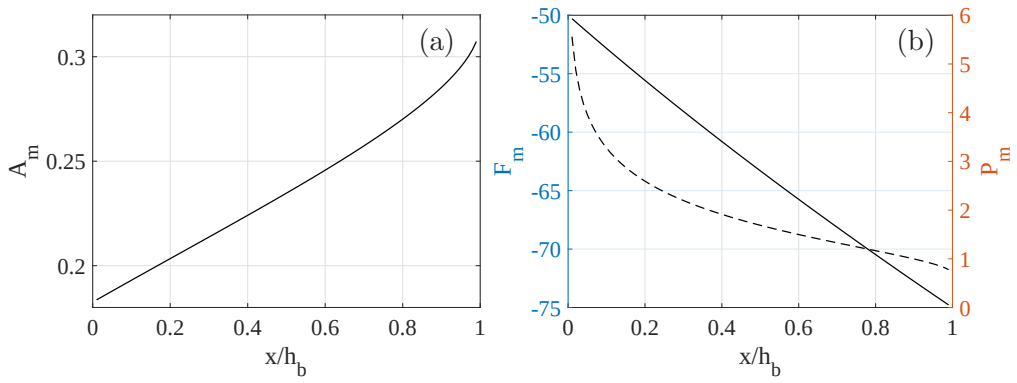

Figure 7.1: Amplitude A_m, Frequency F_m(solid), and Phase P_m(dashed); the parameters changing by x, where $m = 5$, $ak = 5$, $A = 1$, $T_b = 1s$, $h_b = \sqrt{(4a^3)/(27b)}$, $h_b > x > 0$.

lation type is classified depending on the variation parameter; amplitude, frequency, and phase. By this definition, the system under examination performs an analog modulation, as the cubic term in Eq. (6.1) causes a self modulation. As a result, the output's amplitude, frequency, and phase are all varied with the input.

Considering that a step function with an amplitude x is applied to the input. If there is a modulation, there is a carrier signal too, and the input changes one or more parameters of that carrier, which is going to be shown by one of the waveforms, $y_{13}(t)$. A part of it can be taken as a carrier if it is simplified into;

$$y_{13s}(t) = r_3 + \frac{r_1 - r_3}{1 + exp((a - 3br_1^2)t + \ln|r_1/r_3|)} \tag{7.1}$$

where the initial output is set to zero, and the input stays in the limits $\sqrt{(4a^3)/(27b)} > x > 0$ which makes this waveform valid. Then, the fractional term can be considered as a carrier signal written by

$$y_c(t) = \frac{A_m}{1 + exp(F_m t + P_m)} \tag{7.2}$$

The parameters; A_m, F_m and P_m are assumed to be the amplitude, frequency and phase of the modulation, respectively. All these are non-linear functions of input x

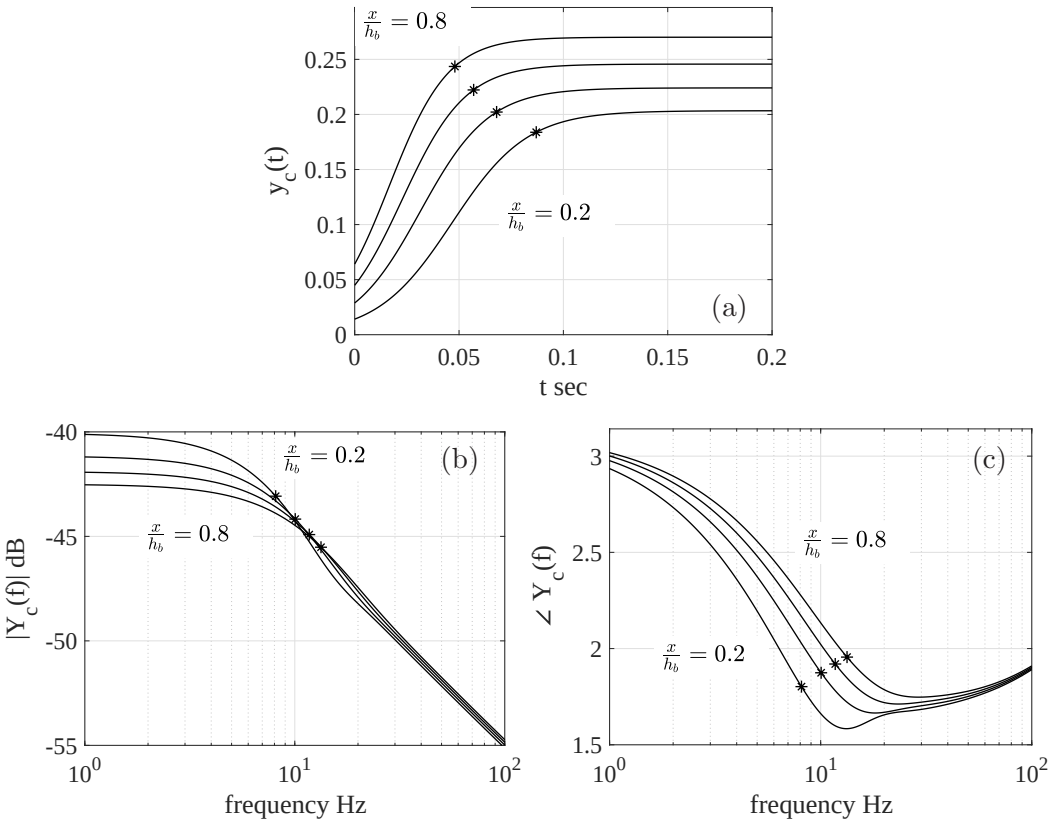

Figure 7.2: The simplified carrier signal, Eq. (7.2), in time and frequency domains, where $x/h_b = 0.2, 0.4, 0.6, 0.8$, $m = 5$, $ak = 5$, $A = 1$, $T_b = 1s$, $h_b = \sqrt{(4a^3)/(27b)}$, $h_b > x > 0$.

as below;

$$\begin{aligned} A_m &= r_1 - r_3 = \tfrac{3}{2}r_1 - \sqrt{\tfrac{a}{b} - \tfrac{3}{4}r_1^2} \\ F_m &= a - 3br_1^2 \\ P_m &= \ln|\tfrac{r_1}{r_3}| = \ln(r_1) - \ln\left(\tfrac{1}{2}r_1 - \sqrt{\tfrac{a}{b} - \tfrac{3}{4}r_1^2}\right) \end{aligned} \tag{7.3}$$

where r_1 is a function of x, given by Eq. (6.13). The dependency of these parameters on x is illustrated in Fig. 7.1. The changes are monotonic. This feature may provide good separation amongst different inputs if the carrier is a sinusoidal. However, y_c is a base-band type signal, so the changes on parameters can not directly take place on the output.

Those changes can be observed in time and frequency domains as in Fig. 7.2. In the time domain (a), it is shown that the final value, which the carrier can

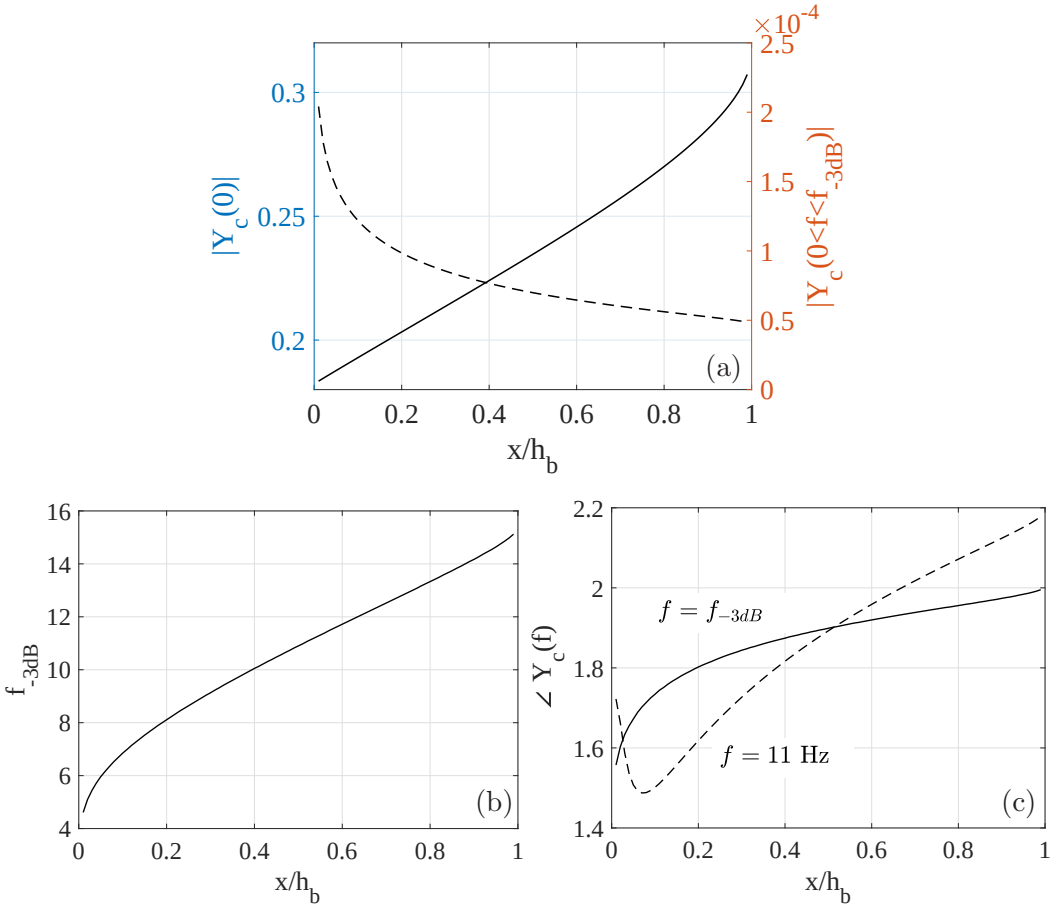

Figure 7.3: The features of simplified carrier; magnitudes at $f = 0$(solid-left) and $0 < f < f_{-3dB}$(dashed-right), corner frequencies, and phases for the input range where $m = 5$, $ak = 5$, $A = 1$, $T_b = 1s$, $h_b = \sqrt{(4a^3)/(27b)}$, $h_b > x > 0$.

reach, directly increases with the input as expected for an amplitude modulation. For the frequency one (a), it is shown that the derivatives of rising curves are slightly different from each other, and the rising times marked with $*$ are getting shorter by increasing the input. In the frequency domain (b), magnitude spectrum shows that increasing the input decreases the magnitudes of baseband components and slightly increases those at high frequencies, which is why the corner frequencies, f_{-3dB} marked with $*$, move forward. For the phase modulation (c), it may be hard to detect the phase difference in time domain, but the phase spectrum indicates that phases at the corner frequencies vary with the input.

As a result of this observation, the magnitude of the DC component, the corner frequency and the phase are directly related to the modulation parameters; A_m, F_m, and P_m, respectively. These features are illustrated in Fig. 7.3 which needs to be compared with Fig. 7.1. Firstly, A_m can be taken directly as an amplitude parameter of the modulation as it is equal to the DC component $|Y_c(f = 0)|$. Secondly, F_m needs to be scaled by -3 as it is approximately equal to $-3f_{-3dB}$. And finally, P_m can be modelled by a linear function of the phases at corner frequencies as such; $P_m = -11\angle Y_c(f_{-3dB}) + 22.5$.

Through this case study, it is shown that the waveform, $y_{13}(t)$, is a modulated signal. It carries the information on its amplitude, frequency and phase. This can be extended for the other waveforms too. However, instead of having such extension, it is necessary to know how these waveforms are chosen and what is the benefit of that. For example, based on the initial conditions and the current input, only one waveform is seen at the output. This dependency on the past and present values with switching waveforms can not be evaluated with in the context of analog modulation. Instead, the digital modulation with memory is found to be quite appropriate to explain such scenario.

7.2 Digital Modulation

The digital modulation is the process of mapping a digital sequence to a signal sequence. The digital sequence is a stream of M messages in the forms of either symbols or binary sequences each of length $k = \log_2 M$ bits. And, the signal sequence is a stream of the waveforms allocated to the messages. These waveforms are different in amplitude or phase or frequency, or some combination of two or more parameters. If the allocation depends on only one message, then this is called *memoryless* modulation. If it depends on the previous messages as well, then it becomes a modulation with *memory*. Therefore, based on this definition, the system, whose

output driven by Eq. (6.1) with its parameters (a, b) being $\mathbb{R}_{>0}$, employs a digital modulation method with memory.

This modulation scheme can be effectively represented by Markov chain. To do that, the sequence of signal waveforms or corresponding indices, m_l, together with the states of the Markov chain, $S_l \in \{1, 2, ..., N\}$, need to be expressed in the form of;

$$\begin{aligned} m_l &= f_m(S_{l-1}, I_l) \\ S_l &= f_s(S_{l-1}, I_l) \end{aligned} \tag{7.4}$$

where l is the time instant, N is the number of states, $I \in \{1, 2, ..., M\}$ is the input sequence, $f_m(.,.)$ and $f_s(.,.)$ are the output function and the function of the internal state dynamics of the Markov chain. Additionally, in the case of messages being represented by binary sequences, each sequence has k bits and similarly each state can be represented by $k(L-1)$ bit. Here, L is the constraint length of the modulation indicating that the modulation depends on the current message and the most recent $L-1$ messages.

Before defining this scheme in the conventional way, the information sequence needs be prepared for the system as following.

7.2.1 Pre-modulation

The system is driven by the DE, so the input needs to be continuous in time. In other words, the symbol sequence must be introduced to the system by a modulated signal. Although this signal can be in any form, the most comprehensive one for the following steps is going to be a pulse amplitude modulated signal.

In that case, the system input, $x(t)$, is a baseband PAM signal conveying the symbol sequence I with pulses whose durations are T_b, and the amplitudes are $x_i = A_s(2i - 1 - M)$ where $i = 1 : M$ and A_s is a positive constant. If T_b is chosen to be long enough in order for outputs to settle down, the number of all states can

be given by

$$N_{all} = M_{|x|>h_b} + 2M_{|x|=h_b} + 3M_{|x|<h_b} \tag{7.5}$$

where $M_{|x|\gtreqless h_b}$ is the number of symbols whose corresponding amplitudes are, respectively, greater than, equal to, and smaller than the system barrier h_b. The reason is that the system has only one real root for $|x| > h_b$. For $|x| = h_b$, all roots are real; one stable state and one metastable state. $|x| < h_b$ has a stable, metastable, and transitional states. In addition to that, it should be noted; for the given input,

$$N_{obs} = M_{|x|>h_b} + (1 + \text{sgn}(M_{x>h_b} M_{x<-h_b}))M_{|x|\leq h_b} \tag{7.6}$$

number of states can be observed, and the rest cannot. Nevertheless, all must be taken into account in the state space, and the reason is that the internal dynamics of Markov chain uses all of them.

7.2.2 States of Markov Chain

The states of Markov chain for the PAM input are the real roots obtained from the r.h.s of Eq. (6.1), and all states, $S_{symbol,type}$, can be given by

$$\begin{aligned} S_{i,s} &= r_i \\ S_{i,t} &= \begin{cases} -\frac{1}{2}r_i + \text{sgn}(r_i)w_i & , |x_i| \leq h_b \\ \varnothing & , \text{otherwise} \end{cases} \\ S_{i,m} &= \begin{cases} -\frac{1}{2}r_i - \text{sgn}(r_i)w_i & , |x_i| \leq h_b \\ \varnothing & , \text{otherwise} \end{cases} \end{aligned} \tag{7.7}$$

where $r_i = f_{r_1}(x = x_i)$ defined by Eq. (6.13), $w_i = \sqrt{a/b - 3r_i^2/4}$, $i = 1, 2, ..., M$, and the second indices (s, t, m) stand for $s$table, $t$ransitional, $m$etastable, respectively. Note that in the case of $|x_i| = h_b$, $S_{i,t}$ and $S_{i,m}$ are equal, which means there is just one state not two. However, this is necessary to determine the new state

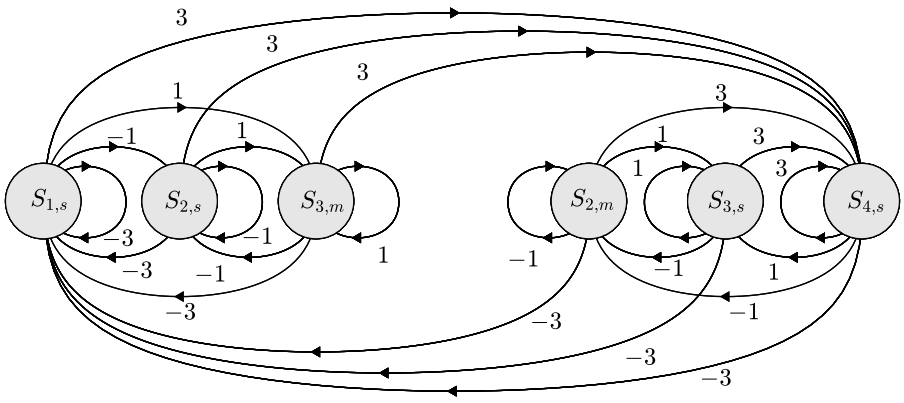

Figure 7.4: State transition diagram where the input is PAM4 signal with $A_s < h_b < 3A_s$, showing the transitions corresponding to the input symbols.

simply by

$$S_l \;= \begin{cases} S_{i,s} & , S_{i,t} = \varnothing \\ S_{i,t} & , S_{l-1} = S_{i,t} \\ S_{i,s} & , S_{l-1} \in \overrightarrow{S_{i,t}S_{i,s}} \;\wedge\; S_{l-1} \neq S_{i,t} \\ S_{i,m} & , S_{l-1} \in \overrightarrow{S_{i,t}S_{i,m}} \;\wedge\; S_{l-1} \neq S_{i,t} \end{cases} \tag{7.8}$$

where S_l and S_{l-1} are the current and previous states, and where $\overrightarrow{S_{i,t}S_{i,m}}$ defines a ray with end point $S_{i,t}$ passing through $S_{i,m}$. From which, the state transition diagram can be obtained as illustrated in Fig. 7.4 for a four-level PAM (PAM4). The transitions are independent of time as the input's pulse duration guarantees to make output settle into the new state at the destination. It also makes this Markov chain homogeneous and discrete in time. Therefore, the transition probabilities can be given in the form of the *state transition matrix*, P, whose rows are for previous states and columns for new ones. For example, P of equiprobable PAM4 in Fig. 7.4

is

$$P_{1>2>1} = \begin{array}{c} \begin{array}{cccccc} S_{4,s} & S_{3,s} & S_{2,m} & S_{3,m} & S_{2,s} & S_{1,s} \end{array} \\ \left[\begin{array}{cccccc} 1/4 & 1/4 & 1/4 & 0 & 0 & 1/4 \\ 1/4 & 1/4 & 1/4 & 0 & 0 & 1/4 \\ 1/4 & 1/4 & 1/4 & 0 & 0 & 1/4 \\ 1/4 & 0 & 0 & 1/4 & 1/4 & 1/4 \\ 1/4 & 0 & 0 & 1/4 & 1/4 & 1/4 \\ 1/4 & 0 & 0 & 1/4 & 1/4 & 1/4 \end{array}\right] \end{array} \begin{array}{c} S_{4,s} \\ S_{3,s} \\ S_{2,m} \\ S_{3,m} \\ S_{2,s} \\ S_{1,s} \end{array} \tag{7.9}$$

where the index of $P_{1>2>1}$ is a short form of $M_{x>h_b}, M_{|x|<h_b}, M_{-h_b>x}$. Then, the *state probability vector* can be obtained from $\lim_{l \longrightarrow \infty} P^l$ and given by

$$p = \begin{array}{c} \begin{array}{cccccc} S_{4,s} & S_{3,s} & S_{2,m} & S_{3,m} & S_{2,s} & S_{1,s} \end{array} \\ \left[\begin{array}{cccccc} 1/4 & 1/8 & 1/8 & 1/8 & 1/8 & 1/4 \end{array}\right] \end{array} \tag{7.10}$$

where l can be considered as a transition count starting from initial state $l = 0$. Therefore, based on this probability vector, the information acquired by the states is 2.5 bits per state, although it is 2 bits/symbol at the input. This measure is basically entropy and it can be determined by the probability vector;

$$H(S) = -\sum_{n=1}^{N_{obs}} p(n) \log_2(p(n)) \tag{7.11}$$

and, if the source of given PAM is equaprobable, and none of $M_{x>h_b}, M_{|x|<h_b}, M_{-h_b>x}$ is zero, it can also be given by

$$H(S) = -\frac{M_{|x|>h_b}}{M} \log_2\left(\frac{1}{M}\right) - \frac{M - M_{|x|>h_b}}{M} \log_2\left(\frac{1}{2M}\right) \tag{7.12}$$

which shows that the information difference between symbols and states are always less than a bit for this configuration. Considering that the difference comes from the coding process, there is no decisions for symbols whose corresponding amplitudes

are greater than h_b, but for others, a decision is made and it contains the information of the previous state's amplitude being greater than that of current transition state. Therefore, there are $k = log_2(M)$ bits for $S_{|x|>h_b}$ and $k+1$ bits for $S_{|x|\leq h_b}$. For the example above, it can be said that $S_{1,s}$ and $S_{4,s}$ are represented by 00 and 11, and similarly, $S_{2,s}$, $S_{2,m}$, $S_{3,s}$, $S_{3,m}$ are by 01 1, 01 0, 10 1, 10 0, respectively.

In this sense, the constraint length, L, is less than 2 but greater than 1 as the transmitted signal is going to carry the information of the current symbol and the most recent $L-1=1$ symbol, which does not happen for all the symbols. Considering the number of states, L can be given by $log_2(N_{obs}/M)$ which is 1.4055 for this PAM4 example.

This finite-state, discrete-time, homogeneous Markov chain is ergodic as well, which requires being aperiodic and irreducible. The elements of the main diagonal of n-step transition matrix P^n are non-zero for any $n > 0$, which means all states are aperiodic. And, starting from any state, it is possible to reach any state within n steps, which makes the Markov chain irreducible.

As the states, $S_{i,j}$, and internal dynamics, $S_l{=}f_s(.,.)$, of the Markov Chain have been defined in detail, the next is to define the waveforms. With that, the representation of modulation scheme will have been completed.

7.2.3 Waveforms

The waveforms used by this modulation scheme differ in amplitude, frequency and phase, which result in a multi-dimensional signalling. In Sec. 6.3, it is shown that there are two different base-waveforms for input $|x| > h_b$ and four for $|x| < h_b$ chosen by the initial condition. Then, in Sec. 7.1, it is examined that, even for waveforms belonging to the same base, parameters; amplitude, frequency, and phase, vary depending on the initial condition and the current state.

The output is a sequence of those waveforms. It can be considered that they are segments taken from the base-waveforms which are illustrated in Fig 7.5; $Z_{s\in 0}$

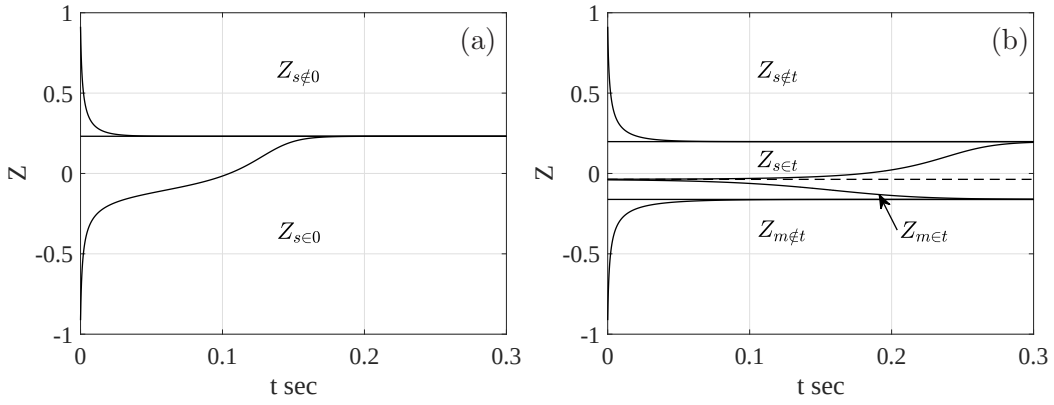

Figure 7.5: The base-waveforms obtained from Eq. (6.14) where $m = 5$, $ak = 5$, $A = 1$, $T_b = 1s$, $h_b = \sqrt{(4a^3)/(27b)}$, $x = \{2h_b, 0.5h_b\}$.

and $Z_{s\notin 0}$ for $|x| > h_b$, $Z_{\{s,m\}\in t}$ and $Z_{\{s,m\}\notin t}$ for $|x| < h_b$. These are functions of the current input x_i, which can be given by $m = Z_{type}(S_{i,s}, t)$ where $0 \leq t \leq \infty$ and where m is the output. Its type is chosen depending on the state transition as

$$Z_l = \begin{cases} Z_{DC} & , S_{l-1} = S_l \\ Z_{s\in 0} & , S_{l-1} \in \overrightarrow{S_{I(l),s}0} \ \wedge \ S_{I(l),t} = \varnothing \ \wedge \ S_{l-1} \neq S_l \\ Z_{s\notin 0} & , S_{l-1} \notin \overrightarrow{S_{I(l),s}0} \ \wedge \ S_{I(l),t} = \varnothing \ \wedge \ S_{l-1} \neq S_l \\ Z_{s\in t} & , S_{l-1} \in \overrightarrow{S_{I(l),t}S_{I(l),s}} \ \wedge \ S_{l-1} \in \overline{S_{I(l),s}S_{I(l),m}} \ \wedge \ S_{l-1} \notin \{S_l, \varnothing\} \\ Z_{s\notin t} & , S_{l-1} \in \overrightarrow{S_{I(l),t}S_{I(l),s}} \ \wedge \ S_{l-1} \notin \overline{S_{I(l),s}S_{I(l),m}} \ \wedge \ S_{l-1} \notin \{S_l, \varnothing\} \\ Z_{m\in t} & , S_{l-1} \notin \overrightarrow{S_{I(l),t}S_{I(l),s}} \ \wedge \ S_{l-1} \in \overline{S_{I(l),s}S_{I(l),m}} \ \wedge \ S_{l-1} \notin \{S_l, \varnothing\} \\ Z_{m\in t} & , S_{l-1} \notin \overrightarrow{S_{I(l),t}S_{I(l),s}} \ \wedge \ S_{l-1} \notin \overline{S_{I(l),s}S_{I(l),m}} \ \wedge \ S_{l-1} \notin \{S_l, \varnothing\} \end{cases} \tag{7.13}$$

Then, in order to have a continuous output, the point at which the current waveform starts can be determined by $t_{sp} = Z^{-1}_{type}(S_{I(l),s}, m = S_{l-1})$ where Z^{-1} is the inverse function. Each waveform also lasts a pulse duration T_b. As a result, the output can be given by

$$m_l = Z_l(S_{I(l),s}, t - Z_l^{-1}(S_{I(l),s}, S_{l-1})), \ t : 0 \longrightarrow T_b \tag{7.14}$$

This process produces a great number of waveforms which can be found by $N_{obs}(M_{|x|>h_b} + M_{|x|<h_b}/2)$. Even for the PAM4, that is $6(2 + 4/2) = 24$. However, they can be categorised to have a simpler analysis. For example, N_{obs} of them are pulse signals with corresponding amplitudes, and due to the symmetry, for each waveform, there is one another with π phase shift. Therefore, $(N_{obs} - 1)M_{|x|>h_b}/2 + (N_{obs}/2 - 1)(M_{|x|<h_b})/2$ number of waveforms need to be analysed, which is $(6 - 1)(2/2) + (6/2 - 1)4/2 = 9$ for PAM4. It can be given in a matrix form by

$$m = \begin{array}{c} \begin{array}{cccccc} S_{4,s} & S_{3,s} & S_{2,m} & S_{3,m} & S_{2,s} & S_{1,s} \end{array} \\ \left[\begin{array}{cccccc} Z_{DC}^{S_{4,s}} & Z_{3,s\notin t}^{S_{4,s}} & Z_{2,m\notin t}^{S_{4,s}} & \varnothing & \varnothing & -Z_{4,s\in 0}^{-S_{4,s}} \\ Z_{4,s\in 0}^{S_{3,s}} & Z_{DC}^{S_{3,s}} & Z_{2,m\notin t}^{S_{3,s}} & \varnothing & \varnothing & -Z_{4,s\in 0}^{-S_{3,s}} \\ Z_{4,s\in 0}^{S_{2,m}} & Z_{3,s\in t}^{S_{2,m}} & Z_{DC}^{S_{2,m}} & \varnothing & \varnothing & -Z_{4,s\in 0}^{-S_{2,m}} \\ Z_{4,s\in 0}^{-S_{2,m}} & \varnothing & \varnothing & -Z_{DC}^{S_{2,m}} & -Z_{3,s\in t}^{S_{2,m}} & -Z_{4,s\in 0}^{S_{2,m}} \\ Z_{4,s\in 0}^{-S_{3,s}} & \varnothing & \varnothing & -Z_{2,m\notin t}^{S_{3,s}} & -Z_{DC}^{S_{3,s}} & -Z_{4,s\in 0}^{S_{3,s}} \\ Z_{4,s\in 0}^{-S_{4,s}} & \varnothing & \varnothing & -Z_{2,m\notin t}^{S_{4,s}} & -Z_{3,s\notin t}^{S_{4,s}} & -Z_{DC}^{S_{4,s}} \end{array}\right] \begin{array}{c} S_{4,s} \\ S_{3,s} \\ S_{2,m} \\ S_{3,m} \\ S_{2,s} \\ S_{1,s} \end{array} \end{array} \tag{7.15}$$

where $m_{i,j}$ is the output waveform at ith row and jth column which is a segment of corresponding base-waveform defined by $Z_{symbol,type}^{startpoint}$.

When all the waveforms are plotted in time domain, due to their monotonic properties, a trellis-like diagram can be obtained. However, the energies of input and output signals are different, for this, one of them may not be noticeable. Therefore, the average output energy needs to be normalized. The energy in waveform $M_{i,j}$ and the average input signal energy can be given by

$$\mathcal{E}_{i,j} = \int_0^{T_b} (m_{i,j})^2 dt \tag{7.16}$$

$$\mathcal{E}_{avg} = \sum_{i=1}^{N_{obs}} \sum_{j=1}^{N_{obs}} p_i P_{i,j} \mathcal{E}_{i,j} \tag{7.17}$$

where $\mathcal{E}_{i,j} = 0$ if $m_{i,j} = \varnothing$, and where P and p are the state transition matrix and

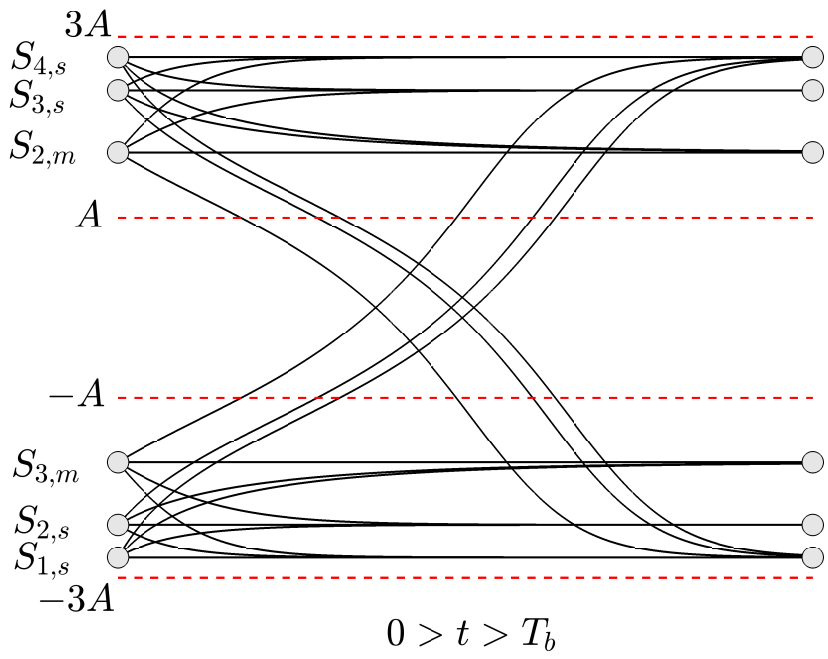

Figure 7.6: Waveforms in time domain with normalized signal energy and the trellis diagram where $a = 25$, $b = 750$, $A_s = 0.75h_b$, $T_b = 0.15\ s$.

probability vector. Then, the energy of PAM signal is

$$\mathcal{E}_{avg,PAM} = \frac{1}{M}\sum_{i=1}^{M}\int_{0}^{T_b} A_i^2 dt \tag{7.18}$$

As a result, the energy normalization can be done by the ratio of average energies, so the scaled waveforms are given by

$$\hat{m}_{i,j} = m_{i,j}\sqrt{\frac{\mathcal{E}_{avg,PAM}}{\mathcal{E}_{avg}}} \tag{7.19}$$

The waveforms for PAM4 are illustrated in Fig. 7.6 which also provides the trellis diagram.

Fig. 7.6 also illustrates that the waveforms differ in frequency spectrum. The indicator is *settling time* which varies from one waveform to another. In order to show the difference between settling times, those waveforms stay below the main

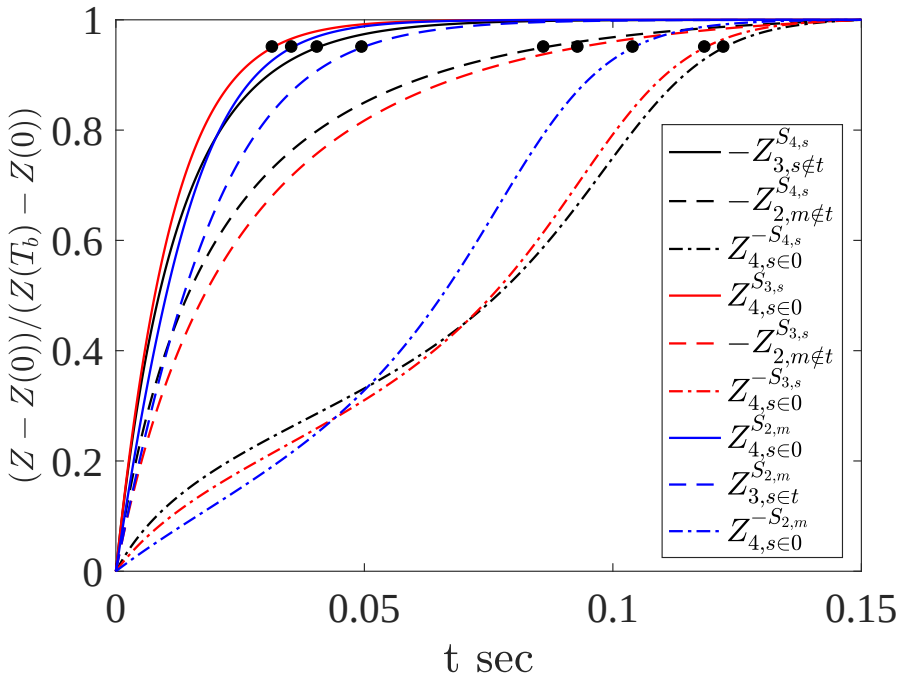

Figure 7.7: Waveform shapes (lines) and settling times (reaching at 95% of final values) (dots) where $a = 25$, $b = 750$, $A_s = 0.75h_b$, $T_b = 0.15$ s.

diagonal of the matrix given by Eq. (7.15) can be taken as specimens, and be linearly scaled to have the same start and end points as in Fig. 7.7, in which, the previous states are indicated by the colours. It can be seen that the settling times vary with not only the current states but also the previous ones.

These differences in settling times require to be observed in frequency spectrums of the waveforms which can be obtained by taking the DFTs. But first, as they are base-band signals and the pulse interval is too short to give the details of this band, there is a need to add a tail to the waveforms in order to improve the resolution. For this, DFTs are taken after inserting a $19 \times T_b$ long pulse with their own end values.

The results, magnitude and phase spectrums are illustrated in Fig. 7.8. The colours and styles are kept the same as in Fig. 7.7. The corner frequencies of waveforms, at which the magnitude falls off -3 dB, are marked by dots. With in the legend's order, these frequencies are given by $20.3, 9.3, 6, 26.3, 8.7, 6.3, 23.7, 17, 7.3$

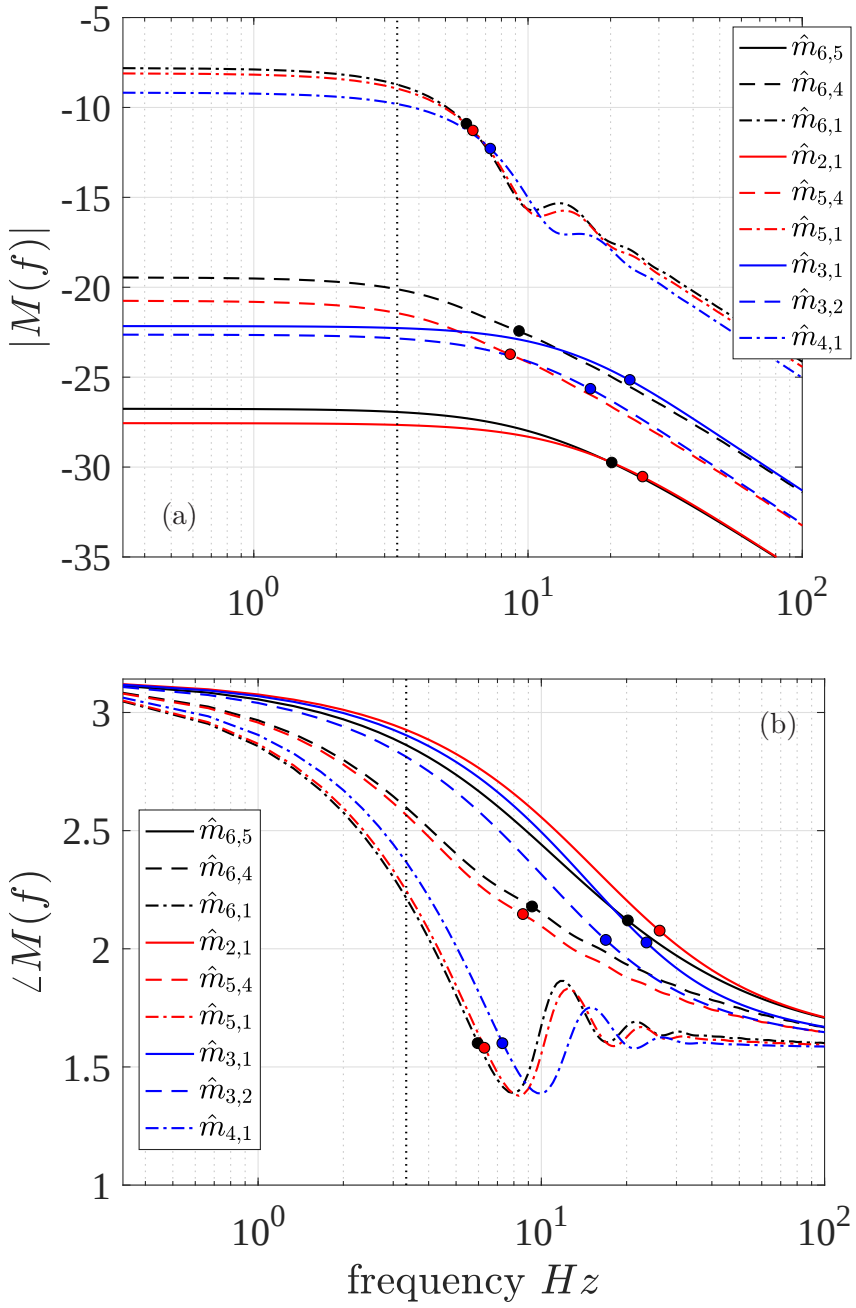

Figure 7.8: Magnitude (in dB) and Phase Spectrums of waveforms with $19T_b$ long tails and corresponding amplitudes where $a = 25$, $b = 750$, $A_s = 0.75h_b$, $T_b = 0.15$ s, 10^4 number of sample per T_b.

Hz. Visually, it is easy to follow that while settling time gets shorten the corner frequency increases. If the corner frequency is considered as bandwidth of a baseband signal, then the information sequence is mapped into a set of bandwidths as well as their amplitudes.

The difference amongst magnitude levels in the baseband also needs to be mentioned. There are two reasons for that; states' amplitudes and waveforms' bandwidths. The amplitude difference indicates the energy of the waveform, and the bandwidth tells us where this energy is spread out. For example, states' amplitudes are $S_{4,s} = -S_{1,s} = 3.66$, $S_{3,s} = -S_{2,s} = 3.17$, $S_{2,m} = -S_{3,m} = 2.26$, and (amplitude difference, bandwidth)s are (1.4, 9.3 Hz) for $-Z_{2,m\notin t}^{S_{4,s}} = \hat{m}_{6,4}$ and (0.9, 8.7 Hz) for $-Z_{2,m\notin t}^{S_{3,s}} = \hat{m}_{5,4}$ and (0.9, 17 Hz) $-Z_{3,s\in t}^{S_{2,m}} = \hat{m}_{3,2}$. Corresponding magnitude levels are 11.3 10^{-3}, 8.4 10^{-3}, and 5.4 10^{-3}, respectively. Now, considering the similar bandwidths 9.3 and 8.7 Hz, the amplitude and magnitude ratios; $1.4/0.9 = 1.56$ and $11.3/8.4 = 1.35$ indicates that there is a linear relation between amplitude and magnitude level. However, when the bandwidth changes considerably as for $8.7/17 = 0.51$ although the amplitudes are the same, the magnitude level ratio $8.4/5.4 = 1.56$ varies with one over square root of the bandwidth ratio; $1/\sqrt{0.51} = 1.4$.

The phase spectrums of those waveforms are also different from each other as in Fig. 7.8. While the phases at corner frequencies can be grouped into two, phases at a certain frequency, such as $1/T_b$, line up in the same order of corner frequencies. Therefore, this modulation scheme maps the information sequence into the output's amplitude, frequency and phase features.

7.3 Noise Effect

A random fluctuation can activate encoding processes on the states. The number of observable states has been given by Eq. (7.6). In the case where there is no input

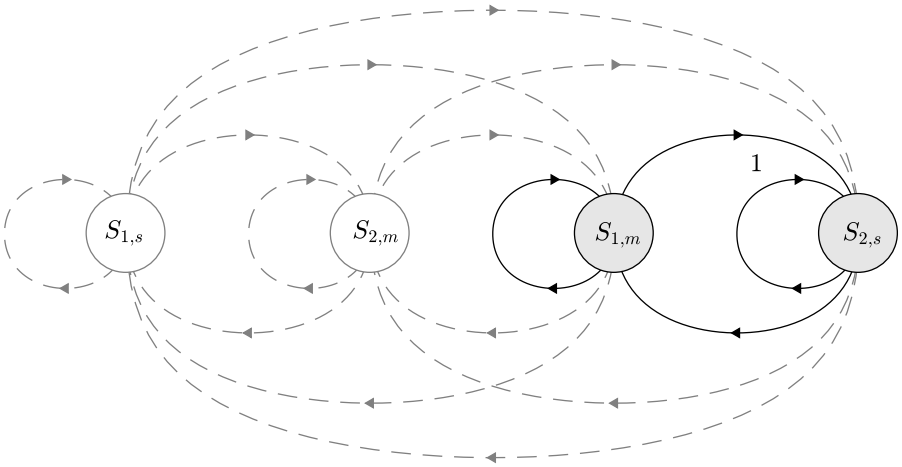

Figure 7.9: State transition diagram for BPAM with $A_s < h_b$. (solid for noise free, dashed for noisy input)

that can make the output cross the zero, it gives that the number of observable states is the same as the number of input levels. In addition to that, if a binary sequence is mapped into only two levels PAM signal as in BPAM, no matter what the levels are, only two states are going to be present. In both cases, the choice of the current state does not depend on the previous state any more. Hence, the entropy of the states probability vector decreases. In order to overcome this limitation, a random fluctuation, namely noise source, can be introduced after the pre-modulation process.

The noise is supposed to make the output jump from one well (either positive amplitudes or negative ones) to another. In the absence of the noise, observable states are placed in one well, and transitions between states are deterministic. If the other states in another well get involved into the process by the help of noise, then the coding applies to the states. However, the noise also enables undesired transitions between states. For example, when a BPAM signal, with amplitudes $(A_s, -A_s)$ and $A_s < h_b$, is applied together with noise, the possible transitions can be shown as in Fig. 7.9.

As mentioned above, the states lose entropy. Therefore, the effect of noise

insertion on the state occurrence needs to be examined, which requires the knowledge of probabilities; zero crossing and state choice. In order to measure the zero crossing dependence on input, a threshold detector can be placed after the modulator, which is similar to the receiver illustrated in Fig. 3.1. Then, as there are four states, two more threshold detector need to be added into the system in order to obtained the state choice probabilities.

The thresholds of these detectors are for detecting which state is observed at the end of each pulse. As the pre-modulated input signal is subject to a random fluctuation, they need to be chosen based on the error probabilities. Defining CDF of the output values $y(nT_b)$ as $F_Y(y) = P(Y \leq y)$, then error probability of a single threshold detector for equiprobable BPAM is given by

$$P_e(y = \theta) = \frac{1}{2}(F_{y^1}(\theta) + 1 - F_{y^0}(\theta)) \tag{7.20}$$

and if there are three threshold detectors, the error probability is

$$\begin{aligned} P_e = \quad & \tfrac{1}{2}(F_{y^1}(\theta_1) + 1 - F_{y^0}(\theta_1) - F_{y^0}(\theta_2))\text{sign}(y < \theta_2) \\ & + \tfrac{1}{2}(F_{y^1}(\theta_3) + 1 - F_{y^0}(\theta_3) - F_{y^1}(\theta_2))\text{sign}(y \geq \theta_2) \end{aligned} \tag{7.21}$$

where $F_{Y^1}(y) = P(Y \leq y \mid X = 1)$ and the input symbols $X = \{0, 1\}$. Here, the thresholds are $\theta = \theta_2 = 0$ and $\theta_3 = -\theta_1$, and the sum of detectors' outputs can take from 0 to 3 for the states from $S_{1,s}$ to $S_{2,s}$, respectively. Considering the input bits $\{0, 1\}$ mapped into the amplitudes $\{-A, A\}$ where $A < h_b$, the states are $\{-kA, -kA(0.5 + \sqrt{ak/(ak+1) - 3/4}), kA(0.5 + \sqrt{ak/(ak+1) - 3/4}), kA\}$. If so, for the noise free case, $\theta_3 = -\theta_1$ can be given by

$$\theta_3 = -\theta_1 = \frac{1}{2}\left[kA + kA\Big(\frac{1}{2} + \sqrt{\frac{ak}{ak+1} - 3/4}\Big)\right] \tag{7.22}$$

where k and a are determined by Eq. (3.21) if A, T_b, ak, m parameters are given.

The CDFs and thresholds of an example system design are given by Fig.

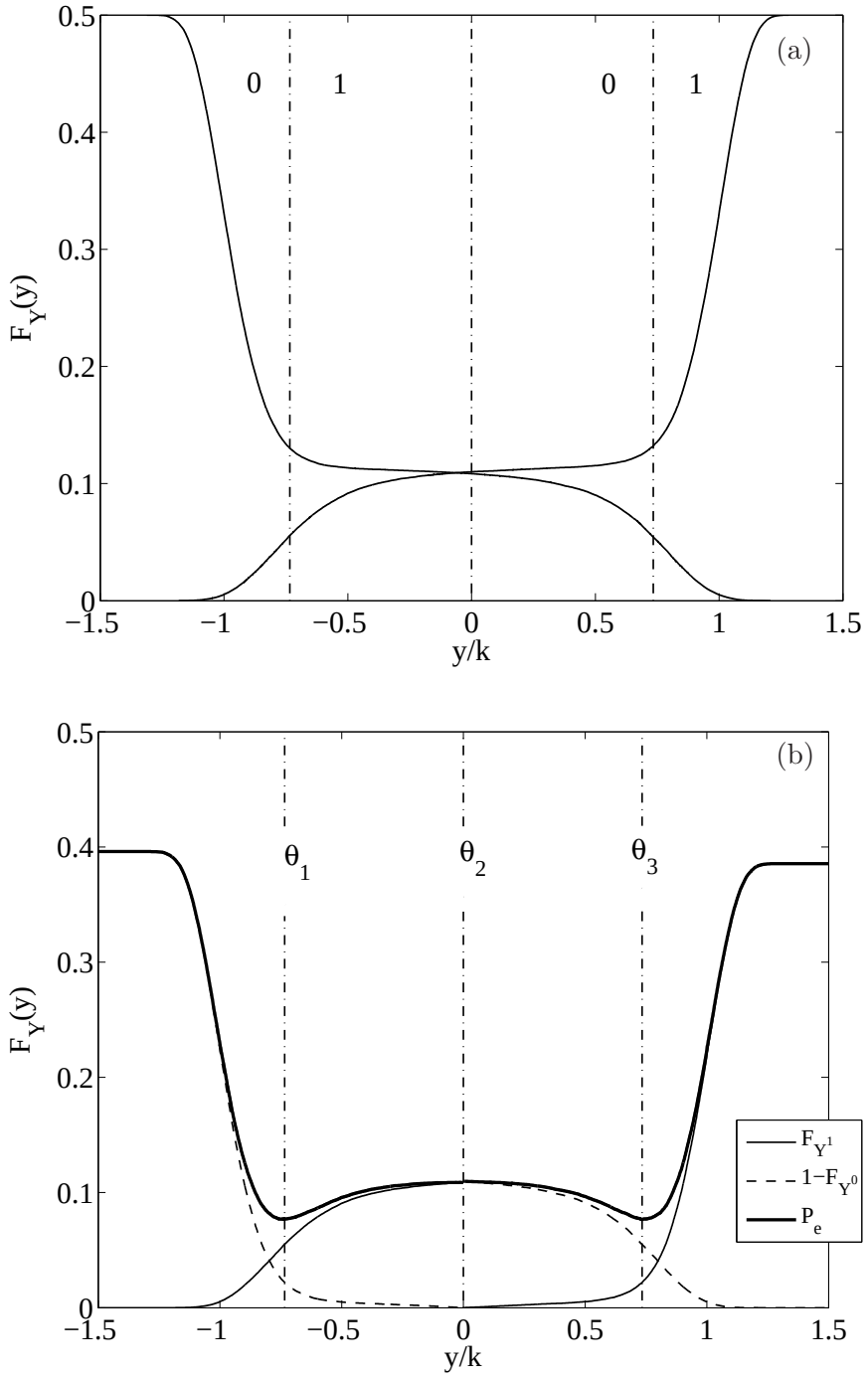

Figure 7.10: The conditional CDFs of output $y(nT_b)$, where $m = 5$, $ak = 5$, $A = 1$, $T_b = 1s$, and the noise is Gaussian distributed with SNR per bit = 8 dB, and where the output y is split in half by $\theta_2 = 0$

7.10. The first plot illustrates the first and second terms on the r.h.s. of Eq. (7.20), similarly, the second plot is for Eq. (7.21). Defining the zero crossing dependence as $1 - 2P_e(\theta = 0)$ (1 means crossing is solely dependent on the input), it is about 6/10 for this example, and the state occurrence probabilities (state probability vector) can be given by $[4/10, 1/10, 1/10, 4/10]$. Then, it can be inferred that the entropy increases from 1 to 1.7.

This could be valid if there was no intersection of the CDFs. For example, when bit 1 comes, y/k is supposed to be either between θ_1 and θ_2 or greater than θ_3, as these are the states assigned to bit 1. However, y/k can be found in values assigned to other states depending on the threshold choice and the noise power. In other words, the probability of finding $y/k > \theta_3$ is less than 4/10. Therefore, the states' entropy needs to be reconsidered after finding the optimum thresholds.

Those thresholds are supposed to provide minimum error probability given by Eq. (7.21). In addition to that, the error probability, consequently the optimum thresholds, vary by noise power and that is illustrated in Fig. 7.11. It can be seen that optimum threshold value for SNR = 8 dB is 0.75, which is already shown in Fig. 7.10. In this case, state probabilities change to $[0.425, 0.075, 0.075, 0.425]$, so the entropy becomes 1.6 while $P_e = 0.15$ is less than 0.2.

Fig. 7.11 also shows P_e of single threshold detector, $\theta = 0$. It is used for determining the zero crossing dependence which goes to zero while SNR is deviating from 4 dB. For lower SNRs, this results in shortening the period between zero crossings while crossing becomes less frequent for high SNRs. In addition to that, as there are optimum threshold values, it can be inferred that states are separable only for SNR $>$ 4 dB.

As a result, the increase in entropy together with a decrease in error probability indicates that the output is encoded. Therefore, by the means of noise, the coding is enabled. Furthermore, as these two properties are inversely related, an optimum noise level can be found for the coding process.

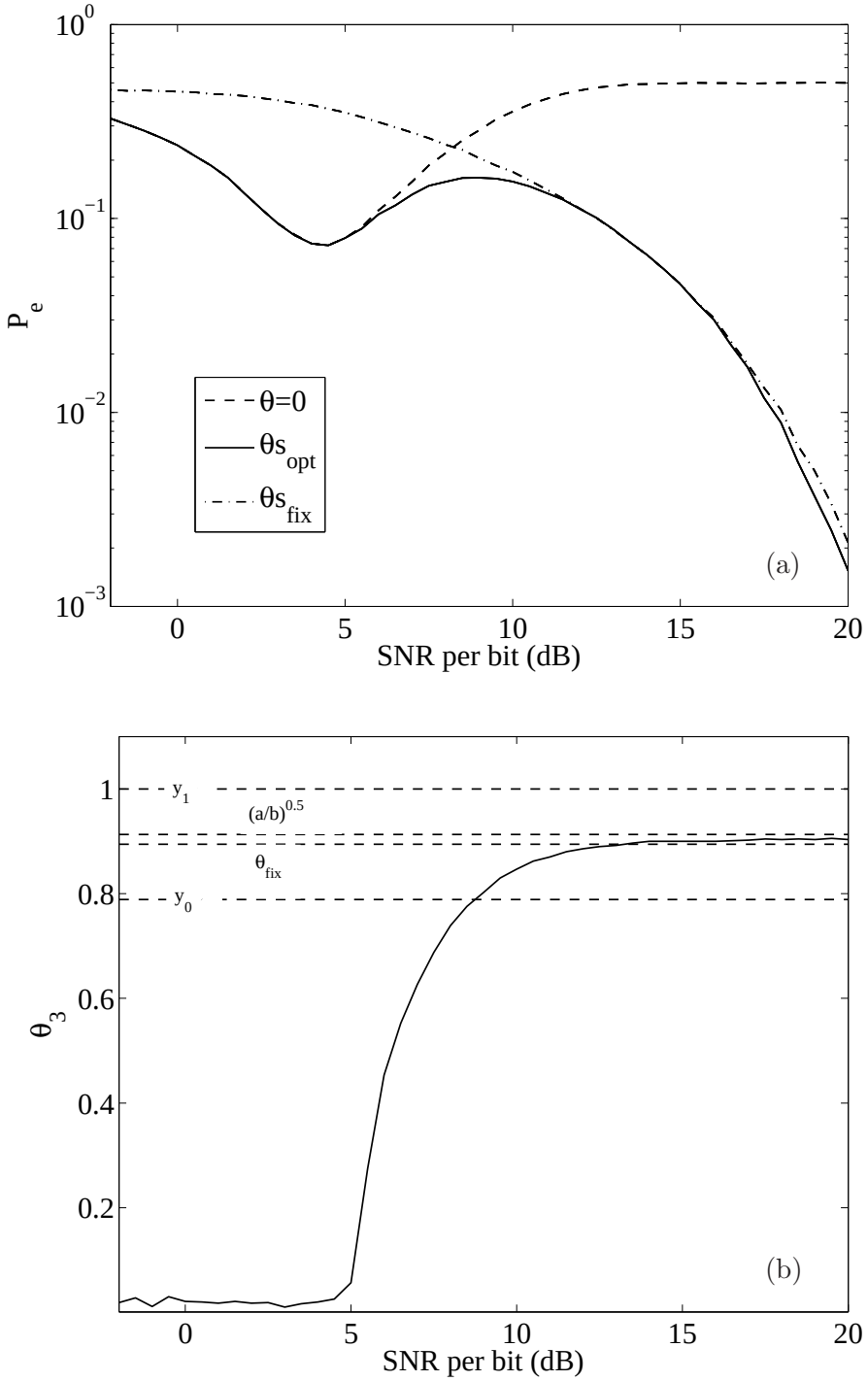

Figure 7.11: The error probabilities of a single threshold $\theta = 0$ case, and three thresholds cases; $\theta_2 = 0, \theta_{1,3} = \mp\theta_{\text{opt}}$ and $\theta_{1,3} = \mp\theta_{\text{fix}}$. Samples are taken at nT_b, where $m = 5$, $ak = 5$, $A = 1$, $T_b = 1s$.

7.4 Pulse Width-Position Modulation

The type of modulation depends on the assessment of output. It has been shown that a noise can activate the coding process for BPAM signal with $A < h_b$. The output of which configuration has been analysed based on the values of states; namely amplitudes, which keeps the modulation in the context of PAM. However, the output also carries the information on its other properties; such as settling time, frequency, etc. Depending on the property examined, the type of modulation differs. When the time domain properties; the zero cross timing and settling time, are taken into account, the modulation type can be named after Pulse Width-Position Modulation (PWPM).

In order to obtain a feasible PWPM signal at the output, the input PAM needs to be rearranged. Although the output is always PWPM for any PAM input, it may not be feasible. For example, any two sequential waveforms given in Sec. 7.2 form a pulse, and that pulse has a shape, amplitude, mean, width, and position. These properties vary from one waveform couple to another. However, PWPM requires to have changes on width and position only. Therefore, the input needs to be determined accordingly.

The shape and amplitude differences at the output can be eliminated by placing a threshold device just after the modulator. As the waveforms are all monotonic in amplitude, the output of threshold device is going to be a sequence of pulses with the same shape and amplitude, whose widths and positions are determined by the threshold cross timing. However, when the input symbol repeats, regardless of the threshold choice, the output does not change. In this case, the amplitudes assigned to symbols can be set higher than h_b, while the phase is changing for every other symbol interval. Therefore, the input $x(t)$ can be given by

$$x(t) = \sum_{i \in \mathbb{Z}} (-1)^i A_{I(i)} g(t - iT) \tag{7.23}$$

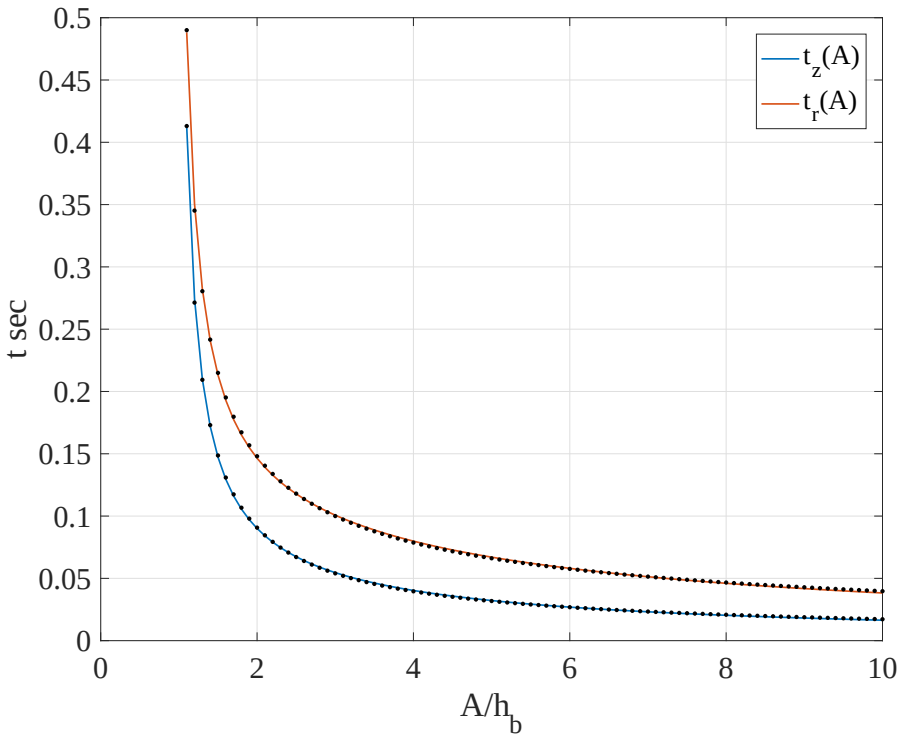

Figure 7.12: The zero cross timing (t_z) and settling time (to 95%) (t_r) functions (solids), and simulation results (dots).

where I is the symbol sequence, $A_{I(i)}$ is the amplitude assigned to ith symbol in the sequence, and $g(t)$ is a pulse with an unit amplitude and T duration. Such an input, together with adequate amplitudes, can guarantee the zero crossing for every symbol.

The input amplitude, A, determines the zero cross timing and settling time, which is illustrated in Fig. 7.12 for the system with parameters $a = 25$ and $b = 750$. The results (dots) belong to the transitions from corresponding states to their negatives. Defining the zero cross timing as a function $t_z(A)$ and settling time as $t_r(A)$, they can be fitted by

$$t(A) = \frac{c_1 A + c_2}{A^2 + c_3 A + c_4} \tag{7.24}$$

where the constants are [0.3025, $0.9526\ 10^{-3}$, 1.124, -4.487] for t_z and [0.819,

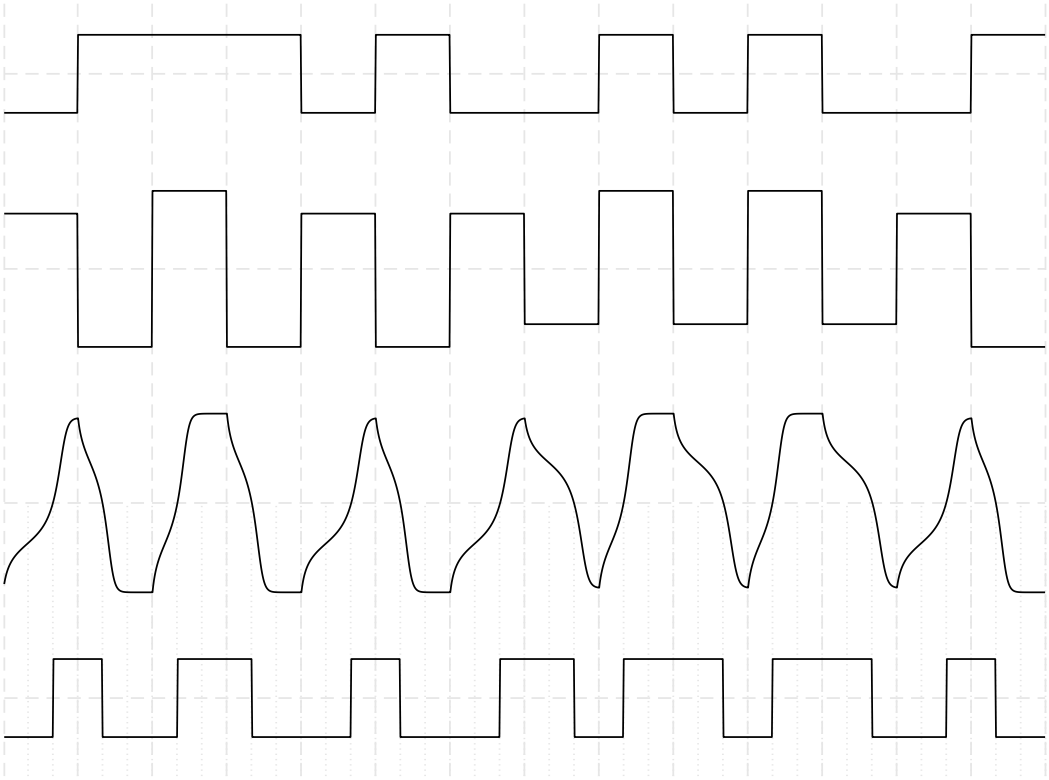

Figure 7.13: The signals at each step of the PWPM creation. By multiplying a square wave, information signal, BPAM (1st), is converted to PAM4 (2nd) applied to the DWP as an input. The output signal (3rd) passing through a sign detector results in PWPM signal (4th).

-0.3987, 3.726, -8.51] for t_r.

For a feasible PWPM signal, widths(W) and positions(P) (at which time pulse starts) needs to be time independent. This can be achieved by setting symbol period T greater than the longest settling time $t_r(A_{min})$. Then, it can be assumed that these properties do not fluctuate by time.

In addition to that, there must be sufficient number of (W,P) couples to match with all symbols. Considering that two sequential symbols with assigned amplitudes A_1 and A_2 form a pulse, then corresponding (W,P) can given by $(T - t_z(A_1) + t_z(A_2), t_z(A_1))$. This results in the same number of (W,P)s and provides one by one mapping between symbols and (W,P)s.

Therefore, the PWPM can be realized by a design of input signal, which is

going to be explained by an example. Considering that zeros cross timings are set to 0.1 s and 0.2 s, then A_1 and A_2 can be found as 1.87 h_b and 1.325 h_b from Eq. (7.24). As the longest settling time becomes $t_r(A_{min} = 1.325\ h_b) = 0.27\ s$, T can be set to 0.3 s. In the case where bits 1 and 0 represent A_1 and A_2, this process creates four pulses with (W,P)s; (0.3,0.1),(0.4,0.1),(0.2,0.2),(0.3,0.2) for four input symbol couples (1,1),(1,0),(0,1),(0,0). This realization can be illustrated by Fig. 7.13 where the information symbols, input signal, outputs of the modulator and threshold device are represented in order.

As a result, the time domain properties; zero cross timing and settling time, are used to create a PWPM output signal. This modulation type is different than the PAM with coding studied in Sec. 7.3. One encodes the information into width and position of the output pulse, another changes only the amplitude. Therefore, depending on the examined property of output signal, the modulation type varies.

7.5 Conclusion

In this chapter, the DWP system has been considered as a modulator and analysed accordingly. The time, frequency and phase parameters of one of the waveform given in Sec. 6.3.3 were defined, which indicated that DWP performs a multivariate analog modulation (involving two or more variable parameters). Then, it was considered that the system converts its input into waveforms having different parameters by the means of these functions. The modulation process was associated with a digital modulation with memory. Therefore, in addition to the conversion, the waveform allocation process was explained by a Markov chain. The results proved that DWP performs a convolutional coding if the input satisfies the given conditions, as the waveform allocation involves the previous states of the system. Furthermore, the SR phenomenon was observed where the background noise with a certain power triggered out the coding process while decreasing BER. Finally, the multidimensional

modulation capability was demonstrated by designing the input signal to create a PWPM signal.

Chapter 8

Conclusions and Future Research

8.1 Conclusions

Over the preceding chapters it has been shown that the DWP, the over-damped Duffing equation with symmetric bistable potential, performs signal processing tasks such as detection, filtering, modulation and encoding which are essentials for a communication system. The beneficial effect of adding stochastic signals as well as deterministic ones on its detection performance has been observed and compared. Meanwhile, the further performance improvement thanks to the resonant cancellation related to the phase matching has been presented by means of two detectors coupled in parallel. As a filter, its noise suppression performance, better than that of a conventional counterpart, has been obtained. In terms of modulation, the system output has been expressed as a function of input; thereby revealing which parameters of output are manipulated by the input. While amplitude, frequency and phase parameters of output are modulated, the analog modulation has been briefly introduced. Considering that the initial condition of the system have a critical control on the output parameters, and the input, a pulse modulated signal, has

discrete amplitudes and pulse durations, the process has been associated with the digital modulation with memory and examined accordingly. Through this examination, the process of convolutional coding has been uncovered. Furthermore, the noise effect triggering the coding process has been observed. These outcomes can be detailed as follows.

In Chapter 3, the detection capability of the DWP has been studied. Although the DE driving the output is responsive to any input signal regardless of strength, the receiver model in literature makes the decision based on the input sign. In order to control the output in a practical way, a novel design of the DWP was introduced. The design was based on the determination of ak, the product of parameter a and amplitude gain k, and the determination of normalized transition time m which was found to be inversely proportional to the gain. This design also simplified the analysis of DWP's response to the BPAM, thereby providing an alternative PSR method. The result shows that any BPAM signal with amplitudes $\pm A$ and bit interval T_b can be detected regardless of its features if the double well is designed to have $ak < 3$ and $m > 2$. Otherwise, a resonant signal is needed to enable the detection. This has been observed by introducing a Gaussian white noise, and then a sine wave.

While the noise with a certain power provided some BER performance improvement, defined as SR, the sine wave with a specific relation between the amplitude and frequency could enhance performance considerably, defined as a deterministic resonance. Such that, the BER of sine-induced resonance was decreased monotonically by the increase in SNR, which cannot be achieved by means of a noise. Although there have been different performance improvements, through Chapter 3, it has been firmly established that the BPAM signal subject to a Gaussian white background noise can be detected by the receiver model accommodating the DWP and a sign detector.

Chapter 4 has been devoted to investigating the effects of various resonant

signals on the output and BER performance. As the sine-induced resonance had such a success, the square and triangle waves were also introduced as a resonant in order to evaluate the underlying reasons of the deterministic resonance and performance improvement. Their resonant parameters; frequencies and amplitudes, were obtained by fitting the surface of minimum BER levels. Despite the variety observed in amplitudes, frequencies, and their relations, these three resonant signals decreased the BER considerably. Their power requirements increasing with the frequency and the strong fluctuations of the corresponding outputs were similar. In order to refine the output, the resonant caused fluctuation at the fundamental frequency was eliminated by the use of two double well coupled in parallel. This refinement was evaluated by their eye patterns showing the improvements on the phase and threshold sensitivities, thereby decreasing BER.

Following to the deterministic signals, various noises; white, f^{β} and band limited ones were introduced to the system input. It has been shown that the white noise with uniform, normal and normal product distributions require almost the same power for resonance, and provide slightly different BERs. This difference was associated with the tails of distribution, such that the longer tail the distribution has, the more errors occur. Then, two parallel double wells have been used to obtain a further BER decrease. While two different resonant noises decreased BER by half, one resonant noise and its negative decreased BER 100 times. This can be construed as a noise cancellation related to phase matching, and such a BER decrease indicates that it takes place within a wide frequency spectrum.

Finally, in Chapter 4, the effect of f^{β} and band limited noises with no background noise have been examined. It was observed that $\beta > 0$ and band limited noise not overlapping with the band of interest also resonated with the system and provided considerable BER improvements, in return, they demanded high powers. For instance, the higher frequency the noise bandwidth moves towards, the more power is required for resonance. Although these resonant signals vary in BER per-

formance, power requirement, and bandwidth, a resonance has been observed in any cases, and this variety extends the detection capability of the DWP.

In Chapter 5, the DWP has been considered as a low pass filter. The design was adapted to pass one single pulse, by defining the passband gain (DC gain) $= k$, and a cut-off frequency $< 1/2k$ (at the frequency where the gain drops to $k/\sqrt{2}$). In order to examine system response, the transfer function defined by the ratio of output and input frequency spectrum, $H(f) = Y(f)/S(f)$, was determined. This transfer function validated the consideration at the beginning as the passband gain $= k$ and cut-off frequency $f_c = 1/5k < 1/2k$, and also provided the stop-band attenuation that is -20 dB/decade. However, the presence of background noise was found to alter these parameters except the slope.

Then, considering the resemblance between transfer functions of the Butterworth filter and this design, both filters with the same cut-off frequency, $f_c = 1/T_b$, were used to obtain the filtered output. Although, the parameters varied depending on noise, BER expression, which was obtained by means of curve fitting, indicated that the noise components above the fixed cut-off frequency were suppressed. In addition, the designed filter provided BER better than 1st order Butterworth did at SNR > 0 dB, than 2nd order at SNR > 7 dB, and 3rd one at SNR > 9 dB, and so on. As the DWP was designed in a conventional way and had a performance, to some extent, better than the Butterworth filter, the filtering capability was demonstrated.

In Chapter 6, the DWP has been considered as a modulator. In order to reveal which parameter of output signal is modified by the input, the DE of the system has been derived where the input $x = 0$, homogeneous case, and $x = A$, inhomogeneous one. In both cases, the root separation method and dummy function approach were used. While the former method was providing the function of output, $y(t)$, which is the inverse function of $t(y)$, the latter one has expressed the general form for that function. As a result, it was found that there are 2 base functions if $|x| > \sqrt{4a^3/27b}$, otherwise there are 4 base functions. Then, they were defined as a

function of input x, initial condition y_0, and time t, so that the modulation property could be examined in Chapter 7.

In terms of modulation, one of the base functions has been analysed by defining and testing its amplitude, frequency and phase parameters in Sec. 7.1. It was shown that all these parameters were varied by the input amplitude. This demonstrates the existence of a multivariate analog modulation. However, the base functions were specified for the DC input, and the input was considered as a PAM signal which consists of discrete amplitudes and durations. Therefore, the direction of analysis was switched to the digital modulation.

As the digital modulation is based on mapping the input information symbols (or bits) into a set of predefined signal segments, called waveforms, the analysis was carried out in Sec. 7.2. First of all, the input information was introduced in the form of PAM signal. Then, the waveforms were considered as some segments of the base functions. The mapping process was also represented by defining the states of Markov chain. The results indicate that if there is at least one PAM level satisfying the condition $|A| < \sqrt{4a^3/27b}$, then there are more states than the PAM levels in total. In addition to that, while some states are observable, some others are hidden. However, regardless of the observation, all states participate in the decision process which determines the current state. Therefore, the mapping can be considered in two steps; the first step is to assign a state to the current input, then, assign a waveform to that state.

In the first step, the current state is chosen depending on not only the current input level but also the previous state, that indicated the presence of a convolutional coding. This was illustrated by the state transition and trellis diagrams as an example for PAM4 input. By presenting the state transition matrix and state probability vector for the same example, the output entropy was obtained as 2.5 bits/symbol where it was 2 bits/symbol for input. As this difference occurred as a result of the redundancy introduced by a coding process, the coding capability was established.

In the second step, each pair of previous and current states was represented by a waveform. The analysis on waveforms of the PAM4 example indicated that a set of properties; amplitude, frequency and phase of a waveform were specific to the corresponding pair. The difference between two waveforms can be in either amplitude, or frequency, or phase or a combination of these, which refers to a multidimensional modulation.

Although, the coding capability has been demonstrated in detail through this analysis, the resonance was not mentioned. Therefore, in order to observe this phenomenon, a simple case where the input was a BPAM signal with amplitudes $\sqrt{4a^3/27b} < -A, A < \sqrt{4a^3/27b}$ has been set in Sec. 7.3. In such a case, while the output is modulated, there is no coding applied, and a noise can benefit the system by enabling the coding process. When the noise is absent, the current state is only determined by the input level. This causes the output to have only two different amplitudes at the end of each bit interval. With the use of an appropriate threshold, the current bit passing through the system can be easily detected, as the mapping is one to one function for the case. However, when a noise is added to the input, two more states become observable. Then, the output cannot be resolved by one threshold, but three thresholds. If a noise starts coding process, it is expected to increase entropy while decreasing error rate where the detection is performed by three thresholds.

This entropy theorem has been tested by means of simulation. The conditional CDFs of output have been determined, and the state occurrence probabilities has been obtained. It has been found that while the entropy was increasing from 1 bit/symbol to 1.6 bits/symbol, the BER decreased from 0.2 to 0.15 where SNR was set to 8 dB. In addition, it was observed that, for lower SNRs, although the state entropy rose to 2 bits/symbol, the optimum thresholds approaching to zero caused uncertainty in the state detection, specifically at SNRs < 5 dB. For SNRs > 14 dB, while thresholds resolved the states with higher certainty, the entropy decreased to

1 bit/symbol within a finite observation. As a result, there was a noise power that enabled the coding in exchange of increasing error probability, thereby optimizing the information conveyed by the output. This is the definitive evidence of SR.

Finally, in Sec. 7.4, the input has been designed to demonstrate and evaluate the multidimensional modulation property. Although it was previously mentioned that the waveforms corresponding to the state pairs differ in amplitude, frequency and phase, only the amplitude property was studied in PAM4 example and the noise effect. Therefore, a case study was also presented for frequency and phase parameters. The output's rise shape and timing were considered to be directly related to its frequency and phase. They were manipulated by a BPAM input. The simulation results indicated that every two symbols was coupled, and a pulse, whose start timing and duration were specific to the corresponding symbol pair, was created. As a result, a PWPM signal was obtained by using a DWP. It can be inferred that depending on the assessment of output, various modulation schemes are attainable.

8.2 Future Research

Throughout the previous section, the conclusions have been drawn from the examination of a DWP in terms of signal processing. As all the tasks specified initially have been accomplished during this Ph.D. research, and it has been concluded that the DWP is an sophisticated signal processing tool, further research activities detailed below are conceived.

In terms of detection and filtering, an array of DWPs in parallel can be designed to detect M-ary PAM, Bandpass PAM, and FSK signals, and a design for an array of DWPs can be used as a bandpass-like filter. For further performance improvement, two DWPs coupled in series can be designed to work as a filter and an amplifier, respectively or reverse, as the amplification and filtering capabilities

can be regulated.

In terms of derivations, the expression of BER of SQPW subject to BPAM input, Eq. (5.11), can be extended to include the error rate of DWP subject to the weak input BPAM. Another possible direction can be a simplification of the output functions, Eq. (6.28), Eq. (6.31), Eq. (6.32).

In terms of modulation and coding properties, the noise free modulated and encoded PAM-like signal, obtained by a DWP and corrupted by adding a background noise, can be resolved by conventional methods to evaluate the modulation and encoding performance of the DWP. Furthermore, the input, in the pre-processing stage, can be designed to obtain FSK and PSK modulated outputs. Two DWPs coupled in parallel and series can be designed to encode and modulate in turn.

In terms of resonance, the optimum Gaussian noise power mentioned in Sec. 7.3 can be determined. The similar resonance effect can be obtained by adding a deterministic signal instead of noise.

Bibliography

[1] J. Proakis and M. Salehi, *Digital Communications*. McGraw-Hill, Edu., Nov 2007.

[2] R. L. Freeman, *Telecommunication System Engineering*. Hoboken, NJ, USA: John Wiley & Sons, Inc., May 2004.

[3] W. J. Witteman, *Detection and Signal Processing*. Springer Berlin Heidelberg, 2006, vol. 22.

[4] T. Wellens, V. Shatokhin, and A. Buchleitner, "Stochastic resonance," *Reports on Progress in Physics*, vol. 67, no. 1, pp. 45–105, 2004.

[5] D. K. Karig, P. Siuti, R. D. Dar, S. T. Retterer, M. J. Doktycz, and M. L. Simpson, "Model for biological communication in a nanofabricated cell-mimic driven by stochastic resonance," *Nano Communication Networks*, vol. 2, no. 1, pp. 39–49, 2011.

[6] T. Nakano, E. Andrew W., and H. Tokuko, *Molecular Communication*. Cambridge University Press, 2013.

[7] M. D. McDonnell, N. G. Stocks, C. E. M. Pearce, and D. Abbott, *Stochastic Resonance*. Cambridge: Cambridge University Press, 2008.

[8] S. Rajasekar and M. A. Sanjuan, *Nonlinear Resonances*. Springer International Publishing, 2016.

[9] J. Zhai, Z. Du, Y. Zhou, J. Shi, W. Xu, G. Sun, L. Kang, J. Chen, and P. Wu, "Noise-induced hopping in an rf squid," *IEEE Transactions on Applied Superconductivity*, vol. 25, no. 3, pp. 1–4, Jun 2015.

[10] S. O. Kasap, "Semiconductor Science and Light Emitting Diodes," in *Optoelectronics and Photonics; Principle and Practices*, 2nd ed. Pearson, 2013, ch. 3, pp. 249–252.

[11] H. G. N. Issaoui and B. Oujia, "Theoretical Simulation of the Infrared Absorption Spectrum of the Strong Hydrogen and Deuterium Bond in 2-Pyridone Dimer," *Open Journal of Physical Chemistry*, vol. 2, no. 4, pp. 228–239, 2012.

[12] G. P. Harmer, B. R. Davis, and D. Abbott, "A review of stochastic resonance: circuits and measurement," *IEEE Transactions on Instrumentation and Measurement*, vol. 51, no. 2, pp. 299–309, Apr 2002.

[13] B. McNamara, K. Wiesenfeld, and R. Roy, "Observation of stochastic resonance in a ring laser," *Physical Review Letters*, vol. 60, no. 25, pp. 2626–2629, Jun 1988.

[14] M. Misono, T. Kohmoto, Y. Fukuda, and M. Kunitomo, "Stochastic resonance in an optical bistable system driven by colored noise," *Optics Communications*, vol. 152, no. 4-6, pp. 255–258, Jul 1998.

[15] M. Misono, T. Kohmoto, M. Kunitomo, and Y. Fukuda, "Information gain in an optical bistable system by stochastic resonance," *Physical Review E*, vol. 67, no. 6, p. 061102, 2003.

[16] K. Wiesenfeld and F. Moss, "Stochastic resonance and the benefits of noise: from ice ages to crayfish and SQUIDs," *Nature*, vol. 373, no. 6509, pp. 33–36, Jan 1995.

[17] B. J. Gluckman, T. I. Netoff, E. J. Neel, W. L. Ditto, M. L. Spano, and S. J. Schiff, "Stochastic resonance in a neuronal network from mammalian brain," *Physical Review Letters*, vol. 77, no. 19, pp. 4098–4101, 1996.

[18] E. Simonotto, M. Riani, C. Seife, M. Roberts, J. Twitty, and F. Moss, "Visual Perception of Stochastic Resonance," *Physiological reviews*, vol. 78, no. 6, pp. 1186–1189, 1997.

[19] G. Giacomelli, M. Giudici, S. Balle, and J. R. Tredicce, "Experimental evidence of coherence resonance in an optical system," *Physical Review Letters*, vol. 84, no. 15, pp. 3298–3301, Apr 2000.

[20] A. Priplata, J. Niemi, M. Salen, J. Harry, L. A. Lipsitz, and J. J. Collins, "Noise-Enhanced Human Balance Control," *Physical Review Letters*, vol. 89, no. 23, p. 238101, 2002.

[21] H. Abbaspour, S. Trebaol, F. Morier-Genoud, M. T. Portella-Oberli, and B. Deveaud, "Stochastic resonance in collective exciton-polariton excitations inside a gaas microcavity," *Physical Review Letters*, vol. 113, no. 5, p. 057401, Jul 2014.

[22] W. J. Venstra, H. J. R. Westra, and H. S. J. van der Zant, "Stochastic switching of cantilever motion." *Nature Communications*, vol. 4, p. 2624, 2013.

[23] I. Lee, X. Liu, C. Zhou, and B. Kosko, "Noise-Enhanced Detection of Subthreshold Signals With Carbon Nanotubes," *IEEE Transactions On Nanotechnology*, vol. 5, no. 6, pp. 613–627, Nov 2006.

[24] F. Moss, L. M. Ward, and W. G. Sannita, "Stochastic resonance and sensory information processing: a tutorial and review of application," *Clinical Neurophysiology*, vol. 115, no. 2, pp. 267–281, 2004.

[25] R. Benzi, A. Sutera, and A. Vulpiani, "The mechanism of stochastic resonance," *Journal of Physics A: Mathematical and General*, vol. 14, no. 11, p. L453, 1981.

[26] L. Gammaitoni, P. Hänggi, P. Jung, and F. Marchesoni, "Stochastic Resonance: A remarkable idea that changed our perception of noise," *The European Physical Journal B*, vol. 69, no. 1, pp. 1–3, May 2009.

[27] R. Benzi, G. Parisi, A. Sutera, and A. Vulpiani, "Stochastic resonance in climatic change," *Tellus*, vol. 34, no. 1, pp. 10–16, 1982.

[28] D. S. Lemons and A. Gythiel, "Paul langevins 1908 paper on the theory of brownian motion [sur la thorie du mouvement brownien, c. r. acad. sci. (paris) 146, 530533 (1908)]," *American Journal of Physics*, vol. 65, no. 11, pp. 1079–1081, 1997.

[29] P. Jung and P. Hänggi, "Amplification of small signals via stochastic resonance," *Physical Review A*, vol. 44, no. 12, pp. 8032–8042, Dec 1991.

[30] B. McNamara and K. Wiesenfeld, "Theory of stochastic resonance," *Phys. Rev. A*, vol. 39, no. 9, pp. 4854–4869, May 1989.

[31] F. Moss, "Stochastic resonance: a signal+noise in a two state system," in *Proceedings of the 45th Annual Symposium on Frequency Control*, May 1991, pp. 649–658.

[32] S. Mitaim and B. Kosko, "Adaptive stochastic resonance," *Proceedings of the IEEE*, vol. 86, no. 11, pp. 2152–2183, Nov 1998.

[33] L. Gammaitoni, "Stochastic resonance and the dithering effect in threshold physical systems," *Physical Review E*, vol. 52, no. 5, pp. 4691–4698, 1995.

[34] F. Chapeau-Blondeau, "Stochastic Resonance and the Benefit of Noise in Nonlinear Systems," in *Noise, Oscillators and Algebraic Randomness*. Berlin, Heidelberg: Springer Berlin Heidelberg, 2000, vol. 550, pp. 137–155.

[35] F. Chapeau-Blondeau and D. Rousseau, "Noise improvements in stochastic resonance: From signal amplification to optimal detection," *Fluctuation and Noise Letters*, vol. 02, no. 03, pp. L221–L233, sep 2002.

[36] L. Gammaitoni, "Stochastic resonance in multi-threshold systems," *Physics Letters A*, vol. 208, no. 4-6, pp. 315–322, 1995.

[37] N. G. Stocks, "Suprathreshold Stochastic Resonance in Multilevel Threshold Systems," *Physical Review Letters*, vol. 84, no. 11, pp. 2310–2313, mar 2000.

[38] N. G. Stocks, "Suprathreshold stochastic resonance: An exact result for uniformly distributed signal and noise," *Physics Letters, Section A: General, Atomic and Solid State Physics*, vol. 279, no. 5-6, pp. 308–312, 2001.

[39] D. Rousseau and F. Chapeau-Blondeau, "Suprathreshold stochastic resonance and signal-to-noise ratio improvement in arrays of comparators," *Physics Letters A*, vol. 321, no. 5-6, pp. 280–290, Feb 2004.

[40] Z. Liu, Y.-C. Lai, and A. Nachman, "Enhancement of noisy signals by stochastic resonance," *Physics Letters A*, vol. 297, no. 1â2, pp. 75–80, 2002.

[41] L. Xu, F. Duan, Y. Ren, and D. Abbott, "Enhanced information transmission with generalized Gaussian signal via suprathreshold stochastic resonance," *2015 International Conference on Noise and Fluctuations, ICNF 2015*, pp. 1–4, 2015.

[42] T. R. Albert, A. R. Bulsara, G. Schmera, and M. Inchiosa, "An evaluation of the stochastic resonance phenomenon as a potential tool for signal processing,"

in *Conference Record of The Twenty-Seventh Asilomar Conference on Signals, Systems and Computers*, Nov 1993, pp. 583–587 vol.1.

[43] H. Yokota, S. Arai, T. Yamazato, and Y. Tadokoro, "Preliminary Study on LED VLC with Simple SR Receiver Using Schmitt Trigger," pp. 61–64, 2014.

[44] L. Gammaitoni, F. Marchesoni, E. Menichella-Saetta, and S. Santucci, "Stochastic Resonance in Bistable Systems," *Physical Review Letters*, vol. 62, no. 4, pp. 349–352, jan 1989.

[45] M. Dykman, R. Mannella, P. V. E. McClintock, and N. G. Stocks, "Comment on "Stochastic Resonance in Bistable Sys- tems"," *Physical Review letters*, vol. 65, no. 20, p. 2606, 1990.

[46] A. Bulsara and A. Zador, "Threshold detection of wideband signals: A noise-induced maximum in the mutual information," *Physical Review E*, vol. 54, no. 3, pp. R2185–R2188, 1996.

[47] M. D. McDonnell and D. Abbott, "What Is Stochastic Resonance? Definitions, Misconceptions, Debates, and Its Relevance to Biology," *PLoS Comput Biol*, vol. 5, no. 5, p. e1000348, 2009.

[48] P. Hänggi, P. Talkner, and M. Borkovec, "Reaction-rate theory: Fifty years after Kramers," *Reviews of Modern Physics*, vol. 62, no. 2, pp. 251–341, apr 1990.

[49] J. A. Revelli, C. E. Budde, and H. S. Wio, "Diffusion in fluctuating media: First passage time problem," *Physics Letters, Section A: General, Atomic and Solid State Physics*, vol. 306, no. 2-3, pp. 104–109, dec 2002.

[50] P. Landa and P. McClintock, "Changes in the dynamical behavior of nonlinear systems induced by noise," *Physics Reports*, vol. 323, no. 1, pp. 1–80, 2000.

[51] R. Mannella, "A Gentle Introduction to the Integration of Stochastic Differential Equations," in *Stochastic Processes in Physics, Chemistry, and Biology*, J. A. Freund and T. Pöschel, Eds. Springer, 2000, pp. 353–364.

[52] N. Berglund and B. Gentz, *Noise-Induced Phenomena in Slow-Fast Dynamical Systems*, ser. Probability and Its Applications. London: Springer-Verlag, 2006.

[53] G. A. Pavliotis, *Stochastic Processes and Applications*, ser. Texts in Applied Mathematics. New York, NY: Springer New York, 2014, vol. 60.

[54] Y. Amadou, G. Betchewe, Douvagai, M. Justin, S. Y. Doka, and K. T. Crepin, "Discrete exact solutions for the double-well potential model through the discrete tanh method," *European Physical Journal Plus*, vol. 130, no. 1, p. 13, 2015.

[55] Hu Gang, G. Nicolis, and C. Nicolis, "Periodically forced Fokker-Planck equation and stochastic resonance," *Physical Review A*, vol. 42, no. 4, pp. 2030–2041, Aug 1990.

[56] C. Zeng, A. Gong, and Y. Luo, "Effect of asymmetry in a bistable system with quantum fluctuations: Strong friction limit," *International Journal Of Modern Physics B*, vol. 25, no. 32, pp. 4331–4338, Dec 2011.

[57] P. S. Landa, I. A. Khovanov, and P. V. E. McClintock, "Theory of stochastic resonance for small signals in weakly damped bistable oscillators," *Physical Review E*, vol. 77, no. 1, p. 011111, Jan 2008.

[58] H. Chen, P. K. Varshney, S. M. Kay, and J. H. Michels, "Theory of the Stochastic Resonance Effect in Signal Detection: Part I - Fixed Detectors," *IEEE Transactions on Signal Processing*, vol. 55, no. 7, pp. 3172–3184, Jul 2007.

[59] H. Chen and P. Varshney, "Theory of the stochastic resonance effect in signal detection - part II: Variable detectors," *IEEE Transactions on Signal Processing*, vol. 56, no. 10, pp. 5031–5041, Oct 2008.

[60] F. Duan and B. Xu, "Parameter-induced stochastic resonance and baseband binary pam signals transmission over an awgn channel," *International Journal of Bifurcation and Chaos*, vol. 13, no. 02, pp. 411–425, Feb 2003.

[61] M. Yu and J. Chen, "Blind adaptive stochastic resonance in base band binary signal processing," *2010 6th International Conference on Wireless Communications, Networking and Mobile Computing, WiCOM 2010*, vol. 3, no. 1, pp. 3–6, 2010.

[62] J. Liu, Z. Li, L. Guan, and L. Pan, "A novel parameter-tuned stochastic resonator for binary pam signal processing at low snr," *IEEE Communications Letters*, vol. 18, no. 3, pp. 427–430, March 2014.

[63] J. Liu and Z. Li, "Lowering the signal-to-noise ratio wall for energy detection using parameter-induced stochastic resonator," *IET Communications*, vol. 9, no. 1, pp. 101–107, 2015.

[64] L. Gammaitoni, F. Marchesoni, and S. Santucci, "Stochastic Resonance as a Bona Fide Resonance," *Physical Review Letters*, vol. 74, no. 7, pp. 1052–1055, Feb 1995.

[65] S. M. Bezrukov and I. Vodyanoy, "Stochastic resonance in non-dynamical systems without response thresholds," pp. 319–321, 1997. [Online]. Available: http://www.ncbi.nlm.nih.gov/pubmed/9002515

[66] L. Gammaitoni, P. Hänggi, P. Jung, and F. Marchesoni, "Stochastic resonance," *Rev. Mod. Phys.*, vol. 70, no. 1, pp. 223–287, 1998.

[67] R. Mingesz, Z. Gingl, and P. Makra, "Marked signal improvement by stochastic resonance for aperiodic signals in the double-well system," *European Physical Journal B*, vol. 50, no. 1-2, pp. 339–344, 2006.

[68] F. Duan and D. Abbott, "Signal detection for frequency-shift keying via short-time stochastic resonance," *Physics Letters A*, vol. 344, no. 6, pp. 401–410, 2005.

[69] S. Wei, T. Zhang, C. Gao, and F. Tan, "The united detection of weak MSK signal using Duffing oscillator and Stochastic resonance," in *4th IEEE Int. Symp. Microwave, Antenna, Propagation, and EMC Technol. (MAPE)*, Nov 2011, pp. 447–453.

[70] D. Rousseau, J. R. Varela, F. Duan, and F. Chapeau-Blondeau, "Evaluation of a Nonlinear Bistable Filter for Binary Signal Detection," *International Journal of Bifurcation and Chaos*, vol. 15, no. 02, pp. 667–679, 2005.

[71] D. Hui, Z. Jinghua, and L. Yonggang, "Research on the nonlinear square wave filter based on concatenation stochastic resonance," *2010 International Conference on Measuring Technology and Mechatronics Automation, ICMTMA 2010*, vol. 3, no. x, pp. 219–222, 2010.

[72] C. Silva and A. Young, "Introduction to chaos-based communications and signal processing," in *2000 IEEE Aerospace Conference. Proceedings (Cat. No.00TH8484)*, vol. 1. IEEE, 2000, pp. 279–299.

[73] S. A. Reshetnyak and V. A. Shcheglov, "On the stochastic resonance from the point of view of filtering properties of a bistable system," *Quantum Electronics*, vol. 33, no. 2, pp. 142–148, 2003.

[74] D. Hui and Z. Li, "Study on Filter Characteristic of Concatenation Stochastic Resonance," *2011 Fourth International Conference on Intelligent Computation Technology and Automation*, pp. 717–719, 2011.

[75] F. Cottone, H. Vocca, and L. Gammaitoni, "Nonlinear Energy Harvesting," *Physical Review Letters*, vol. 102, no. 8, p. 080601, Feb 2009.

[76] A. Palonpon, J. Amistoso, J. Holdsworth, W. Garcia, and C. Saloma, "Measurement of weak transmittances by stochastic resonance," *Opt. Lett.*, vol. 23, no. 18, pp. 1480–1482, Sep 1998.

[77] J. C. Comte and S. Morfu, "Stochastic resonance: another way to retrieve subthreshold digital data," *Physics Letters A*, vol. 309, no. 1, pp. 39–43, 2003.

[78] F. Chapeau-Blondeau and D. Rousseau, "Noise-aided SNR amplification by parallel arrays of sensors with saturation," *Physics Letters A*, vol. 351, no. 4-5, pp. 231–237, Mar 2006.

[79] Y. Guo and J. Tan, "Suprathreshold stochastic resonance in multilevel threshold system driven by multiplicative and additive noises," *Communications in Nonlinear Science and Numerical Simulation*, vol. 18, no. 10, pp. 2852–2858, Oct 2013.

[80] X. Zhang and W. Xu, "Stochastic resonance in an asymmetric bistable system with coloured noises and periodic rectangular signal," *Physica A: Statistical Mechanics and its Applications*, vol. 385, no. 1, pp. 95–104, 2007.

[81] S. Zozor and P.-O. Amblard, "Stochastic resonance in locally optimal detectors," *IEEE Transactions on Signal Processing*, vol. 51, no. 12, pp. 3177–3181, Dec 2003.

[82] K. Cuomo, A. Oppenheim, and S. Strogatz, "Synchronization of Lorenz-based chaotic circuits with applications to communications," *IEEE Transactions on Circuits and Systems II: Analog and Digital Signal Processing*, vol. 40, no. 10, pp. 626–633, 1993.

[83] G. Kolumban, M. P. Kennedy, and L. O. Chua, "The role of synchronization in digital communications using chaos. i . fundamentals of digital communications," *IEEE Transactions on Circuits and Systems I: Fundamental Theory and Applications*, vol. 44, no. 10, pp. 927–936, Oct 1997.

[84] G. Kolumban, M. Kennedy, and L. Chua, "The role of synchronization in digital communications using chaos. II. Chaotic modulation and chaotic synchronization," *IEEE Transactions on Circuits and Systems I: Fundamental Theory and Applications*, vol. 45, no. 11, pp. 1129–1140, 1998.

[85] M. I. Yousefi and F. R. Kschischang, "Information transmission using the nonlinear fourier transform, part I: Mathematical tools," *IEEE Transactions on Information Theory*, vol. 60, no. 7, pp. 4312–4328, 2013.

[86] Z. Dong, S. Hari, T. Gui, K. Zhong, M. I. Yousefi, C. Lu, P. K. A. Wai, F. R. Kschischang, and A. P. T. Lau, "Nonlinear frequency division multiplexed transmissions based on nft," *IEEE Photonics Technology Letters*, vol. 27, no. 15, pp. 1621–1623, Aug 2015.

[87] W. Chen, J. Wang, H. Li, and S. Li, "Stochastic resonance noise enhanced spectrum sensing in cognitive radio networks," *GLOBECOM - IEEE Global Telecommunications Conference*, no. 2008, 2010.

[88] R. A. Wannamaker, S. P. Lipshitz, and J. Vanderkooy, "Stochastic resonance as dithering," *Physical Review E*, vol. 61, no. 1, pp. 233–236, Jan 2000.

[89] M. D. McDonnell, N. G. Stocks, C. E. M. Pearce, and D. Abbott, "Optimal information transmission in nonlinear arrays through suprathreshold stochastic resonance," *Physics Letters, Section A: General, Atomic and Solid State Physics*, vol. 352, no. 3, pp. 183–189, 2006.

[90] F. Duan, F. Chapeau-Blondeau, and D. Abbott, "Encoding efficiency of suprathreshold stochastic resonance on stimulus-specific information,"

Physics Letters, Section A: General, Atomic and Solid State Physics, vol. 380, no. 1-2, pp. 33–39, 2016.

[91] H. Gang, T. Ditzinger, C. Z. Ning, and H. Haken, "Stochastic resonance without external periodic force," *Physical Review Letters*, vol. 71, no. 6, pp. 807–810, Aug 1993.

[92] L. Gammaitoni, M. Löcher, A. Bulsara, P. Hänggi, J. Neff, K. Wiesenfeld, W. Ditto, and M. Inchiosa, "Controlling Stochastic Resonance," *Physical Review Letters*, vol. 82, no. 23, pp. 4574–4577, Jun 1999.

[93] J. J. Collins, C. C. Chow, and T. T. Imhoff, "Aperiodic stochastic resonance in excitable systems," *Physical Review E*, vol. 52, no. 4, pp. R3321–R3324, Oct 1995.

[94] D. Nozaki, J. J. Collins, and Y. Yamamato, "Mechanism of stochastic resonance enhancement in neuronal models driven by 1/f noise," *Physical review E, Statistical physics, plasmas, fluids, and related interdisciplinary topics*, vol. 60, no. 4, pp. 4637–4644, 1999.

[95] P. S. Landa and P. V. E. McClintock, "Vibrational resonance," *Journal of Physics A: Mathematical and General*, vol. 33, no. 45, pp. L433–L438, Nov 2000.

[96] Y. Ren and F. Duan, "Theoretical and experimental implementation of vibrational resonance in an array of hard limiters," *Physica A: Statistical Mechanics and its Applications*, vol. 456, pp. 319–326, 2016.

[97] R. H. Shao and Y. Chen, "Stochastic resonance in time-delayed bistable systems driven by weak periodic signal," *Physica A: Statistical Mechanics and its Applications*, vol. 388, no. 6, pp. 977–983, 2009.

[98] J. F. Lindner, B. K. Meadows, W. L. Ditto, M. E. Inchiosa, and A. R. Bulsara, "Array Enhanced Stochastic Resonance and Spatiotemporal Synchronization," *Physical Review Letters*, vol. 75, no. 1, pp. 3–6, Jul 1995.

[99] F. Duan, F. Chapeau-Blondeau, and D. Abbott, "Stochastic resonance with colored noise for neural signal detection," *PLoS ONE*, vol. 9, no. 3, p. e91345, Mar 2014.

[100] Y. Guo, Y. Shen, and J. Tan, "Stochastic resonance in a piecewise nonlinear model driven by multiplicative non-Gaussian noise and additive white noise," *Communications in Nonlinear Science and Numerical Simulation*, vol. 38, pp. 257–266, 2016.

[101] C. J. Wang, F. Long, P. Zhang, and L. R. Nie, "Controlling of stochastic resonance and noise enhanced stability induced by harmonic noises in a bistable system," *Physica A: Statistical Mechanics and its Applications*, vol. 471, pp. 288–294, Apr 2017.

[102] N. Güneş, M. D. Higgins, and M. S. Leeson, "Stochastic resonator to detect bipolar binary pulse amplitude modulated signals; analysis, parameter-induced SR designs and sine-induced SR," *IET Signal Processing*, vol. 10, no. 9, pp. 1017–1023, Dec 2016.

[103] M. Kocaoglu, B. Gulbahar, and O. B. Akan, "Stochastic resonance in graphene bilayer optical nanoreceivers," *IEEE Transactions on Nanotechnology*, vol. 13, no. 6, pp. 1107–1117, Nov 2014.